Title
Developing zebrafish behavioral assays for high-throughput psychoactive drug discovery

Author
Kinser, Reid

Publication Date
2022

Peer reviewed|Thesis/dissertation

Developing zebrafish behavioral assays for high-throughput psychoactive drug discovery

by
Reid Kinser

DISSERTATION
Submitted in partial satisfaction of the requirements for degree of
DOCTOR OF PHILOSOPHY

in

Pharmaceutical Sciences and Pharmacogenomics

in the

GRADUATE DIVISION
of the
UNIVERSITY OF CALIFORNIA, SAN FRANCISCO

Approved:

DocuSigned by:
Su Guo
607F1205C317481...

Su Guo
Chair

DocuSigned by:
Michael Keiser

Michael Keiser

DocuSigned by:
Roy Gerona
B8A076B0924B41B...

Roy Gerona

Committee Members

For my parents

Acknowledgements

First, I must thank my advisor, Su Guo; thank you for generously taking me into your lab and sharing all of your wisdom with me. Next, I'd like to thank my committee members, Roy Gerona and Mike Keiser. Thank you both for the mentorship you've given me over the past few years, and for the opportunities to collaborate and learn from you. I also want to thank the members of my lab for their friendship, the many enthusiastic conversations, and for sharing their expertise with me. In particular, I thank Matt McCarroll for his leadership and commitment to the students in the lab. Finally, I want to express my gratitude to my close friends and family – I couldn't have done it without your support and encouragement.

Contributions

Some chapters of this dissertation contain previously published material or work that is currently in review. In some instances, these materials have been altered for the purpose of this dissertation and therefore may differ from the published articles.

Basis for Chapter 1:

Adapted from an unpublished manuscript currently in review;

Kinser, R. *et al.* (2022) “Zebrafish buoyancy as a sensitive phenotypic endpoint for high-throughput neuroactive drug discovery”.

Basis for Chapter 2:

McCarroll, M.N., Gendelev, L., Kinser, R. *et al.* Zebrafish behavioural profiling identifies GABA and serotonin receptor ligands related to sedation and paradoxical excitation. *Nature Communications* **10**, 4078 (2019). https://doi.org/10.1038/s41467-019-11936-w

Developing zebrafish behavioral assays for high-throughput psychoactive drug discovery

Reid Kinser

Abstract

Neurological and psychiatric disorders (such as depression, neurodegeneration, and drug addiction) are among the greatest challenges faced by modern medicine. Though they are some of the most prevalent and debilitating illnesses in the world, current treatment options leave much to be desired due to limited efficacy or intolerable side effects. Our understanding of the nervous system is still rudimentary, preventing the development of new drugs that precisely target the pathogenic mechanisms of disease.

Instead, most neuroactive drugs in clinical use were either developed decades ago or are chemical derivatives of these legacy drugs. Typical target-based approaches to drug screening have had limited success in psychiatric drug discovery due to inadequate mechanistic understanding and the multifactorial nature of the disorders they aim to treat. As a result, neuroactive drug development has stagnated while pharmaceutical companies focus their resources on less risky endeavors.

How can we overcome these challenges to accelerate psychoactive drug discovery in the future? One approach is phenotypic drug screening based on observations of animal behavior. This strategy has the potential to uncover behaviorally active compounds with unprecedented mechanisms but is limited by the difficulty of efficiently measuring animal behaviors at scale. This dissertation documents

contributions to phenotypic drug screening utilizing the zebrafish model organism, including the identification of meaningful behavioral phenotypes which are accessible in a large-scale context and new methods to automate the quantification of these behaviors.

In Chapter 1, the influence of neuroactive drugs on zebrafish buoyancy is investigated using a computational method to approximate the depth of larvae in a 96-well plate. This approach is easily scaled up, allowing us to rapidly screen thousands of molecules to discover new ligands for adrenergic and serotonergic receptors which alter behavior *in vivo*. In Chapter 2, we explore phenotypes related to paradoxical excitation during early-stage general anesthesia – a complex and poorly understood behavioral state that would be very difficult to study in systems other than intact animals. By identifying compounds from a behavioral screen that phenocopy the response of zebrafish to anesthetics like etomidate and propofol, we uncovered new $GABA_A$ receptor modulators with potential anesthetic activity *in vivo*. In summary, the work included in this dissertation provides new methods to quantify zebrafish behavior on a high-throughput scale and demonstrates their use by identifying several new behavior-modifying small molecules.

Table of Contents

List of Figures

List of Tables

Chapter 1: Zebrafish buoyancy as a sensitive phenotypic endpoint for high-throughput neuroactive drug discovery

1.1 Abstract

In nature, fish occupy a characteristic depth in the water column centered around the position where they achieve hydrostatic equilibrium (neutral buoyancy). The nervous system integrates sensory information from the internal and external environment, and initiates physiological changes in whole-body density to maintain an ideal buoyancy for survival. Here we developed a high-throughput assay to identify floating zebrafish larvae and found that buoyancy homeostasis is highly sensitive to neuroactive compounds. We used this method to interrogate 647 chemical probes, revealing adrenergic, cholinergic, serotonergic, and dopaminergic involvement in buoyancy regulation. Harnessing the potential of zebrafish for drug discovery, we next screened 9,600 uncharacterized molecules to identify buoyancy-modifying compounds. Results from *in vitro* receptor binding assays and cheminformatics-based target prediction suggest that some hit compounds represent new chemical entities that target α_{1B} and 5-HT_{1D} receptors, while others might interact with kinases or other enzymes. Our findings demonstrate the value of this zebrafish buoyancy assay as a scalable, non-invasive method to identify new neuroactive substances.

1.2 Introduction

Despite technological advancements which have made most aspects of science more efficient, discovery of new drugs has remained a challenge. Modern pharmaceutical companies have generally favored a target-based approach, but retrospective analysis of FDA approved drugs indicates that these "rational" screening strategies have done little to improve the rate of success during drug discovery. In particular, the discovery of new drugs to treat nervous system disorders is limited by our understanding of the relevant pathogenesis. Instead, "phenotypic" screening has historically been a more successful avenue for discovery of drugs with new mechanisms [1]; in this approach, substances which cause a unique or desirable response in a living organism are flagged for further study [2]. The benefit is that powerful bioactive substances can be identified without relying on any mechanistic knowledge or preconceptions about how drugs may work *in vivo*. Widespread adoption of phenotypic screens is limited by the challenge of observing and quantifying animal phenotypes at a scale that is comparable to current *in vitro* options.

Zebrafish larvae are an attractive model organism for conducting phenotypic screens to find new neuroactive drugs. As vertebrates, zebrafish are genetically and physiologically similar to humans [3,4], are sensitive to many of the same neuroactive compounds [5], and develop complex behaviors at young ages [6,7]. Larvae are small enough to fit in standard 96-well plates and can absorb drugs from the water, allowing pharmacological experiments to be conducted at a scale that wouldn't be practical with larger animals. The relatively simple and inexpensive maintenance of fish makes it feasible for individual labs to conduct these screens. Zebrafish phenotypic screens have

previously discovered bioactive molecules with phenotypic relevance to sleep [8], anesthesia [9], appetite [10], morphological development [11], and glucose regulation [12].

Reflexive adjustments to swim bladder volume allow fish to compensate for changes in their environment such as fluctuations in atmospheric pressure, water temperature or salinity, which will change the density of the surrounding medium. Maintaining neutral buoyancy promotes homeostasis by minimizing the energetic cost of resisting gravity. Fish depth is also reflective of complex behaviors, such as risk-assessment [13] and circadian rhythms [14,15], which may be disrupted in human pathological states. These qualities suggest fish depth preference could be a potentially informative endpoint for behavioral screening. However, current depth assays are designed for low-throughput single fish experiments and rely on cumbersome camera arrangements that aren't readily adapted for large-scale screening [16].

In this work, we establish a high-throughput behavioral assay to approximate larval zebrafish depth from top-down videos. Using this method, we investigated the pharmacology regulating the swimbladder, the fish buoyancy organ. We found that swimbladder hyperinflation could be induced by drugs targeting receptors of the autonomic nervous system (including muscarinic agonists, α_1 blockers, and β-adrenergic agonists). Several classes of psychiatric drugs, including antidepressants, antipsychotics, and ergoline derivatives were broadly active in the assay, as well as a variety of vasodilator drugs. Additionally, serotonin receptor agonists were identified as neural regulators of zebrafish buoyancy. Finally, we identified several buoyancy modulating compounds in a high-throughput screen of previously uncharacterized molecules. Though some of these compounds were found to bind to anticipated receptor targets,

most have undetermined mechanisms of action, representing "dark chemical matter" with potentially novel pharmacology.

1.3 Methods

1.3.1 Fish lines and husbandry

Wild-type “Singapore”-strain zebrafish (ZFIN:ZDB-GENO-980210-24) were used; husbandry was performed as described previously [20]. Briefly, embryos were collected after group mating and raised to 7 dpf on a 14/10-hour light/dark cycle in 28°C egg water. All experiments were done with institutional IACUC approval at the University of California, San Francisco.

1.3.2 Chemicals and screening libraries

The “Biomol” library (SCREEN-WELL Neurotransmitter library, Enzo) contained 647 ligands with annotated pharmacological activity at a variety of different neurotransmitter receptors. Compounds were dissolved in a biocompatible solvent (DMSO, water, or N-methyl-2-pyrrolidone) at a concentration of 10 mM (1 mM for peptides) and screened at a final concentration of 30 μM (peptides at 3 μM). The resulting dataset included multiple replicates (median 11, range 5-26) of each compound randomly located in different wells of the 96-well plate.

The “ChemBridge” library included 9,600 structurally diverse, drug-like molecules with uncharacterized activity (a subset of the DIVERSet-EXP library, ChemBridge Corporation). Compounds were dissolved in DMSO at a concentration of 1 mM and screened at a final concentration of 10 μM in the well. Each compound has a

numeric catalog ID (**Supplemental Table 1.2**) to simplify purchasing a sample for further study of the active molecules identified in this work (Hit2Lead.com, ChemBridge Corporation).

In addition, the following probe compounds were used to characterize zebrafish buoyancy or other depth-related phenotypes: ABE, atropine, prazosin, selegiline, 8-OH-DPAT, and 3-CPMT were obtained from Cayman. Isoprenaline and Salbutamol were obtained from Sigma.

1.3.3 Measuring locomotor activity

Zebrafish locomotion in each well was quantified with a frame differencing approach performed by custom Python scripts using the OpenCV library. First, the maximum change in intensity across 3 sequential frames was calculated pixel-wise according to the following formula:

$$m'(t) = \max\left((frame_t - frame_{t-1}), (frame_t - frame_{t+1})\right)$$

The locomotion score m was obtained by counting the pixels in the difference image m' which exceeded a fixed threshold after applying a gaussian blur to suppress noise. The sum of the locomotion scores over every frame in the video (the “total motion”) was used to identify potentially toxic treatments that immobilized the larvae.

1.3.4 Approximating depth of zebrafish larvae

To estimate the depth of zebrafish in a 96-well plate from top-down videos, the average radial position of the larvae within the well was measured. To automatically mask the locations of larvae in a video frame, we developed a filtering procedure based on mathematical morphology, an image processing approach well-suited for detecting features based on shape. Through a series of morphological and algebraic operations targeting round objects with a strong intensity gradient, we obtained robust masks of the head/abdomen region for all larvae in the frame. The masked pixels were used to increment an accumulator image, producing a heatmap indicating the cumulative number of frames where each pixel was occupied.

For each well, the heatmap was used to calculate the mean distance from the center of the well using a weighted average given by:

$$d = \frac{\sum_{r=1}^{n}(w_r * x_r * r)}{\sum_{r=1}^{n}(w_r * x_r)}$$

where x_r is the value of a pixel in the heatmap located at distance r from the center of the well and w_r is the corresponding weight, which is inversely proportional to the relative frequency of pixels located at distance r (i.e., if there are twice as many pixels sharing the same distance, they will have half the weight). As a consequence, the pixels along the maximum inscribed circle within the square well receive a weight of 0, and pixels near the center or corners of the well are highly weighted. This weighting function minimizes the contribution from intermediate-distance positions in the well which take up a disproportionate amount of the well's area.

1.3.5 12-hour assay for zebrafish larvae depth approximation

For probe compound characterization and hit validation, a 12-hour video of zebrafish behavior was captured at a framerate of 1 fps. The extended observation period is important to ensure that the maximum effect is measured, despite potential differences in the rate of onset of the phenotype. Larvae were distributed in each well of a 96-well plate (3 larvae per well for the 12-hour assays), filled with 300 µL of egg water. All plates used for this project were 650 µL “square-well” plates (Whatman Uniplate 7701-1651). After addition of the compounds, the plate was immediately placed in the screening chamber and recording was started within 1 minute. Only the frames from the last 3 hours of the video were used to calculate the average radial position of the larvae within the well (representing their position from 9-12 hours after first addition of the drug) using the formula described above.

1.3.6 High-throughput behavioral screens

Pre-existing video data from phenotypic screens of the “Biomol” and “ChemBridge” libraries [20] were re-analyzed to identify compounds that increase zebrafish buoyancy resulting in accumulation at the water surface. In brief, the format of this data was 20-minute long videos (2k resolution, 100 frames per second) of 96-well plates filled with egg water (300 µL) and zebrafish larvae (7 dpf, n = 8 larvae per well) treated with either compound or vehicle control. To identify compounds that potentially caused the zebrafish to float, all frames from the 20-minute videos were included in the calculation of the time-averaged radial position. Compounds that suppressed locomotion to less

than 20% of the average vehicle-treated control value were considered potentially toxic and removed from further consideration.

1.3.7 *In vitro* receptor binding profiles, K_i determination, and receptor activation assays.

Receptors used for *in vitro* assays were all cloned human receptors, except for TSPO and the benzodiazepine binding site (rat brain tissue). All *in vitro* assays were performed by the National Institute of Mental Health Psychoactive Drug Screening Program (PDSP) at University of North Carolina, Chapel Hill. For a detailed description of the assay protocols, see the *NIMH PDSP Assay Protocol Book* (Version 3): https://pdsp.unc.edu/pdspweb/content/PDSP%20Protocols%20II%202013-03-28.pdf.

1.3.8 Chemoinformatics-based target prediction

A SEA library was constructed as following. ChEMBL 29 (RRID: 014042) activity data were filtered for binding (type 'B') subject to PCHEMBL ≥ 5 (10 μM) and target confidence ≥ 3. We restricted targets to target single protein, protein family, protein complex, protein complex group, nucleic-acid, or macromolecule; and required that the target species was in euteleostomi in a cladistic sense (UniProt taxon 117571). Targets were dropped if there were fewer than 10 distinct ligands meeting these requirements. These filters resulted in 1,030,636 activity annotations over 1,705 targets and 565,905 molecules. Distinct sets were then generated for 6 affinity thresholds: PCHEMBL ≥ 5 (10 μM), ..., PCHEMBL ≥ 10 (100 pM). A target was dropped out of a set if it had fewer than 10 ligands or fewer than 20 annotations meeting the required threshold. For target

predictions, compounds were normalized by applying rdkit (RRID: 014274) sanitization. They were then linked semi-automatically to ChEMBL 29.0. ECFP fingerprints with radius 4 and 4096 bits were calculated by SEA on the normalized structures.

1.4 Results

1.4.1 Developing a high-throughput method to identify floating larvae

Short-term changes in fish buoyancy are primarily mediated by adjustments in swimbladder gas volume. Like other internal organs, the activity of the swimbladder is regulated by the autonomic nervous system (ANS) [17,18,19]. It is thought that the sympathetic ("fight or flight") branch of the ANS is responsible for deflation of the swimbladder, while the parasympathetic ("rest and digest") branch facilitates inflation. To determine if zebrafish buoyancy could serve as an indicator of pharmacological activity for screening purposes, we tested if drugs targeting ANS receptors could stimulate swimbladder inflation.

We selected the α_1-blocker, prazosin, and the muscarinic agonist, arecaidine but-2-ynyl ester (ABE), to represent a withdrawal of sympathetic tone (decreased stimulation of adrenergic receptors by norepinephrine) and gain in parasympathetic tone (increased muscarinic receptor signaling), respectively (**Figure 1.1a**). Larvae were incubated with either drug in the wells of a 96-well plate (**Figure 1.1b**). We soon observed that these larvae had become positively buoyant and displayed an enlarged swimbladder when inspected under a microscope (**Figure 1.1c–1.1d**). From a side perspective (**Figure 1.1e**), untreated larvae are typically observed near the bottom of the well, while treated larvae are clearly restricted to the top portion of the well (**Figure 1.1f**). Interestingly, when

viewed from above, untreated larvae were typically distributed semi-randomly throughout the area of the well (**Figure 1.1g**), but the floating larvae accumulated along the edges due to the interaction with the meniscus at the surface (**Figure 1.1h**).

Next, we leveraged this edge-accumulation phenomenon to develop an automated, high-throughput method for quantifying larval depth. To do this, we analyzed videos of larvae in 96-well plates recorded from a top-down view [20], the most common method of acquiring larval zebrafish behavioral data [21]. We selected microplates featuring deep, square-shaped wells that taper in width towards the bottom (**Figure 1.2a**). By tracking the location of larvae over the course of the video, we were able to generate a heatmap of preferred locations within the well (**Figure 1.2b–1.2d**). This data was then used to calculate the average radial position of the larvae (measured from the well's center when viewed from above) throughout the duration of the video (**Figure 1.2e**). To compensate for potential differences in drug bioavailability and solubility, a significant issue with bath application of drugs [22], we determined the potency of both compounds from 12-hour videos captured overnight (**Figure 1.2f**).

We found that prazosin concentrations as below 100 nM prompted a robust floating phenotype in most larvae (**Figure 1.2g**). The potency of this interaction suggests that α_1-adrenoceptors play an important role in regulating swimbladder volume in larval zebrafish, consistent with other fish species [23,24]. The muscarinic agonist, ABE, also potently stimulated swimbladder inflation (**Figure 1.2h**). To verify that this compound was acting on muscarinic receptors, we attempted to block swimbladder inflation by pretreating the larvae with atropine, a muscarinic antagonist. We found that a 2-hour pretreatment with atropine (100 μM) suppressed the inflation reflex following exposure to ABE

(**Supplemental Figure 1.1**). Atropine pretreatment was unable to prevent prazosin-induced inflation (data not shown).

In summary, these experiments show that perturbation of autonomic signaling, that is, decreased sympathetic tone (through blockade of α_1 receptors) or increased parasympathetic tone (agonism of muscarinic receptors) can manipulate larval zebrafish buoyancy by causing swimbladder inflation. Floating larvae can be identified automatically from top-down video recordings due to their tendency to remain along the edges of the well, enabling behavioral screening in a simple, high-throughput format.

1.4.2 Screen of 647 probe compounds highlights specific chemical classes and suggests β-adrenergic, serotonergic, and dopaminergic regulation of buoyancy.

To find additional mechanisms that regulate zebrafish depth preference, we analyzed videos from a phenotypic screen of 647 compounds from the SCREEN-WELL Neurotransmitter library ("Biomol" dataset), following the screening process described briefly in **Figure 1.3a.** This library consists of ligands with annotated pharmacological activity at one or more receptors for 13 different neurotransmitter systems (**Figure 1.3b**). The videos were obtained from a previously conducted screen [20] and included multiple replicates for each compound (median *n* replicates: 11; range: 6–27) at a single concentration (30 μM).

We quantified the mean radius of the larvae in each well over the full 20-minute video. For each unique ligand in the dataset, we recorded the median result obtained from replicate wells. After discarding 36 "toxic" compounds which suppressed locomotor activity in most replicate experiments, we selected all the compounds with a radius

value more than two standard deviations above the control mean (using data from 1,012 DMSO-treated control wells screened simultaneously). This left us with 46 compounds from the neuroactive reference library (**Figure 1.3c**) which putatively inflated the larval zebrafish swimbladder (**Supplemental Table 1.1**).

Of the 13 different neurotransmitter systems, >90% of the hit compounds (43 of 46) were annotated for adrenergic, cholinergic, serotonergic, or dopaminergic activity (**Figure 1.3d**). Inspection of this collection of compounds revealed substantial overlap between the represented chemical classes (**Figure 1.3e**). We were able to group most of the compounds into 8 categories with shared pharmacological profiles and/or chemical structures (**Supplemental Figure 1.2**). For example, arylpiperazine derivatives (such as tricyclic antidepressants and antipsychotics) comprised the majority of all compounds, possibly due to synergistic polypharmacology.

The presence of cholinergic and adrenergic compounds among the hits is consistent with our earlier observation that ANS-targeting drugs can cause hyperinflation of the larval zebrafish swimbladder. However, aside from α-blockers, a small group of β agonists were among the adrenergic drugs; this was an unexpected finding, as a previous study of (adult) zebrafish swimbladder tissue showed that β receptor agonism causes deflation via smooth muscle contraction [18]. To verify the pro-inflation effect of β adrenergic agonists on larval zebrafish swimbladder, we investigated the ability of isoprenaline (a non-selective β agonist) and salbutamol (a β_2 selective agonist) [25,26] to induce a floating phenotype. We found that both of these drugs caused a dose-dependent increase in the mean radius of larvae from the center of the well (**Figure 1.3f, 1.3g**), suggestive of increasing buoyancy. Visual inspection confirmed the presence of an overinflated

swimbladder in larvae treated with β agonists. These findings indicate that β adrenergic agonists can inflate the swimbladder of larval zebrafish, and that this phenomenon may involve receptors with β_2-like pharmacology.

Serotonergic hit compounds from the reference ligand screen had both agonist (at 5-HT_{1A}) and antagonist (at 5-HT_{2A}) mechanisms. To better understand how serotonin might regulate swimbladder inflation, we investigated if 5-HT receptor agonism can cause swimbladder inflation. Practical issues with drug efficacy and selectivity motivated us to verify the involvement of serotonin indirectly by disrupting its metabolism. For this experiment, we treated larvae with selegiline, a monoamine oxidase inhibitor (MAOI). Unlike humans, which have two versions of this protein (MAO-A and MAO-B) and use them to break down several monoamine neurotransmitters, zebrafish possesses only a single MAO enzyme and it appears to degrade 5-HT primarily [27,28]. We observed that selegiline treatment caused a buoyant phenotype in zebrafish, evident by an increase in mean radius inside the well (**Figure 1.3h**). Given the frequency of the 5-HT_{1A} receptor as a target for ligands promoting swimbladder inflation, we investigated if the 5-HT agonism component of the inflation phenotype might be due to 5-HT_{1A} agonism. We tested the post-synaptic 5-HT_{1A} agonist, 8-OH-DPAT, and the potent azapirone 5-HT_{1A} full agonist, eptapirone. Both compounds phenocopied the floating behavior caused by increased 5-HT levels *in vivo* (**Figure 1.3i, 1.3j**). These findings suggest that an increased serotonergic tone, possibly via 5-HT_{1A} agonism, can contribute to swimbladder inflation in larval zebrafish.

Though compounds with dopaminergic target annotations formed the largest single group of active reference compounds, most of these molecules are known for their

extensive polypharmacology, including both adrenergic and serotonergic actions. This includes, for example, antipsychotics such as ziprasidone and clozapine, and ergoline derivatives such as lisuride. To selectively probe the effect of dopaminergic neurotransmission on zebrafish depth phenotypes, we used the dopamine transporter (DAT) inhibitor, 3-CPMT, to increase dopamine levels *in vivo*. 3-CPMT treatment caused a dose-dependent decrease in average radial position of larvae in the well, consistent with a shift towards the bottom of the well (**Figure 1.3k**). To visualize this behavior more clearly, we captured lateral-view videos of treated larvae in a large (53×44×59 cm) tank. These experiments captured a clear "bottom-dwelling" phenotype not displayed by control larvae (**Figure 1.3l**). This result suggests that increased dopamine signaling causes zebrafish larvae to prefer to remain deeper in the water column.

1.4.3 Screen of 9,600 uncharacterized compounds identifies small molecules that promote swimbladder inflation.

Video-based phenotypic screens are a powerful application of zebrafish larvae in early drug discovery efforts. Using both custom and commercially available recording chambers, researchers are capable of efficiently screening large chemical libraries in a standard 96-well format. The high-content videos resulting from such screens can be readily repurposed to test new hypotheses. The ease of detecting buoyant larvae based on their position in the well makes this a valuable phenotypic endpoint for finding compounds that promote swimbladder inflation. To demonstrate the value of this approach, we analyzed video data from a behavioral screen of 9,600 unique compounds

from the ChemBridge DIVERSet library, a collection of structurally diverse, drug-like molecules with unknown pharmacological activity.

To identify compounds that likely cause swimbladder inflation, we considered both the locomotor activity of treated larvae and their mean radial position from the center of the well. This dataset included 2,032 DMSO-treated control wells, which were used to set the criteria for defining hit compounds. Potentially toxic compounds were removed from consideration by excluding wells where very little locomotor activity was observed (less than 20% of the average locomotion of the control wells). A strict threshold of 5 standard deviations above the control mean radius was used to isolate compounds presumed to promote swimbladder inflation. In the end, 84 unique molecules met the above criteria (**Figure 1.4a**). Hierarchical clustering by structural similarity (represented as a dendrogram in **Figure 1.4b**) showed that these compounds could be broadly grouped into 6 clusters. For validation experiments, we re-ordered 24 compounds sampled from the largest branches of the dendrogram to fairly represent the various chemotypes. We then tested the ability of these compounds to inflate the larval swimbladder at a range of concentrations.

Toxicity was assessed by evaluating the vitality of the larvae after prolonged exposure. Larvae survival was assessed after 24 hours of incubation with these compounds. If applicable, we recorded the test concentration where 50% of larvae displayed signs of toxicity when inspected under a microscope. This value represents the 24-hour LC_{50} of the test compound and was used as an indicator of potential toxicity or off-target effects (**Supplemental Table 1.2**).

Video analysis showed most retested compounds (18 of 24) successfully increased the radial position of larvae in the well with at least one tested concentration (**Figure 1.4c**). Most retested compounds were effective around the concentration of 12.5 μM, close to the concentration in the original screen (10 μM). A subset of compounds performed exceptionally well, producing the floating phenotype at a wide range of concentrations.

For example, **compound W** appeared to be the top performing hit. It caused swimbladder inflation at concentrations as low as 1.56 μM, without visible toxic effects after 24 hours of exposure, even at concentrations of 100 μM (see also, **Figure 1.5b**). The structurally related compounds, **Q** and **I**, also potently modified larval buoyancy. However, we noticed suboptimal phenotypic strength for **compound Q** at the 24-hour timepoint; the reduced efficacy of this compound after extended incubation might reflect off-target toxicity. **Compound U** also showed high potency and a wide effective range but produced toxicity at concentrations >25 μM. Our findings demonstrate that zebrafish buoyancy is a scalable endpoint for phenotypic drug screening and have provided at least 18 molecules that cause swimbladder hyperinflation for future studies of this phenomenon.

1.4.4 *In vitro* receptor binding assays suggest human translatability of the discovered compounds.

To investigate their receptor targets, the 18 validated hit compounds were screened for binding against a panel of 45 human and rodent receptors by the NIMH Psychoactive Drug Screening Program (**Figure 1.5a**). Primary binding assays were carried out with the

objective to identify, for each compound, receptors which it might interact with. This was done by performing radioligand displacement experiments using a single, saturating concentration (10 μM) of the test compound. The percentage of radioactive probe that remained bound to the receptor was measured to quantify the extent of the test compound's affinity for the receptor. Compounds that managed to displace at least 50% of the radioligand were continued to secondary binding experiments. Secondary binding consisted of further radioligand displacement studies against a range of test compound concentrations, yielding a complete dose-response curve for precise calculation of the compound's affinity for the receptor.

In total, 13 of the 18 compounds displayed affinity for at least one target with a K_i of at least 10,000 nM, with 9 of these compounds demonstrating an affinity less than 1,000 nM. These high-affinity targets were mostly restricted to adrenergic and serotonergic receptors. **Compound O** was found to be a ligand of the serotonin transporter (490 nM), suggesting an indirect serotonergic mechanism in which the compounds prevent the clearance of this neurotransmitter from the extracellular space. Other targets included histamine receptors (H_1, H_2, and H_3) and σ receptors. The σ_2 receptor had (mostly low affinity) interactions with 8 ligands, but σ receptors are known for indiscriminate binding with many types of drug-like molecules [29], and low-affinity σ receptor binding has been a common observation in previous studies characterizing hit molecules from zebrafish screens [9,30].

A small group of four compounds stood out from the rest as having multiple high-affinity binding partners (purple box in **Figure 1.5b**). We noticed that these molecules were substantially more potent than most others in our *in vivo* assay, which might be

explained by a synergistic combination of targets. The binding profile of these compounds shared many similarities, including a strong preference for the α_{1B} and 5-HT_{1D} receptors over the other members of their subfamilies. In primary binding experiments, these compounds readily competed against the radioligand for the binding site of their preferred subtype, yet typically very weak interactions with others (**Figure 1.5c**). We noted a sharp decrease in potency for the **compound G**, which has good affinity for serotonergic receptors but lacks the α-adrenergic activity of the other compounds (**Figure 1.5d**). This observation supports the hypothesis that extensive polypharmacology at both adrenergic and serotonergic targets (especially α_{1B} and 5-HT_{1D}) contribute to the strong phenotypic effects of certain hit compounds.

To further investigate how interactions between these molecules and receptors may lead to changes in zebrafish buoyancy, we selected **compound U** to carry forward for functional assays. This compound is special because it has considerable muscarinic receptor affinity as well as α_{1B} and 5-HT_{1D} selectivity. *In vitro* Tango assays, which measures β-arrestin translocation as a proxy for receptor activation [31], were performed to determine if this ligand had agonist activity at the 5-HT_{1D} or muscarinic (M_{1-4}) receptors. We found **compound U** to be a partial agonist of 5-HT_{1D}, activating the receptor with ~40% the efficacy of serotonin itself (**Figure 1.5e**). At the muscarinic receptors, however, we observed no receptor activation at any of the concentrations tested (data not shown). Surprisingly, we found that **compound U** was able to inhibit the activation of receptors that were pre-treated with the muscarinic agonist, carbachol, indicating that it is an antagonist in this system (**Figure 1.5f**). M_2 and M_4 receptors were especially sensitive to this antagonist behavior, while the M_1 and M_3 receptors were less so.

In summary, these findings showed that molecules discovered in our zebrafish screen can retain their activity against human receptors. Furthermore, these results demonstrate the tendency of phenotypic screens to yield compounds sharing a similar profile of biological activities rather than a singular molecular target. The rich polypharmacology of such compounds may be a desirable property of future CNS drugs, where a “magic shotgun” approach may be superior to a “magic bullet” [32].

1.4.5 Chemoinformatic analysis suggests lipid signaling and kinases as potential targets of other hit compounds.

Though we were able to identify targets for many of the validated hits from our screen, some compounds were more elusive. These included compounds **W**, **I**, **M**, and **Q**, which were of interest to us due to their high potency and low toxicity relative to other hits (grey box in **Figure 1.5b**), and because they have a common molecular scaffold. In fact, more than a quarter of the hit compounds (23 of 84) were members of this chemical class (**Figure 1.6a**), bearing only minor structural modifications (**Figure 1.6b**). This large cluster of hit compounds may provide a lead compound with many possibilities for optimization by medicinal chemists. However, in *in vitro* binding experiments that tested this group of 4 compounds against 45 targets, only a single binding interaction with K_i below 10,000 nM was observed: **compound W** bound to the 18 kDa translocator protein (TSPO) with a binding affinity of 871 nM. The relevance of this interaction to the studied phenotype is unknown, though we did not observe a buoyant phenotype caused by any TSPO ligands in our screen of 647 reference compounds (such as PK-11195, FGIN-1-27, and FGIN-1-

43). Therefore, we hypothesize that TSPO is not the primary target of **compound W** responsible for making it the most potent compound identified in this work.

Bioactive molecules with no known mechanism of action despite testing against many possible targets, like the 4 compounds in this group, have been referred to as "dark chemical matter" [33]. Compounds like this have the potential to be developed into new drugs with unique activity or fewer side effects. To identify possible targets of our own "dark matter" molecules, we turned to the Similarity Ensemble Approach (SEA), a chemoinformatic method for predicting the protein targets of a molecule by comparing its structure against a database of molecules with known interactions [34]. We populated our database with compound-target binding data from ChEMBL, a massive repository of drug activity data for >2 million compounds [35].

To verify the accuracy of these predictions, we first compared SEA predictions for the hit compounds on the targets evaluated in the *in vitro* binding assays. We noted a generally good overlap between the SEA results (**Supplemental Figure 1.3**) and the empirically determined receptor affinity data (**Figure 1.5**). The consistency between the *in silico* predictions and *in vitro* binding profiles increased our confidence in this method to identify prospective molecular targets of the hit compounds recovered from our zebrafish screen. SEA predictions for compounds **W**, **I**, and **M** suggested targets that included mostly a variety of kinases, along with a few GPCR targets (**Figure 1.6c**); there were no statistically significant predictions for **compound Q**, likely explained by its unique sulfonyl group in place of the more common amide moiety. Brief descriptions of the biological activities for the top predicted targets shared by these compounds are provided in **Figure 1.6d**.

1.5 Discussion

We report the development and validation of a high throughput assay that identifies floating larval zebrafish in 96-well plates as a sensitive phenotypic endpoint for discovering new neuroactive compounds. Fish depth has been used a readout for behavioral states of interest to psychiatric drug discovery, such as anxiety and circadian locomotor rhythms [14,15,16]. Although many labs include a depth-measurement assay in their behavioral characterization of genetic mutants or pharmacological treatments, existing assays have a low throughput. Our method estimates larval zebrafish depth from overhead videos of 96-well plates, allowing us to observe a similar behavioral endpoint with much greater efficiency. Using this approach, we were able to observe changes in depth following treatment with thousands of diverse bioactive compounds.

We found that drugs can modify zebrafish buoyancy, most frequently by disrupting swimbladder homeostasis. The swimbladder is the main organ that fish use to regulate their buoyancy and is thought to be regulated by signals from the autonomic nervous system conveyed by the sympathetic and parasympathetic branches [17]. The parasympathetic ("rest and digest") branch regulates smooth muscle contraction and glandular activity by activating muscarinic acetylcholine receptors on visceral organs. We found that bath application of muscarinic agonists can induce a robust swimbladder inflation phenotype in larval zebrafish, in agreement with a report that the muscarinic agonist, pilocarpine, promotes inflation of the swimbladder in pike [36]. Studies performed on isolated swimbladder tissue have found that muscarinic agonism (using carbachol) may promote inflation by stimulating metabolic activity in specialized “gas gland” cells, which facilitates the diffusion of oxygen into the swimbladder from the blood [37]. The

sympathetic ("fight or flight") branch is generally thought to cause deflation of the swimbladder, consistent with our finding that blockade of α_1 receptors results in inflation. This may be explained by adrenergic receptor-mediated vasoconstriction restricting the oxygen supply to the swimbladder in fish that rely on the bloodstream to supply oxygen to inflate the swimbladder [38,39]. Alternately, in salmon, an adrenergic antagonist was able to suppress the reflexive ejection of air bubbles from the mouth as fish dive deep in the water when startled [40]. Further experiments will be necessary to verify if autonomic regulation of the zebrafish swimbladder proceeds through mechanisms similar to those previously observed in other fish.

Additionally, we observed that serotonergic and dopaminergic ligands appeared to consistently modify zebrafish depth, albeit in opposing ways. Others have previously demonstrated that 5-HT causes larval zebrafish to display an attraction to the surface [28,41], but it has been generally assumed that this behavior is indicative of an anxiolytic effect. In different fish species (eel, carp, and goldfish), others have made the serendipitous (but unexplained) discovery that 5-HTP treatment causes swimbladder inflation and buoyancy [42,43]. This response to 5-HT may be due to direct action on the swimbladder, as 5-HT-positive innervation has been shown in the swimbladder of zebrafish [17] and other fish species [44]. Alternatively, the surfacing response to 5-HT could originate elsewhere in the nervous system. For example, serotonin signaling is important in the detection of hypoxic conditions in zebrafish [45,46], and hypoxia results in increased respiration behaviors at the surface, which is augmented by 5-HT exposure [47].

Studies of zebrafish mutants lacking a dopamine transporter (DAT KO) have noted a persistent “bottom-dwelling” phenotype [48], similar to our observation of wild-type larvae

treated with a DAT-inhibitor. Bottom-dwelling can be attenuated by treating DAT KO fish with a D_1-like antagonist (SCH23390) or D_2-like antagonist (sulpiride) [48]. Likewise, we found that SCH23390 and other dopamine antagonists could cause floating phenotypes in our assay. Our results indicate that dopamine signaling might influence zebrafish depth by modulating buoyancy.

By enabling depth approximation in a 96-well format, we were able to identify floating larvae and use this endpoint for a high-throughput behavioral screen of 9,600 uncharacterized molecules. To discover molecules with interesting effects on the nervous system, we selected a subset of compounds from this screen that appeared to cause a buoyant phenotype. We found we could successfully identify compounds that caused swimbladder inflation from the screening data. *In vitro* experiments showed that some of these compounds bound to human receptors, like 5-HT_{1D}, demonstrating the value of this behavioral endpoint for identifying neuroactive molecules with potential for human translatability. Many of the identified compounds didn't bind to any of the 45-target panel; these compounds represent chemical "dark matter" that may serve as useful probe compounds in future research exploring depth-related phenotypes in zebrafish.

Because depth is often measured in (adult) zebrafish behavioral assays and widely assumed to be an indication of mood, our findings have important implications for the interpretation of such depth-related phenotypes. Specifically, it may be especially critical to consider fish buoyancy as a confounding variable when interpreting “anxiety” behaviors in the novel tank test [16].

1.6 Acknowledgements

K_i determinations, receptor binding profiles, and agonist/antagonist functional data were generously provided by the National Institute of Mental Health's Psychoactive Drug Screening Program, Contract # HHSN-271-2018-00023-C (NIMH PDSP). The NIMH PDSP is Directed by Bryan L. Roth MD, PhD at the University of North Carolina at Chapel Hill and Project Officer Jamie Driscoll at NIMH, Bethesda MD, USA.

1.7 Figures

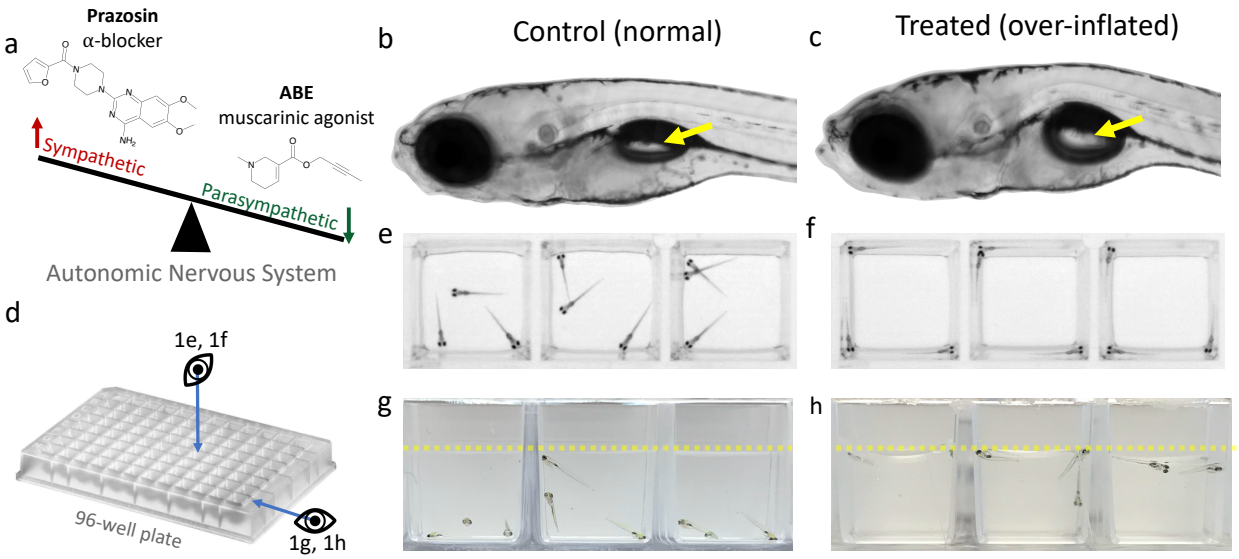

Figure 1.1. Autonomic control of zebrafish swimbladder inflation.
a, Diagram depicting the pharmacological interventions that cause swimbladder inflation by targeting the autonomic nervous system to disrupt sympathovagal balance. **b**, an image of a 96-well plate. The points-of-view for e-h are represented by eyes either looking down into the wells or looking though the side of the wells. **c** and **d**, Lateral images of larvae with normal morphology (**c**) and the drug-induced, over-inflated swimbladder phenotype (**d**), respectively. Yellow arrows indicate the swimbladder. **e** and **f**, side-view displaying the vertical distribution of larvae inside a well with normal (untreated) and buoyant (over-inflated) phenotypes, respectively. Untreated fish rarely occupy the top portion of the water column (surface indicated by the dotted line), while floating larvae are restricted to the surface. **g** and **h**, Top-down view of normally behaving larvae (**g**), which spend most of their time in close proximity to the bottom of the well, and floating larvae with over-inflated swimbladders (**h**), which become trapped in the corners of the well due to insurmountable surface tension and buoyant forces.

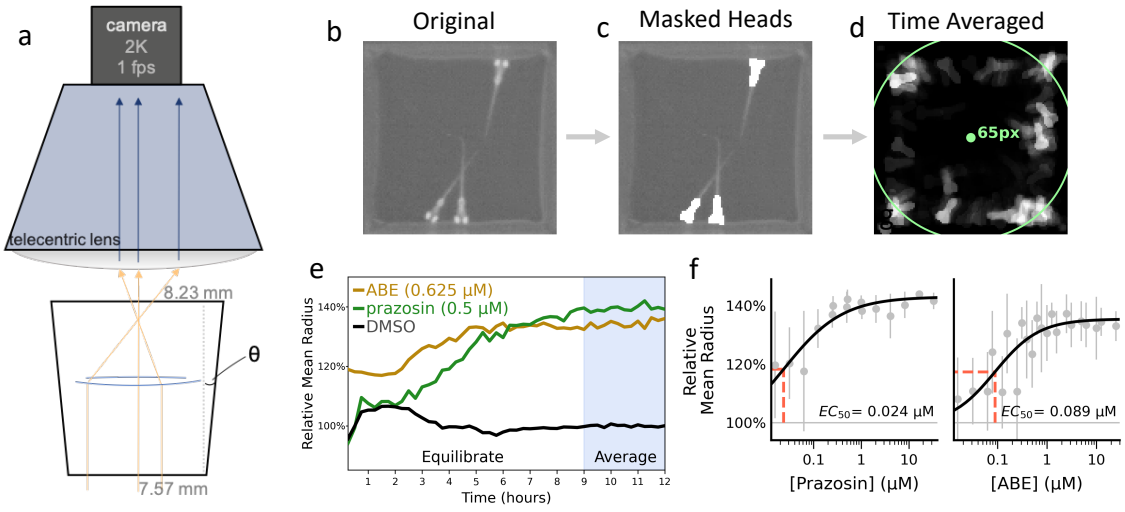

Figure 1.2. A scalable assay to approximate larval zebrafish depth.
a, Schematic showing the dimensions inside a single well and the overhead recording hardware. The well's cross-sectional width is larger at the top than the bottom, so objects at the surface may access locations with a greater distance from the well's vertical axis. Rays of IR light (yellow/blue arrows) from LED backlights refract through the meniscus (blue lines) at the surface of the water, exaggerating the relationship between depth and position. A telecentric lens provides an orthographic perspective without parallax. **b-d**, Procedure to calculate the average radial position of larvae over the course of a video (12 hours of video at 1 frame per second during this assay), which is directly influenced by depth in the well. **b**, The original intensity image (inverted) of a single well containing 3 larvae. **c**, Automatic masking of the pixels where zebrafish heads are in the original image. Masked pixels are white. **d**, Mask (head) pixels are accumulated across all the frames in the video clip, which is represented as a heatmap. All the observed pixel locations are included to calculate of a "time-averaged" radial position (green circle) from the center of the well. **e**, Timeseries of the radial position over a 12-hour continuous recording, showing the onset of floating phenotypes from prazosin or ABE treatment. Values indicate the mean radial position calculated independently on each 15-minute video segment. DMSO-treated control larvae (n = 872 replicates) typically have a peak in radial position during the first 3 hours of the assay, likely due to an initial exploratory period or increased locomotion following the sudden transition to complete darkness. The muscarinic agonist, ABE (n = 12), produces a faster increase in mean radial position (less than 1 hour), while the α-blocker, prazosin (n = 12), has a more gradual onset over several hours but causes a slightly greater maximum response. To produce comparable dose-response curves expressing the potency of buoyancy-promoting drugs (for example, **f** and **g**), differing rates of onset are compensated for by considering only the final 3 hours of the video (from 9–12 hours incubation time, indicated by a blue background in **e**). **f–g**, Dose-response curves fit using this approach for prazosin (**f**) and ABE (**g**) indicate the extreme potency of these compounds *in vivo*, with approximate EC_{50} values of 24 and 89 nM, respectively.

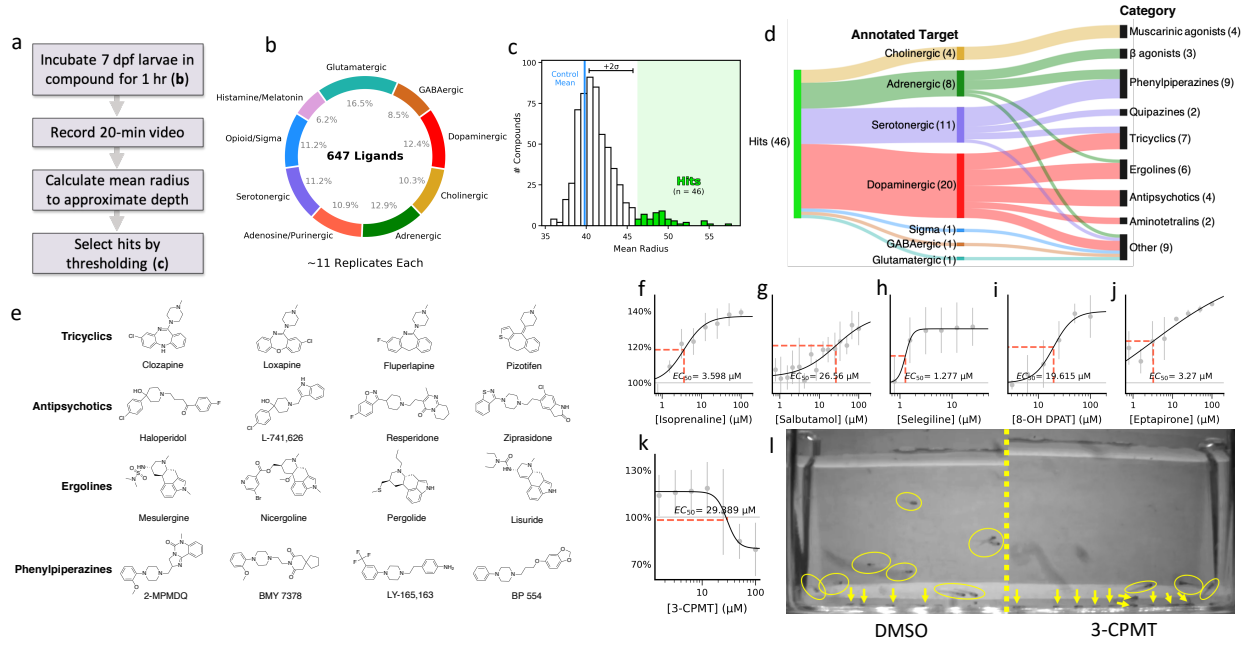

Figure 1.3. Reference compound screen identifies chemical classes and receptor targets controlling zebrafish buoyancy.

a, Flowchart summarizing the process of performing the phenotypic screen and determining which ligands might cause changes in zebrafish buoyancy. **b**, Pie chart detailing the composition of the "Biomol" library used in this screen. Each included ligand is known to target one (or more) of the 13 neurotransmitter systems from the chart. **c**, Histogram of average radial position values (median of all replicates) for all 647 reference compounds in this library. A threshold of 2 standard deviations above the average from simultaneously screened DMSO-treated wells (blue vertical line, n = 1,012) is used as the cutoff for the selection of 46 hit compounds (green background color and histogram bins). **d**, Sankey diagram decomposing the 46 hits according to their manufacturer-provided target annotations and manually assigned chemical structure cluster. Most hits originated from the dopaminergic, serotonergic, and adrenergic portions of the library, strongly suggesting these pathways contribute to buoyancy regulation *in vivo*. **e**, Examples of hit compound structures sharing a similar chemical structure. **f–j**, Dose-response curves for drugs that inflate zebrafish swimbladders by acting as β adrenergic agonists (**f –g**), a MAOI-inhibitor (**h**), and agonists of the 5-HT_{1A} receptor (**i –j**). **k**, Dose-response curves for the DAT-inhibitor, 3-CPMT, which increases zebrafish larvae depth in the well. **l**, Side-by-side comparison of still frames from lateral-view videos, showing the vertical distribution of larvae within a large tank after incubation with either DMSO or the DAT inhibitor, 3-CPMT (50 μM). These videos were recorded through the side of the tank to allow direct observation of depth. Yellow arrows indicate larvae resting on the bottom surface, while other visible larvae are circled. DMSO-treated fish (left) can be seen throughout the water column, while larvae treated with 3-CPMT (right) remain in contact with the tank bottom for almost the entire duration, with the occasional upward swim bout followed by rapid sinking.

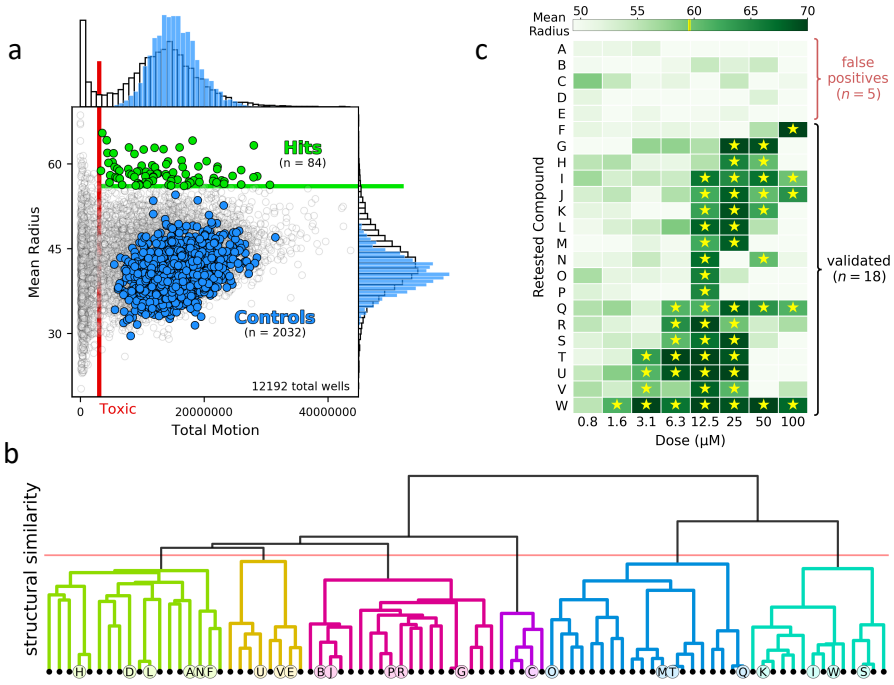

Figure 1.4. High-throughput screen identifies uncharacterized compounds that regulates swimming depth.
a, Scatterplot of average radial position vs locomotion for each well in the novel compound screen dataset. Hit compounds were selected by thresholding 5 standard deviations (green horizontal line) above the control average (*n* = 2,032 DMSO wells, blue markers) and rejecting "toxic" compounds with a total motion less than minimum threshold (red vertical line). Only 84 wells from the entire dataset met these criteria (green markers). **b,** Dendrogram representing the structural diversity of the 84 selected hit compounds. The 24 compounds labeled with a bold font were chosen to re-order for validation experiments. **c**, Heatmap of results from 12-hour validation assays with the re-ordered hit compounds. Heatmap intensity reflects the average score from 4 replicates per concentration. Most of the retested compounds were validated as having at least 1 active dose.

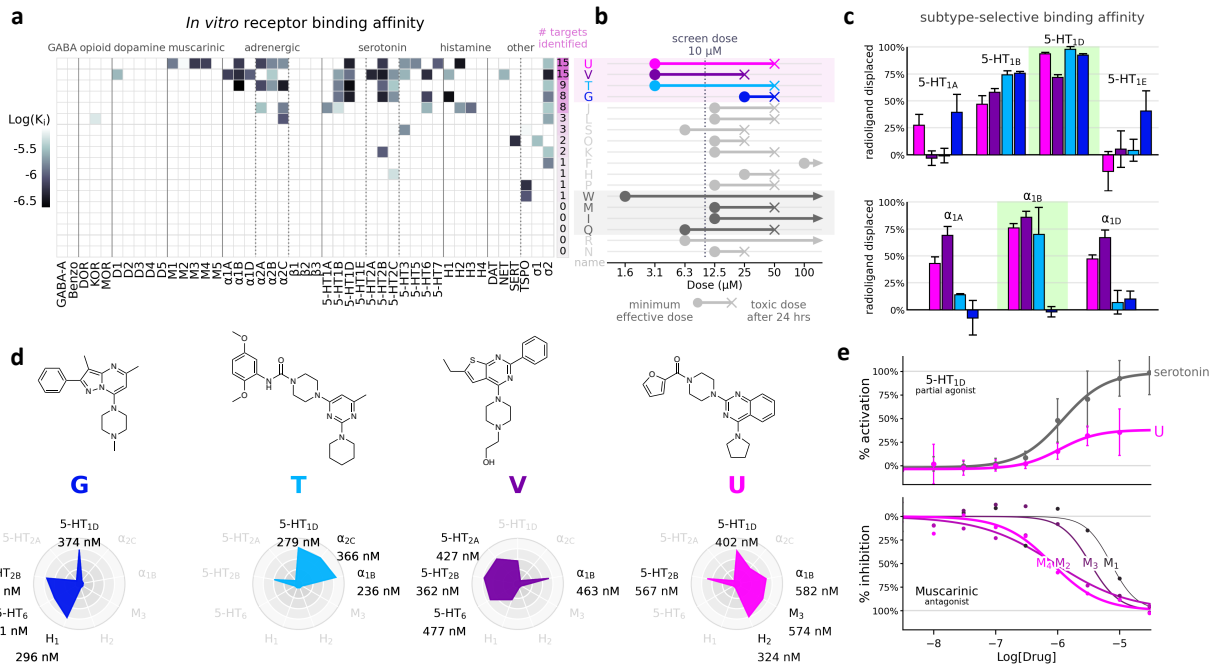

Figure 1.5. *In vitro* receptor binding assays identify compounds that target α_{1B}, 5-HT_{1D}, 5-HT_{2B}, and muscarinic receptors.

a, Heatmap representing the binding affinity (K_i) of 18 validated hit compounds against 45 major CNS drug targets, determined by *in vitro* radioligand competition assays. Several compounds bind to multiple targets with nanomolar affinity, while others have few or no binding partners. **b**, Effective range ("therapeutic window") of 18 active hits. A group of potent compounds with similar polypharmacology is highlighted in purple, and a cluster of structurally related compounds is highlighted in grey. **c**, Compounds with multiple targets appear to share selectivity for 5-HT_{1D} (top) and α_{1B} (bottom) receptor subtypes. Bar plots indicate the relative affinity for each subtype, measured as the fraction of a bound radioligand displaced by 10 μM of the test compound. **d**, Molecular structures and radar plots representing the polypharmacology of 4 compounds highlighted in B. Despite the diverse structures, these molecules share several high-affinity targets, such as α_{1B}, 5-HT_{1D}, and 5-HT_{2B} receptors. **e**, Functional activity of **compound U** at 5-HT_{1D} (top) and muscarinic M_1–M_4 receptors (bottom). Top: Partial agonism at 5-HT_{1D} (E_{max} ~40% of serotonin). Bottom: Antagonist activity at muscarinic receptors, pre-treated with an agonist (carbachol) to achieve ~50% maximum activation of the receptor. **Compound U** has functional selectivity for M_4 and M_2 subtypes over M_1 and M_3.

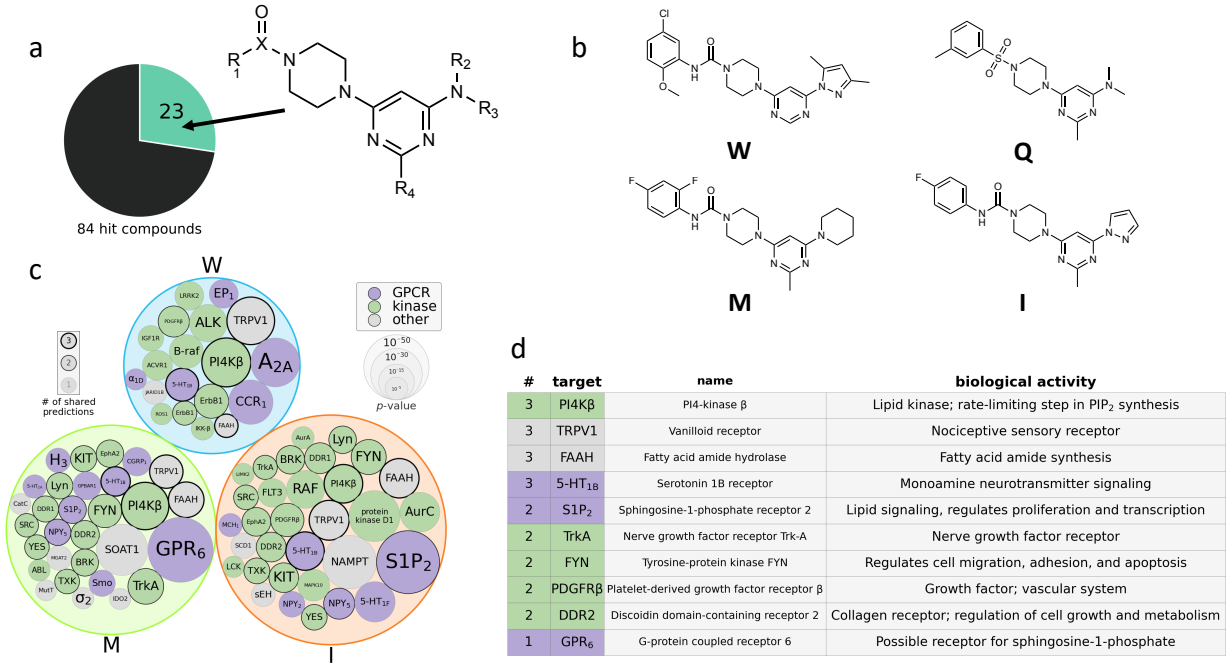

#	target	name	biological activity
3	PI4Kβ	PI4-kinase β	Lipid kinase; rate-limiting step in PIP_2 synthesis
3	TRPV1	Vanilloid receptor	Nociceptive sensory receptor
3	FAAH	Fatty acid amide hydrolase	Fatty acid amide synthesis
3	$5\text{-}HT_{1B}$	Serotonin 1B receptor	Monoamine neurotransmitter signaling
2	$S1P_2$	Sphingosine-1-phosphate receptor 2	Lipid signaling, regulates proliferation and transcription
2	TrkA	Nerve growth factor receptor Trk-A	Nerve growth factor receptor
2	FYN	Tyrosine-protein kinase FYN	Regulates cell migration, adhesion, and apoptosis
2	PDGFRβ	Platelet-derived growth factor receptor β	Growth factor; vascular system
2	DDR2	Discoidin domain-containing receptor 2	Collagen receptor; regulation of cell growth and metabolism
1	GPR_6	G-protein coupled receptor 6	Possible receptor for sphingosine-1-phosphate

Figure 1.6. SEA algorithm predictions of possible targets for a group of structurally related hit molecules.
a, A large fraction of the identified hit molecules can be described by a single Markush structure. **b**, Chemical structures of the 4 validated hit compounds sharing this scaffold. **c**, Circle packing representation of the set of targets predicted by the SEA algorithm for each of the specified compounds. The size of the inner circles is proportional to the p-value of the prediction. GPCRs and kinases make up the majority of the predicted targets. Compound Q had no predicted interactions and therefore is not depicted. **d**, Table describing the biological functions of the top predicted targets. Many of these proteins are involved in lipid homeostasis/signal transduction.

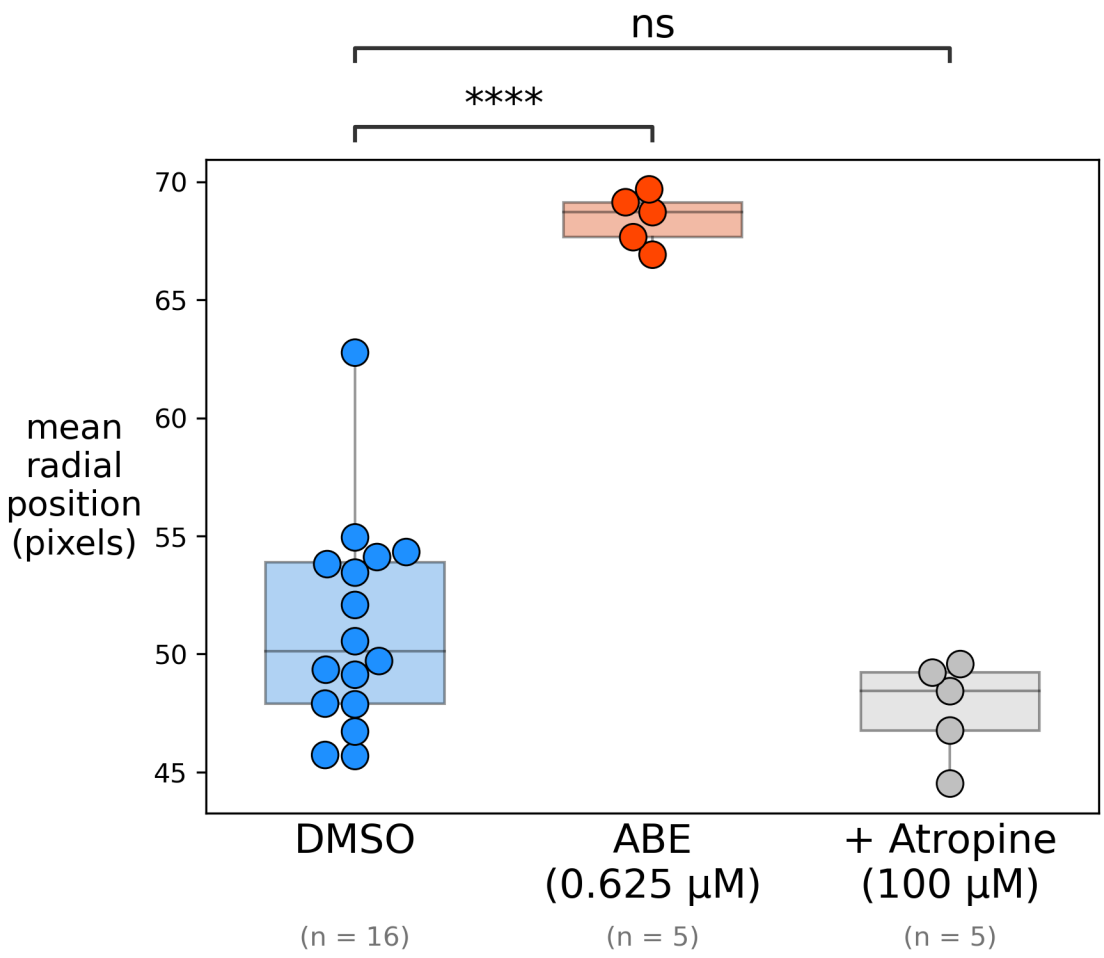

Figure 1.S1. Atropine pre-treatment blocks ABE-induced swimbladder inflation. The floating phenotype caused by ABE (a muscarinic agonist) can be attenuated by a 2-hour pre-incubation with the muscarinic antagonist, atropine. This observation provides strong evidence of a buoyancy-regulating mechanism that is controlled by muscarinic receptor signaling.

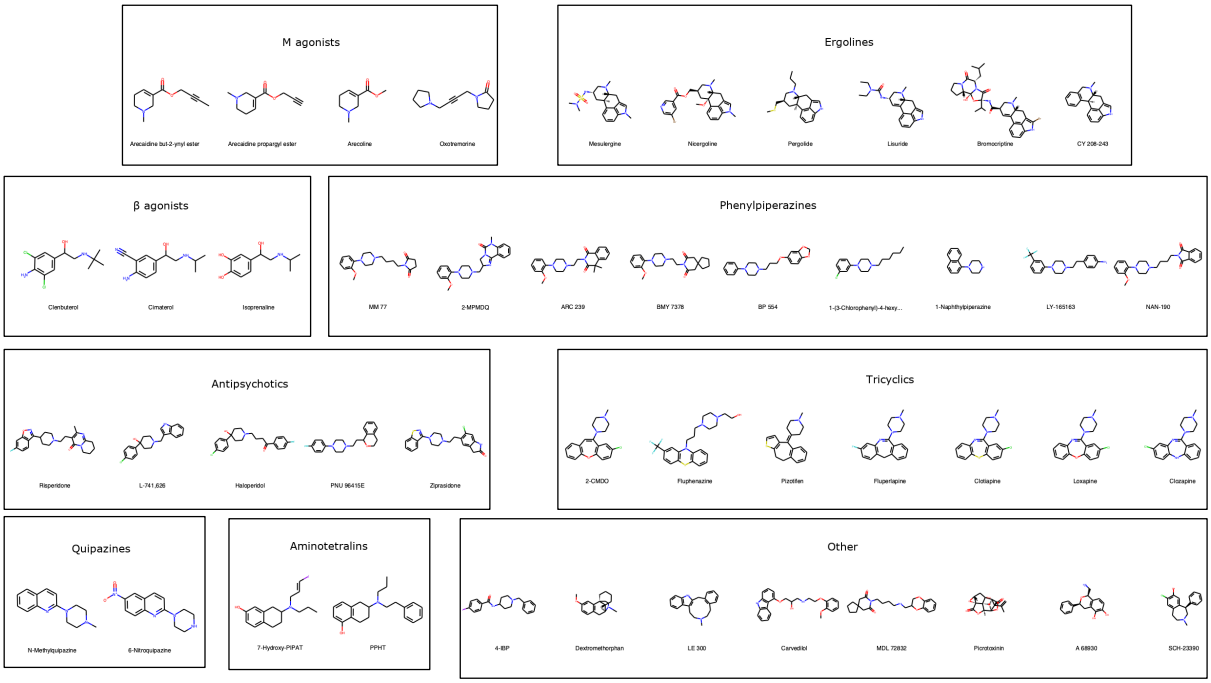

Figure 1.S2. Chemical structures of the 46 reference ligands which putatively inflate the zebrafish swimbladder.
These compounds from the Biomol library are grouped based on their pharmacological profiles and structural characteristics.

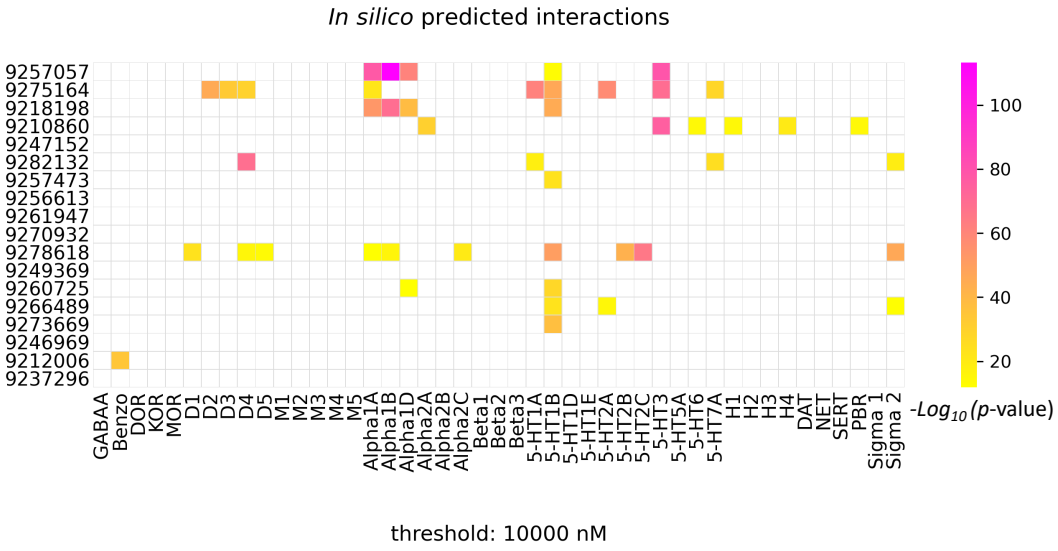

Figure 1.S3. Heatmap of SEA target predictions.
Heatmap of predicted activity at select receptors (p-values) for 18 validated hit compounds discovered in our phenotypic screen. The 5-HT_{1B} receptor (which shares significant pharmacology with the 5-HT_{1D} receptor) is the most frequently predicted target.

1.8 Tables

Supplemental Table 1.1. Reference compounds which putatively increase zebrafish buoyancy.
These 46 compounds from the Biomol library reliably increased the mean radial position of larvae across multiple replicates in the screening dataset.

Compound	Target	Category	Annotation
Clenbuterol	Adrenergic	β agonists	β2 adrenergic agonist
Cimaterol	Adrenergic	β agonists	β adrenergic agonist
Isoprenaline	Adrenergic	β agonists	β adrenergic agonist
Clozapine	Dopaminergic	Tricyclics	D4 and D2 antagonist
Clotiapine	Dopaminergic	Tricyclics	D4 and D2 antagonist
Fluperlapine	Serotonergic	Tricyclics	5-HT6 / 5-HT7 ligand
Pizotifen	Serotonergic	Tricyclics	Serotonin antagonist
Fluphenazine	Dopaminergic	Tricyclics	Dopamine antagonist
2-CMDO	Dopaminergic	Tricyclics	D4 receptor ligand
Loxapine	Dopaminergic	Tricyclics	D4 and D2 antagonist
6-Nitroquipazine	Serotonergic	Quipazines	SERT inhibitor
N-Methylquipazine	Serotonergic	Quipazines	5-HT3 agonist
1-(3-Chlorophenyl)-4-hexylpiperazine	Serotonergic	Phenylpiperazines	5-HT1 ligand
MM 77	Serotonergic	Phenylpiperazines	5-HT1A ligand
1-Naphthylpiperazine	Serotonergic	Phenylpiperazines	5-HT1 agonist; 5-HT2 antagonist
BP 554	Serotonergic	Phenylpiperazines	5-HT1A agonist
LY-165163	Serotonergic	Phenylpiperazines	5-HT1A agonist
BMY 7378	Adrenergic	Phenylpiperazines	5-HT1A partial agonist
NAN-190	Serotonergic	Phenylpiperazines	5-HT1A antagonist
ARC 239	Adrenergic	Phenylpiperazines	Alpha2B antagonist
2-MPMDQ	Adrenergic	Phenylpiperazines	Alpha1 antagonist
4-IBP	Opioid	Other	Sigma1/sigma2 ligand
SCH-23390	Dopaminergic	Other	Potent D1 antagonist
A 68930	Dopaminergic	Other	Selective D1 agonist
Picrotoxinin	GABAergic	Other	GABA(A) antagonist
Dextromethorphan	Gllutamatergic	Other	NMDA antagonist
LE 300	Dopaminergic	Other	Potent D1 antagonist
MDL 72832	Serotonergic	Other	5-HT1A ligand
Carvedilol	Adrenergic	Other	β antagonist
Arecaidine propargyl ester	Cholinergic	M agonists	Muscarinic agonist
Arecaidine but-2-ynyl ester	Cholinergic	M agonists	Muscarinic agonist

Compound	Target	Category	Annotation
Oxotremorine	Cholinergic	M agonists	Muscarinic agonist
Arecoline	Cholinergic	M agonists	Muscarinic agonist
CY 208-243	Dopaminergic	Ergolines	Selective D1 agonist
Lisuride	Dopaminergic	Ergolines	D2 agonist / D1 antagonist
Mesulergine	Dopaminergic	Ergolines	Dopaminergic agonist
Nicergoline	Adrenergic	Ergolines	Alpha antagonist
Pergolide	Dopaminergic	Ergolines	Dopamine agonist
Bromocriptine	Dopaminergic	Ergolines	Dopamine agonist
L-741,626	Dopaminergic	Antipsychotics	D2 antagonist
Risperidone	Dopaminergic	Antipsychotics	D2 antagonist
Haloperidol	Dopaminergic	Antipsychotics	Dopamine antagonist
PNU 96415E	Dopaminergic	Antipsychotics	D4 receptor ligand
Ziprasidone	Dopaminergic	Antipsychotics	D2 antagonist
PPHT	Dopaminergic	Aminotetralins	D2 agonist
7-Hydroxy-PIPAT	Dopaminergic	Aminotetralins	D3 dopamine ligand

Supplemental Table 1.2. Retested hit compounds from the ChemBridge library. Identifiers for the ChemBridge hit compounds that were reordered for validation experiments, including the manufacturer's catalogue ID and SMILES string encoding the chemical structure. These compounds were tested at 8 concentrations for activity in the zebrafish buoyancy assay; compounds that caused hyperinflation of the swimbladder are flagged as "validated" compounds. The concentration causing toxic effects in most larvae after 24 hours of incubation is also provided.

Symbol	Hit2Lead ID	SMILES	Validated	24-hour LC_{50}
A	9205822	Cc1nc(C(=O)Nc2cccc(Cl)c2Cl)co1	No	N/A
B	9257526	Cc1ccc(-c2nc3c4c(C)c(C)n(CCCN5CCOCC5)c4ncn3n2)cc1	No	12.5 μM
C	9223376	CSc1nc2nccc(-c3ccsc3)n2n1	No	25 μM
D	9251190	COc1ccc(-c2nnc(SC3COC(=O)C3)n2C)cc1	No	N/A
E	9221443	CCc1nc(N2CCCC(C(=O)O)C2)c2cc(CC)sc2n1	No	100 μM
F	9270932	CC(C)CCn1ccc2nc3ccn(-c4ccccn4)c(=O)c3cc2c1=O	Yes	N/A
G	9210860	Cc1cc(N2CCN(C)CC2)n2nc(-c3ccccc3)c(C)c2n1	Yes	50 μM
H	9278618	COC(=O)c1cccc(NC(=O)N2CCc3cc(OC)c(OC)cc3C2)c1	Yes	50 μM
I	9273669	Cc1nc(N2CCN(C(=O)Nc3ccc(F)cc3)CC2)cc(-n2cccn2)n1	Yes	N/A
J	9247152	Cc1c(C)n(CCN(C)C)c2ncn3nc(Cc4ccccc4)nc3c12	Yes	50 μM
K	9261947	O=C(c1ccccc1C(F)(F)F)N1CCN(c2cc(-n3cccn3)ncn2)CC1	Yes	50 μM
L	9282132	Fc1cccc(-c2nn3c(CN4CCN(c5ccccc5)CC4)nnc3s2)c1	Yes	50 μM
M	9266489	Cc1nc(N2CCCCC2)cc(N2CCN(C(=O)Nc3ccc(F)cc3F)CC2)n1	Yes	50 μM
N	9237296	Cc1ccc(-n2ccc3nc(N4CCCCC4)ncc3c2=O)cc1C	Yes	25 μM
O	9256613	Cc1nc(N2CCCC2)cc(N2CCN(C(=O)c3sc(-c4ccccc4)nc3C)CC2)n1	Yes	25 μM
P	9249369	COc1ccccc1-c1cc(C(F)(F)F)n2ncc(C(=O)N3CCCC3c3cc(C)no3)c2n1	Yes	50 μM

Symbol	Hit2Lead ID	SMILES	Validated	24-hour LC_{50}
Q	9246969	Cc1cccc(S(=O)(=O)N2CCN(c3cc(N(C)C)nc(C)n3)CC2)c1	Yes	50 μM
R	9212006	COCc1nn2c(nnc3c(=O)n(CCc4ccccc4)ccc32)c1-c1ccccc1	Yes	N/A
S	9257473	Cc1cc(C)cc(NC(=O)N2CCN(c3ccc(-n4nc(C)cc4C)nn3)CC2)c1	Yes	25 μM
T	9218198	COc1ccc(OC)c(NC(=O)N2CCN(c3cc(C)nc(N4CCCCC4)n3)CC2)c1	Yes	50 μM
U	9257057	O=C(c1ccco1)N1CCN(c2nc(N3CCCC3)c3ccccc3n2)CC1	Yes	50 μM
V	9275164	CCc1cc2c(N3CCN(CCO)CC3)nc(-c3ccccc3)nc2s1	Yes	25 μM
W	9260725	COc1ccc(Cl)cc1NC(=O)N1CCN(c2cc(-n3nc(C)cc3C)ncn2)CC1	Yes	N/A

1.9 References

1. Swinney DC and Anthony J. How were new medicines discovered?. *Nat Rev Drug Discov*. 2011; 10:507-19. doi: 10.1038/nrd3480
2. Wiley DS, *et al*. Chemical screening in zebrafish for novel biological and therapeutic discovery. *Methods Cell Biol*. 2017; 138:651-679. doi: 10.1016/bs.mcb.2016.10.004
3. Howe K, *et al*. The zebrafish reference genome sequence and its relationship to the human genome. *Nature*. 2013; 496:498-503. doi: 10.1038/nature12111
4. Shin JT and Fishman MC. From Zebrafish to human: modular medical models. *Annu Rev Genomics Hum Genet*. 2002; 3:311-40. doi: 10.1146/annurev.genom.3.031402.131506
5. MacRae CA and Peterson RT. Zebrafish as tools for drug discovery. *Nat Rev Drug Discov*. 2015; 14:721-31. doi: 10.1038/nrd4627
6. Guo S. Linking genes to brain, behavior and neurological diseases: what can we learn from zebrafish?. *Genes Brain Behav*. 2004; 3:63-74. doi: 10.1046/j.1601-183x.2003.00053.x
7. Horstick EJ, *et al*. Motivated state control in larval zebrafish: behavioral paradigms and anatomical substrates. *J Neurogenet*. 2016; 30:122-32. doi: 10.1080/01677063.2016.1177048
8. Rihel J, *et al*. Zebrafish behavioral profiling links drugs to biological targets and rest/wake regulation. *Science*. 2010; 327:348-51. doi: 10.1126/science.1183090

9. McCarroll MN, *et al*. Zebrafish behavioural profiling identifies GABA and serotonin receptor ligands related to sedation and paradoxical excitation. *Nat Commun*. 2019; 10:4078. doi: 10.1038/s41467-019-11936-w
10. Jordi J, *et al*. High-throughput screening for selective appetite modulators: A multibehavioral and translational drug discovery strategy. *Sci Adv*. 2018; 4:eaav1966. doi: 10.1126/sciadv.aav1966
11. Peterson RT, *et al*. Small molecule developmental screens reveal the logic and timing of vertebrate development. *Proc Natl Acad Sci U S A*. 2000; 97:12965-9. doi: 10.1073/pnas.97.24.12965
12. Matsuda H, *et al*. Whole-Organism Chemical Screening Identifies Modulators of Pancreatic β-Cell Function. *Diabetes*. 2018; 67:2268-2279. doi: 10.2337/db17-1223
13. Harvey B and White J. Axes of fear for stream fish: water depth and distance to cover. *Environmental Biology of Fishes*. 2017; 100:565-573. doi: 10.1007/s10641-017-0585-2
14. Ben-Moshe Livne Z, *et al*. Genetically Blocking the Zebrafish Pineal Clock Affects Circadian Behavior. *PLoS Genet*. 2016; 12:e1006445. doi: 10.1371/journal.pgen.1006445
15. Lin Q and Jesuthasan S. Masking of a circadian behavior in larval zebrafish involves the thalamo-habenula pathway. *Sci Rep*. 2017; 7:4104. doi: 10.1038/s41598-017-04205-7
16. Cachat J, *et al*. Measuring behavioral and endocrine responses to novelty stress in adult zebrafish. *Nat Protoc*. 2010; 5:1786-99. doi: 10.1038/nprot.2010.140

17. Finney JL, *et al*. Structure and autonomic innervation of the swim bladder in the zebrafish (Danio rerio). *J Comp Neurol*. 2006; 495:587-606. doi: 10.1002/cne.20948
18. Dumbarton TC, *et al*. Adrenergic control of swimbladder deflation in the zebrafish (Danio rerio). *J Exp Biol*. 2010; 213:2536-46. doi: 10.1242/jeb.039792
19. Smith FM and Croll RP. Autonomic control of the swimbladder. *Auton Neurosci*. 2011; 165:140-8. doi: 10.1016/j.autneu.2010.08.002
20. Myers-Turnbull, D., Taylor, J. C., Helsell, C., Tummino, T. A., McCarroll, M. N., Alexander, R., Ki, C. S., Gendelev, L., & Kokel, D. (2020). Simultaneous classification of neuroactive compounds in zebrafish. https://doi.org/10.1101/2020.01.01.891432
21. Tan JL and Zon LI. Chemical screening in zebrafish for novel biological and therapeutic discovery. *Methods Cell Biol*. 2011; 105:493-516. doi: 10.1016/B978-0-12-381320-6.00021-7
22. Milan DJ, *et al*. Drugs that induce repolarization abnormalities cause bradycardia in zebrafish. *Circulation*. 2003; 107:1355-8. doi: 10.1161/01.cir.0000061912.88753.87
23. Nilsson S. Adrenergic innervation and drug responses of the oval sphincter in the swimbladder of the cod (Gadus morhua). *Acta Physiol Scand*. 1971; 83:446-53. doi: 10.1111/j.1748-1716.1971.tb05102.x
24. Nilsson S. Autonomic vasomotor innervation in the gas gland of the swimbladder of a teleost (Gadus morhua). *Comp Gen Pharmacol*. 1972; 3:371-5. doi: 10.1016/0010-4035(72)90050-x

25. Baker JG. The selectivity of beta-adrenoceptor agonists at human beta1-, beta2- and beta3-adrenoceptors. *Br J Pharmacol*. 2010; 160:1048-61. doi: 10.1111/j.1476-5381.2010.00754.x
26. Baker JG. The selectivity of beta-adrenoceptor antagonists at the human beta1, beta2 and beta3 adrenoceptors. *Br J Pharmacol*. 2005; 144:317-22. doi: 10.1038/sj.bjp.0706048
27. Maximino C and Herculano AM. A review of monoaminergic neuropsychopharmacology in zebrafish. *Zebrafish*. 2010; 7:359-78. doi: 10.1089/zeb.2010.0669
28. Sallinen V, *et al*. Hyperserotonergic phenotype after monoamine oxidase inhibition in larval zebrafish. *J Neurochem*. 2009; 109:403-15. doi: 10.1111/j.1471-4159.2009.05986.x
29. Schmidt HR and Kruse AC. The Molecular Function of σ Receptors: Past, Present, and Future. *Trends Pharmacol Sci*. 2019; 40:636-654. doi: 10.1016/j.tips.2019.07.006
30. Bruni G, *et al*. Zebrafish behavioral profiling identifies multitarget antipsychotic-like compounds. *Nat Chem Biol*. 2016; 12:559-66. doi: 10.1038/nchembio.2097
31. Kroeze WK, *et al*. PRESTO-Tango as an open-source resource for interrogation of the druggable human GPCRome. *Nat Struct Mol Biol*. 2015; 22:362-9. doi: 10.1038/nsmb.3014
32. Roth BL, *et al*. Magic shotguns versus magic bullets: selectively non-selective drugs for mood disorders and schizophrenia. *Nat Rev Drug Discov*. 2004; 3:353-9. doi: 10.1038/nrd1346

33. Wassermann AM, *et al*. Dark chemical matter as a promising starting point for drug lead discovery. *Nat Chem Biol*. 2015; 11:958-66. doi: 10.1038/nchembio.1936
34. Keiser MJ, *et al*. Relating protein pharmacology by ligand chemistry. *Nat Biotechnol*. 2007; 25:197-206. doi: 10.1038/nbt1284
35. Mendez D, *et al*. ChEMBL: towards direct deposition of bioassay data. *Nucleic Acids Res*. 2019; 47:D930-D940. doi: 10.1093/nar/gky1075
36. Dreser H. Notiz über eine Wirkung des Pilocarpins. *Archiv für Experimentelle Pathologie und Pharmakologie*. 1892; 30:159-160. doi: 10.1007/bf01960501
37. Pelster B. Lactate Production in Isolated Swim Bladder Tissue of the European Eel Anguilla anguilla. *Physiological Zoology*. 1995; 68:634-646. doi: 10.1086/physzool.68.4.30166349
38. Pelster B. Adrenergic control of swimbladder perfusion in the European eel Anguilla anguilla. *J Exp Biol*. 1994; 189:237-50. doi: 10.1242/jeb.189.1.237
39. Stray-Pedersen S. Vascular responses induced by drugs and by vagal stimulation in the swimbladder of the eel, Anguilla vulgaris. *Comp Gen Pharmacol*. 1970; 1:358-64. doi: 10.1016/0010-4035(70)90030-3
40. Harvey H, et al. Sounding Response of the Kokanee and Sockeye Salmon. *Journal of the Fisheries Research Board of Canada*. 1968; 25:1115-1131. doi: 10.1139/f68-098
41. Stewart AM, *et al*. Perspectives on experimental models of serotonin syndrome in zebrafish. *Neurochem Int*. 2013; 62:893-902. doi: 10.1016/j.neuint.2013.02.018

42. Olivereau M and Olivereau J. Effect of serotonin on prolactin- and MSH-secreting cells in the eel. Comparison with the effect of 5-hydroxytryptophan. *Cell Tissue Res*. 1979; 196:397-408. doi: 10.1007/BF00234736
43. Olivereau M, *et al*. Responses of MSH and prolactin cells to 5-hydroxytryptophan (5-HTP) in amphibians and teleosts. *Cell Tissue Res*. 1980; 207:377-85. doi: 10.1007/BF00224614
44. Lundin K and Holmgren S. The occurrence and distribution of peptide- or 5-HT-containing nerves in the swimbladder of four different species of teleosts (Gadus morhua, Ctenolabrus rupestris, Anguilla anguilla, Salmo gairdneri). *Cell and Tissue Research*. 1989; 257:641-647. doi: 10.1007/bf00221475
45. Pan YK and Perry SF. Neuroendocrine control of breathing in fish. *Mol Cell Endocrinol*. 2020; 509:110800. doi: 10.1016/j.mce.2020.110800
46. Pan YK, *et al*. Disruption of tph1 genes demonstrates the importance of serotonin in regulating ventilation in larval zebrafish (Danio rerio). *Respir Physiol Neurobiol*. 2021; 285:103594. doi: 10.1016/j.resp.2020.103594
47. Abdallah SJ, *et al*. Aquatic surface respiration and swimming behaviour in adult and developing zebrafish exposed to hypoxia. *J Exp Biol*. 2015; 218:1777-86. doi: 10.1242/jeb.116343
48. Kacprzak V, *et al*. Dopaminergic control of anxiety in young and aged zebrafish. *Pharmacol Biochem Behav*. 2017; 157:1-8. doi: 10.1016/j.pbb.2017.01.005

Chapter 2: Zebrafish behavioural profiling identifies GABA and serotonin receptor ligands related to sedation and paradoxical excitation

2.1 Abstract

Anesthetics are generally associated with sedation, but some anesthetics can also increase brain and motor activity—a phenomenon known as paradoxical excitation. Previous studies have identified $GABA_A$ receptors as the primary targets of most anesthetic drugs, but how these compounds produce paradoxical excitation is poorly understood. To identify and understand such compounds, we applied a behavior-based drug profiling approach. Here, we show that a subset of central nervous system depressants cause paradoxical excitation in zebrafish. Using this behavior as a readout, we screened thousands of compounds and identified dozens of hits that caused paradoxical excitation. Many hit compounds modulated human $GABA_A$ receptors, while others appeared to modulate different neuronal targets, including the human serotonin-6 receptor. Ligands at these receptors generally decreased neuronal activity, but paradoxically increased activity in the caudal hindbrain. Together, these studies identify ligands, targets, and neurons affecting sedation and paradoxical excitation in vivo in zebrafish.

2.2 Introduction

Anesthetics and other central nervous system (CNS) depressants primarily suppress neural activity, but sometimes they also cause paradoxical excitation[1]. During paradoxical excitation, brain activity increases[2,3] and produces clinical features such as confusion, anxiety, aggression, suicidal behavior, seizures, and aggravated rage[4,5]. These symptoms primarily affect small but vulnerable patient populations including psychiatric, pediatric, and elderly patients[6,7]. Understanding paradoxical excitation is important for discovering, understanding, and developing CNS depressants and for understanding how small molecules affect the vertebrate nervous system. However, relatively few compounds have been identified that cause paradoxical excitation, and few model systems have been identified that reproducibly model paradoxical excitation in vivo.

Many ligands that cause paradoxical excitation are agonists or positive allosteric modulators (PAMs) of $GABA_A$ receptors ($GABA_ARs$), the major type of inhibitory receptors in the CNS[8]. However, it is likely that other mechanisms also affect paradoxical excitation. One such mechanism may involve serotonin imbalance, which affects behavioral disinhibition[9,10], and has paradoxical effects on neuronal circuit output[11]. For example, the serotonin-6 receptor (HTR6) is an excitatory G protein-coupled receptor (GPCR) reported to modulate cholinergic and glutamatergic systems by disinhibiting GABAergic neurons[12]. In serotonin syndrome, excessive serotonergic signaling causes agitation, convulsions, and muscle rigidity. Despite these excitatory effects of excessive serotonergic signaling, several serotonin receptor agonists are used as anxiolytics, hypnotics, and anticonvulsants[13]. Examples include clemizole and

fenfluramine, which promote 5-HT signaling and have anticonvulsant properties in humans and zebrafish[13,14]. By contrast, serotonin antagonists and inverse agonists improve sleep and are used for treating insomnia[15]. Furthermore, serotonin receptors are secondary and tertiary targets of some anesthetics, suggesting that 5-HT receptors may contribute to sedation[16]. However, the potential impact of serotonin receptors on anesthesia and paradoxical excitation is poorly understood.

In principle, large-scale behavior-based chemical screens would be a powerful way to identify compounds that cause sedation and paradoxical excitation. The reason is that phenotype-based screens are not restricted to predefined target-based assays. Rather, phenotype-based screens can be used to identify targets and pathways that produce poorly understood phenotypes. Indeed, virtually all CNS and anesthetic drug prototypes were originally discovered based on their behavioral effects before their targets were known[17]. Furthermore, these compounds were valuable tools for understanding the mechanisms of anesthesia and sedation. Although behavior-based chemical screens in vertebrates would be most relevant for human biology, behavioral assays in mice, primates, and other mammals are difficult to scale.

Zebrafish are uniquely well-suited for studying the chemical biology of sedation and paradoxical excitation. Zebrafish are vertebrate animals with complex brains and behaviors, they are small enough to fit in 96-well plates, and they readily absorb compounds dissolved in the fish water. Compared with humans, zebrafish share many conserved genes and neurotransmitter signaling pathways[18]. For example, the zebrafish genome contains orthologs for all but two human $GABA_AR$ subunit isoforms[19]. The α-isoform family is the largest and most diverse family of $GABA_AR$ subunits in both

humans and zebrafish[20]. The zebrafish genome also encodes orthologs of serotonin receptors, including orthologs of HTR6[21,22]. Additionally, there are several important differences between the species. One such difference is that the zebrafish genome encodes a $GABA_AR$ β_4-subunit, which does not have a clear ortholog in mammals[19]. Another difference is that whereas mammals have six $GABA_AR$ α-subunit isoforms, zebrafish have eight[20]. Previously, drug profiling studies in zebrafish have identified neuroactive compounds related to antipsychotics, fear, sleep, and learning[23-26]. However, specific behavioral profiles for compounds that cause paradoxical excitation have not been previously described in zebrafish.

The purpose of these studies is to identify and understand compounds that cause paradoxical excitation. First, we develop a scalable model of paradoxical excitation in zebrafish. Then, we use this model in large-scale chemical screens to identify dozens of compounds that cause paradoxical excitation. Third, we use these compounds as research tools to identify receptors affecting sedation and paradoxical excitation. Finally, we map whole-brain activity patterns during these behavioral states. Together, these studies improve our understanding of how small molecules cause sedation and paradoxical excitation and may help to accelerate the pace of CNS drug discovery.

2.3 Methods

2.3.1 Fish maintenance, breeding, and compound treatments

We collected a large number of fertilized eggs (up to 10,000 embryos per day) from group matings of wild-type zebrafish (from Singapore). All embryos were raised on a 14/10-hour light/dark cycle at 28 °C until 7 dpf. Larvae were distributed 8 animals per well into square 96-well plates (GE Healthcare Life Sciences) with 300 µL of egg water. Compound stock solutions were applied directly to the egg water and larvae were incubated at room temp for 1 h before behavioral analysis. To determine the impact of group size on this assay, we analyzed eASR behaviors from animals in different group sizes (1, 2, 4, 8, 12, 16, 32 animals per well). Although animals in all groups responded similarly to the stimulus, the largest differences between treated and controls were seen in groups of 8 and 16 animals (**Supplemental Figure 2.19**). We, therefore, used 8 animals to balance small group size with a strong MI signal. All zebrafish procedures were and approved by the UCSF's Institutional Animal Care Use Committee (IACUC), and in accordance with the Guide to Care and Use of Laboratory Animals (National Institutes of Health 1996) and conducted according to established protocols that complied with ethical regulations for animal testing and research.

2.3.2 Compounds and chemical libraries

All chemical libraries were dissolved in DMSO. The Chembridge library (Chembridge Corporation) contains 10,000 compounds at 1 mM. The Prestwick library (Prestwick Chemical) contains 1280 approved drugs at 10 mM. All compounds were diluted in E3 buffer and screened at 10 µM final concentration in < 1% DMSO. Controls were treated

with an equal volume of DMSO. Compounds were validated in 3-12 replicate wells, on 3 replicate plates. For dose-response behavioral assays, compounds were tested at 7 concentrations that ranged from 0.1 to 100 μM, unless otherwise indicated.

2.3.3 Automated behavioral phenotyping assays

Digital video was captured at 25 frames per second using an AVT Pike digital camera (Allied Vision). Each assay duration was 30–120 s, and consisted of a combination of acoustic and light stimuli[23]. Low (70 db) and high (100 db) amplitude acoustic stimuli were delivered using push-style solenoids (12 V) to tap a custom built acrylic stage where the 96-well plate was placed. Acoustic stimuli were recorded using a contact microphone (*Aquarian Audio Products*, model# H2a) and the freeware audio recording software Audacity (http://www.audacityteam.org). Digital acoustic stimulus was generated as a 70 ms sine wave at various frequencies using Audacity. A computer was used to playback the audio stimulus as an mp3 using an APA150 150 W powered amplifier (Dayton Audio) played through surface transducers adhered to the acrylic stage. Stimulus volume was measured using a BAFX 3608 digital sound level meter (BAFX Products). Light stimuli were delivered using high intensity LEDs (LEDENGIN) at violet (400 nm, 11 μW/mm^2), blue (560 nm, 18 μW/mm^2), and red (650 nm, 11 μW/mm^2) wavelengths. Stimuli and digital recordings were applied to the entire 96-well plate simultaneously. Instrument control and data acquisition were performed using custom scripts written in MATLAB and Python. The zebrafish motion index (MI) was calculated as follows: $MI = sum(abs(frame_n - frame_{n-1}))$. Normalized MI (nMI) was calculated as follows: $nMI = (MI-min(MI))/max(MI)$. Startle magnitude was calculated using numerical

integration via the trapezoidal method (Matlab function *trapz*) of MI values during stimulus.

2.3.4 Computing the phenoscore

To quantify distances between multi-dimensional behavioral profiles, we first defined a prototypic behavioral profile to compare everything else against. Etomidate's prototypical behavioral profile was determined from 36 replicate wells treated with etomidate (6.25 μM) on 3 different plates (12 replicates per plate). Using a simulated annealing procedure (described in the supplement) we identified 12 replicate profiles with the most consistent eASR response that was also most distant from the control (DMSO) wells. The reference profile was the average of these 12 profiles. Phenoscore distances were computed between each well and the reference profile by calculating the correlation distance (using the correlation distance module from the scipy package in python). The correlation distance (phenoscore) has a range from −1 to +1. Positive and negative values represent positive and negative correlation, respectively. Negative values represent anti-correlation. Experimentally, phenoscores tended to saturate at around 0.7, a value that represents substantial positive correlation given that the MI time series is a large vector with >10,000 values. Although etomidate and propofol are both anesthetic $GABA_AR$ PAMs with similar behavioral profiles in zebrafish, etomidate is more soluble than propofol, so we used etomidate as the archetypal positive control.

2.3.5 Ranking the screening hits

Phenoscores were computed to assign each compound in the screening library a rank order. Hit compounds were defined as the top 125 compounds from this ranked list.

2.3.6 Calculating response magnitude Z-scores

Response magnitudes were calculated by averaging the maximum motion index value during 3 repeated violet stimuli or 6 repeated acoustic stimuli. These Motion index magnitudes were converted to Z-scores using the following equation: Z-score = (magnitude − mean)/SD. Z-scores were then normalized from 0-1 using the scikit function sklearn.preprocessing.normalize written for python.

2.3.7 In vitro receptor profiling

In vitro binding assays and Ki data were generated by the National Institute of Mental Health's Psychoactive Drug Screening Program (PDSP), contract no. HHSN-271-2008-00025-C (NIMH PDSP), for assay details: http://pdsp.med.unc.edu/PDSP%20Protocols%20II%202013-03-28.pdf. Normalized Ki (npKi) values were generated as follows: npKi = 4 + (−log10 (Ki)) [64].

2.3.8 FLIPR

We used the FLIPR system (Molecular Devices) to quantify GABA-evoked activity of human GABAARs. We chose a membrane potential dye (Molecular Devices) to measure changes in membrane potentials and stably transfected HEK293 cells that expressed α_1, β_2 and γ_2. Since we observed an increase in GABA-evoked responses

when transfected with γ_2 transiently, we describe the cells as having a low level of γ-subunit expression, indicating heterogeneity of $GABA_AR$ compositions in the cell ($\alpha_1\beta_2$ or $\alpha_1\beta_2\gamma_2$). To assay for direct agonists, fluorescence was subtracted pre- and post compound addition. To assay for PAMs, cells were treated with compound at 20 uM and then with 5 uM GABA.

2.3.9 Whole-brain activity mapping

Following behavioral experiments, animals were immediately fixed in 4% paraformaldehyde in PBS and incubated overnight at 4 °C. Larvae were then washed in PBS + 0.25% Triton-X (PBT), incubated for 15 min at 70 °C in 150 mM Tris-HCl, pH9, washed in PBT, permeabilized in 0.05% Trypsin-EDTA for 30-45 min on ice and washed with PBT. Animals were then blocked for 1 h at room temperature (PBT, 1% bovine serum albumin, 2% normal goat serum, 1% DMSO, and 0.02% sodium azide)[38]. The following primary antibodies were diluted into blocking buffer and incubated overnight at 4 °C: α-5HT (1:500, ImmunoStar), α-tERK (1:750, Cell Signaling), α-pERK (1:750, Cell Signaling). Secondary fluorescent antibodies (Life Technologies) were used at 1:500 and incubated in blocking buffer overnight at 4 °C in the dark. Whole-mount fluorescent images were obtained using a Leica SP8 confocal microscope. Image processing was performed in imageJ. Image registration was performed using the Computational Morphometry Toolkit (https://www.nitrc.org/projects/cmtk) and a user interface with the command string defined by Owen Randlett (-awr 010203 -T 8 -X 52 -C 8 -G 80 -R 3 -A '--accuracy 0.4' -W '--accuracy 1.6'). Multiple brains from each condition were then averaged using Matlab scripts to obtain a representative neural activity image.

Brightness and contrast were adjusted using Fiji (imageJ). MAP-map calculations (whole-brain ΔpERK significance heat maps) were performed using the analysis code for MAP-map which can be downloaded from the website (http://engertlab.fas.harvard.edu/Z-Brain/).

2.3.10 Cortisol detection assay

Cortisol levels were measured in zebrafish[65]. Briefly, 15, 7-day old larvae were treated with the indicated compounds for 1 h. Larvae were anesthetized in ice-cold egg water and then snap-froze in an ethanol/dry ice bath. Larvae were then homogenized in 100 µL of water. Cortisol was extracted from the homogenate with 1 mL of ethyl acetate, the resulting supernatant was collected and the solvent allowed to evaporate. Cortisol was dissolved in 0.2% bovine serum albumin (A7030, Sigma) and frozen at −20 °C. For cortisol ELISA experiments, 96-well plates (VWR International) were treated with cortisol antibody (P01-92-94M-P, EastCoast Bio; 1.6 g/mL in PBS) for 16 h at 4 °C, washed, and blocked with 0.1% BSA in PBS. Cortisol samples and cortisol-HRP (P91-92-91H, EastCoast Bio) were incubated at room temperature for 2 h and washed extensively with PBS containing 0.05% Tween-20 (Invitrogen). Detection of HRP was performed using tetramethylbenzidine (TMB: 22166-1, Biomol) and Tetrabutylammonium borohydride (TBABH: 230170-10 G, Sigma). Reaction was stopped using 1 M H_2SO_4. Absorbance was read at 450 nm in an ELISA plate reader (SpectraMax MS, Molecular Devices).

2.3.11 Software

Data acquisition and analysis were carried out using custom scripts in Matlab (MathWorks) and Python. Figures were prepared using Matlab, Python, ImageJ (NIH), Prism (GraphPad), and Adobe Illustrator.

2.4 Results

2.4.1 $GABA_AR$ ligands produce paradoxical excitation in zebrafish

To determine how sedatives affect zebrafish behavior, we assembled a set of 27 CNS depressants in ten functional classes (**Figure 2.1a**, **Supplemental Table 2.1**) and tested these compounds in a battery of automated behavioral assays. The behavioral assays were originally devised to discriminate between a broad range of neuroactive compounds[23]. Here, the assays were used to profile anesthetics and other CNS-depressants. In one assay, we used excitatory violet light stimuli to identify compounds that reduce motor activity (**Figure 2.1b**). In another assay, we used low-volume acoustic stimuli to identify compounds that enhance startle sensitivity (**Figure 2.1b**). Most CNS depressants caused a dose-dependent decrease in animals' average motion index (MI) (**Supplemental Figure 2.1**), however, we noticed a striking exception.

Two anesthetic $GABA_AR$ ligands, etomidate and propofol, caused enhanced acoustic startle responses (eASRs). These eASRs occurred in response to a specific low-volume acoustic stimulus, but not to other stimuli (**Figure 2.1a, 2.1b, Supplemental Figures 2.2 and 2.3**). Unlike vehicle-treated controls, all the animals in a well treated with etomidate showed robust eASRs. High speed video revealed that the eASRs

resembled short latency C-bends (**Figure 2.1c**). Multiple eASRs could be elicited with multiple stimuli (**Figure 2.1d**). Etomidate's half maximal effective concentration (EC_{50}) for causing eASRs was 1 μM, consistent with its EC_{50} against $GABA_A$Rs in vitro (**Figure 2.1e**)[27]. Neither etomidate or propofol was toxic at the concentrations that caused eASRs (**Supplemental Table 2.2**). The eASRs persisted for several hours and rapidly reversed after drug washout (**Figure 2.1b, f**). Curiously, not all anesthetics caused eASR behaviors in zebrafish, including isoflurane (a volatile inhalational anesthetic that is relatively toxic in zebrafish), dexmedetomidine (a veterinary anesthetic and alpha-adrenergic agonist), and tricaine (a local anesthetic and sodium channel blocker) (**Figure 2.1a**). Together, these data suggest that a subset of $GABA_A$R ligands produce sedation and paradoxical excitation in zebrafish.

To determine if other $GABA_A$R ligands caused similar phenotypes, we used the phenoscore metric to quantify similarities between the archetypal profile caused by etomidate (6.5 uM) and a diverse range of GABAergic compounds (**Supplemental Table 2.3**). Average phenoscores of DMSO-treated negative controls were significantly less than etomidate-treated positive controls (0.2 versus 0.71, $P < 10^{-10}$, Kolmogorov–Smirnov test) (**Supplemental Figure 2.20**). Average phenoscores for the test compounds fell on a continuum between the positive and negative controls (**Figure 2.1g**). Based on statistical simulations, these phenoscores were subdivided into three categories: weak, intermediate, and strong.

Compounds with the strongest phenoscores ($0.71 < x < 1$) included several anesthetic and neurosteroid PAMs including etomidate, propofol, progesterone, and 11-deoxycorticosterone (DOC) (**Figure 2.1g**). The highest scoring treatments for these

compounds produced behavioral profiles that were both strongly sedating and produced high-magnitude eASRs (**Supplemental Figure 2.2**). These profiles were not statistically different from the positive controls ($P > 0.05$, Kolmogorov–Smirnov test, **Supplemental Figure 2.20**). Together, these data suggest that a subset of $GABA_AR$ PAMs cause sedation and paradoxical excitation in zebrafish. However, due to the overlapping pharmacology of numerous $GABA_AR$ subtypes, these data do not clearly point to any specific subset of receptor subtypes as being necessary or sufficient for these behaviors.

In humans, the M-current is a low-threshold, non-inactivating, voltage-dependent current that limits repetitive action potentials and has been implicated in propofol-induced paradoxical excitation[28,29]. To determine if M-currents affect eASRs in zebrafish, we tested several M-current activators and inhibitors. In animals treated with M-current activators (flupirtine[30,31] and ICA-069673[32]), eASR magnitudes significantly decreased (**Supplemental Figure 2.6**, $P < 0.01$, two-tailed *t*-test, $n = 6$ wells; 8 fish/well). By contrast, in animals treated with M-current inhibitors (linopirdine, XE-991, and oxotremorine[33]) eASR magnitudes significantly increased (**Supplemental Figure 2.6**, $P < 0.000001$, two-tailed *t*-test, $n = 6$ wells; 8 fish/well). These data suggest that zebrafish eASRs are a form of paradoxical excitation affected by potassium channel M-currents.

2.4.2 Large-scale behavioral screening identifies hit compounds

To prepare for large-scale screening, we calculated phenoscores for hundreds of positive and negative control wells (treated with etomidate or DMSO, respectively).

The average phenoscores of the positive controls were significantly greater than the negative controls (0.7, ± 0.11 SD versus 0.1 ± 0.05 SD), suggesting that a large-scale screen would have an expected false positive and negative rate of 2% and 0.4%, respectively (at a threshold of 3 SD) (**Figure 2.2a**, *Z*-factor = 0.7, *n* = 944 wells).

Then, we screened a library of 9512 structurally-diverse compounds plus 2336 DMSO-treated negative controls, and analyzed their effects on sedation and paradoxical excitation. Visualized as a contour plot, the highest density of phenoscores occurred in three major regions (**Figure 2.2b**). The first region contained 11,679 compounds and DMSO-treated control wells that did not phenocopy etomidate. The second region contained 44 potentially toxic compounds that immobilized zebrafish but did not cause paradoxical excitation. The third region contained 125 compounds that both produced immobilization and phenocopied etomidate and were considered primary screening hits (**Supplemental Figure 2.7**).

To organize these hit compounds by structural similarity, we clustered them based on Tanimoto similarities and visualized the results as a dendrogram that contained 14 clusters (**Figure 2.2c**). Several clusters included compounds previously associated with $GABA_AR$s (**Figure 2.2c, d**). For example, Cluster 10 included several dihydro/quinazolinones that are structurally-related to methaqualone, a sedative hypnotic drug (**Figure 2.2c, d**). A second cluster, Cluster 14, included several isoflavonoids, which are structurally-related to flavonoid sedatives[34]. Overall, we selected a broad range of 57 primary hit compounds across all the clusters to re-purchase and re-test. Each compound was re-tested in a dose-response format from 0.1 to 100 μM and scored based on its ability to immobilize zebrafish and increase

eASRs. Together, 81% of these primary hit compounds (46/57) caused reproducible eASR phenotypes at one or more concentrations (**Figure 2.2e**, **Supplemental Figure 2.8**), indicating a high rate of reproducibility from the primary screen.

To determine if these compounds targeted human $GABA_AR$s, we tested them in a fluorescent imaging plate reader (FLIPR) assay on HEK293 cells transfected with $\alpha_1\beta_2$ and $\alpha_1\beta_2\gamma_2$ human $GABA_AR$ subtypes. In this cell line, etomidate, tracazolate, and propofol increased fluorescence in the presence of GABA, as expected for $GABA_AR$ PAMs. In addition, half of the tested hit compounds (23/46) also showed PAM activity (**Figure 2.2f**, **Supplemental Figure 2.9**). By contrast, PAM activity was not observed with negative control compounds including BGC 20-761 (an HTR6 antagonist) and PTX (a $GABA_AR$ channel blocker) which likely reduced $GABA_AR$ activity due to inhibition of constitutively active $GABA_AR$s in the system. Interestingly, the PAM activity of two hit compounds, 7013338 and 5942595, was significantly greater than the positive controls (**Figure 2.2f**, $P < 0.0001$, two-tailed *t*-test, $n = 4$). While some of the compounds appeared to function in this assay as negative allosteric modulators (NAMs), reductions in fluorescence were likely due to toxicity-induced cell loss (**Figure 2.2f**). In addition to the PAM assay, four hit compounds directly activated $GABA_AR$s in the absence of GABA, including 5860357, 6091285, 5835629, and 7284610 (**Supplemental Figure 2.9**). The strongest direct activator, 5835629, did not further enhance $GABA_AR$ activation in the PAM assay, presumably because the cells were already maximally activated by the compound before GABA was added. These data suggest that behavioral screens in zebrafish can enrich for compounds with activity at specific

human receptors. In addition, these data suggest that many of the hit compounds identified in the screen cause sedation and paradoxical excitation via $GABA_AR$s.

2.4.3 Hit compounds act on targets including GABAAR and HTR6

To determine if any of the hit compounds acted on non-$GABA_AR$ targets, we used the Similarity Ensemble Approach (SEA)[35] to predict targets based on 'guilt-by-association' enrichment factor scores (EFs). Among the top-ranked 1000 screening compounds, 150 targets were enriched. As we analyzed subsets of hit compounds with increasing phenotypic stringency, the number of enriched targets decreased (**Figure 2.3a, b**). The most stringent set of 30 top-ranked hit compounds contained 25 enriched targets including $GABA_AR$s, 5α-reductase, mGluRs, and 5-HTRs. By contrast, this stringent set of hit compounds were not enriched for other sporadically predicted targets such as histone deacetylase, matrix metalloproteinase, and carbonic anhydrase (**Figure 2.3b**). As additional negative controls, we tested 48 reference compounds targeting receptors with relatively low EF scores and confirmed they did not cause eASR phenotypes at any concentration. Together, these data suggest that the hit compounds may act on $GABA_AR$s, 5α-reductase, mGluRs, or 5-HTRs.

A second approach to target identification was to test the binding affinity of hit compounds against a panel of 43 human and rodent neurotransmitter-related targets. Of 46 hit compounds, 33 of them bound to at least one of 19 receptors at a $K_i < 10$ μM (**Figure 2.3c, d**). Several hit compounds bound to multiple targets, including compound 7145248, which bound to TSPO, the benzodiazepine receptor (BZP), dopamine transporter, and the alpha 2b receptor (**Figure 2.3d**). The most common targets

(binding > 5 compounds) included BZP, sigma 2, HTR2A/B/C, HTR6, and TSPO (**Figure 2.3c, d**). TSPO, previously known as the peripheral benzodiazepine receptor (PBR) (because it was originally identified as a binding site for benzodiazepine anxiolytic drugs), is a mitochondrial protein that supplies cholesterol to steroid-producing enzymes in the brain[36]. TSPO ligands are thought to enhance GABAergic signaling by increasing neurosteroid production. However, some TSPO ligands, including benzodiazepines and zolpidem, also bind to $GABA_A$Rs directly[37]. We found that 14 hit compounds bound to TSPO in vitro (**Figure 2.3c, d**), and that two TSPO reference ligands, PK 11195 and AC 5216, both caused eASRs in vivo (**Figure 2.3e**). Of the 14 compounds that bound to TSPO in vitro, 5 compounds potentiated $GABA_A$R in FLIPR assays (**Figure 2.3c,** green arrowheads). These data suggest that TSPO ligands promote anesthetic-related phenotypes via direct interactions with $GABA_A$Rs, indirect effects on neurosteroidogenesis, or both.

Both target identification approaches, SEA and the in vitro receptor binding assays, implicated HTR6. For example, SEA predicted that seven hit compounds, six benzenesulfonamides and one piperazine, targeted HTR6 (**Figure 2.4a**). These compounds reproducibly caused eASRs in vivo (**Figure 2.4b**). In vitro, six of these hit compounds bound to HTR6 at nanomolar concentrations (Ki = 54–807 nM) (**Figure 2.4c**). To determine their functional effects, we tested them for agonist and antagonist activity in G-protein and β-arrestin pathways at eight serotonin receptor subtypes (1A, 2A, 2B, 2C, 4, 5A, 6, and 7A). Six of the compounds antagonized HTR6 in vitro. Most of them antagonized both G-protein and β-arrestin pathways, suggesting that the compounds were unbiased HTR6 antagonists (activity range 3.30 nM–18.2 μM)

(**Figure 2.4d**). By contrast, a structurally-related piperazine, 5801496, did not cause eASRs in vivo.

To determine if any annotated HTR6 antagonists also caused eASRs, we analyzed six structurally-diverse HTR6 reference antagonists. Two of these reference antagonists, BGC 20-761 and idalopirdine, reproducibly caused eASRs in vivo (**Figure 2.4b**). It is unclear why only 2/6 reference HTR6 antagonists caused eASRs in zebrafish, but it may be related to issues with absorption, metabolic stability, and/or structural differences between human and zebrafish receptors. A panel of 36 additional 5-HT modulating ligands at various serotonergic targets did not cause eASRs at any concentration tested. Together, these data suggest that a subset of HTR6 antagonists cause eASRs in zebrafish.

2.4.4 A neural substrate for paradoxical excitation

To determine which regions of the brain were active during eASRs, we visualized whole-brain activity patterns by pERK labeling[38]. In DMSO-treated control animals, pERK labeling showed broad patterns of activity in the optic tectum, telencephalon, and other brain regions (**Figure 2.5a, b**). By contrast, in animals treated with etomidate or propofol, pERK labeling was broadly reduced (**Figure 2.5c–e;** $P < 0.0005$, Mann–Whitney *U* test). Acoustic stimuli significantly activated a cluster of neurons in the caudal hindbrain at the base of the 4th ventricle near the auditory brainstem and the nucleus of the solitary tract (NST)[39] at the level of the area postrema (**Figure 2.5f, g**; $P < 0.0005$, Mann–Whitney *U* test)[40], suggesting that this hindbrain neuron cluster represented a specific substrate of eASR behavior.

To determine if activity in this region specifically occurred during eASRs, we analyzed pERK labeling in this region during four other robust motor behaviors. First, in animals stimulated by optovin (a reversible photoactivatable TRPA1 ligand)[24], neuronal activity increased in many brain regions including the telencephalon and optic tectum but not in the hindbrain (**Figure 2.5j, k**). Second, in DMSO-treated control animals stimulated by light, neuronal activity increased in the telencephalon and pineal gland but not in the hindbrain (**Supplemental Figure 2.13**). Third, in animals stimulated by the $GABA_AR$ antagonist picrotoxin (PTX), neuronal activity increased in the telencephalon but not in the hindbrain (**Supplemental Figure 2.13**). Finally, in DMSO-treated animals stimulated by a strong acoustic stimulus (hard tap), pERK labeling increased in the midbrain but not in the caudal hindbrain (**Supplemental Figure 2.13**). Compared to lower concentrations of etomidate (6 μM), higher concentrations of etomidate (50 μM) suppressed eASRs and decreased pERK labeling in the caudal hindbrain (**Supplemental Figure 2.13**). Like etomidate, BGC 20-761 reduced neuronal activity throughout most of the brain and increased activity in the caudal hindbrain neuron cluster in response to acoustic stimuli (**Figure 2.5h, i**). Together, these data suggest that the labeled neurons in the caudal hindbrain are a specific substrate of eASR behaviors.

2.4.5 Hit compounds produce distinct side effect profiles

To prioritize hit compounds for further development, we tested them for specific side effects. For example, a serious side effect of etomidate is that it suppresses corticosteroid synthesis due to off-target activity on 11β-hydroxylase, the enzyme that

synthesizes cortisol in humans and zebrafish. To determine if any of the hit compounds suffered from similar liabilities, we measured their effects on cortisol levels. As a positive control, we used carboetomidate, a close structural analog of etomidate that was rationally designed to retain etomidate's activity on $GABA_AR$s, while disrupting its ability to suppress cortisol synthesis. Both etomidate and carboetomidate immobilized zebrafish and caused eASRs (**Figure 2.1g**). As expected, etomidate lowered cortisol levels in zebrafish, whereas carboetomidate did not, suggesting that these compounds have similar side effects in humans and zebrafish (**Figure 2.6a**). Next, we tested 12 hit compounds in the cortisol assay, including eight $GABA_AR$ ligands (found to be positive in the FLIPR assay), one compound predicted to target $GABA_AR$ by SEA (5951201), two HTR6 antagonists (6225936 and 6029941), and one mysterious compound with no target leads (5736224). None of these compounds reduced cortisol levels in zebrafish (**Figure 2.6a**), indicating that these ligands cause sedation and paradoxical excitation without suppressing cortisol levels.

To determine if any of the hit compounds may be analgesic, we used optovin-induced motor activity as a potential analgesia-related assay. In humans, general anesthetics reduce perceptions of pain and suffering. Although it is unclear if fish feel pain, painful stimuli in humans also cause behavioral responses in zebrafish. For example, activation of the TRPA1 ion channel causes pain in humans[41], and optovin, a photoinducible TRPA1 ligand, induces strong behavioral responses in zebrafish[24]. As a positive control, we found that etomidate suppressed the optovin response at the same concentrations that caused eASRs (**Figure 2.6b**). Similarly, we found that two GABAergic hit compounds, 7114005 and 5942595, also blocked optovin-induced motor

activity at the same concentrations that caused eASRs (**Figure 2.6b**). By contrast, compounds 5658603 and 7013338 did not suppress the optovin response (**Figure 2.6b**). The HTR6 antagonist BGC 20-761 also blocked the optovin response (**Supplemental Figure 2.16**), however serotonergic hit compounds 6225936, 6028165, and 6212662 only reduced the optovin response at concentrations that also reduced eASRs (**Supplemental Figure 2.16**). Together, these data suggest that the mechanisms controlling sedation and eASRs may be separable from analgesia, and that some eASR-causing compounds may cause analgesic-related effects in zebrafish.

To determine if eASRs also occur in adult zebrafish, we treated adult animals with etomidate and the hit compound 7013338, the most effective hit compound in the FLIPR assays (**Figure 2.2f**). We found that both of these compounds also worked in adult animals, reducing the violet light response, while increasing acoustic startle (**Figure 2.6c**). These data suggest that the mechanisms underlying eASR phenotypes are not limited to larvae but also exist in adult zebrafish.

In humans, therapeutic windows for many inhalational anesthetics are only 2-fold, while therapeutic indices for intravenous anesthetics are not much better[42]. Many of the hit compounds also had relatively narrow efficacy windows (**Figure 2.6d**). Numerous analogs of key hit compounds including thiophenes, aryloxycarboxamides, quinazolines, and sulfonamides had lower activity than the original hits (**Supplemental Figure 2.17**), suggesting that substantial medicinal chemistry would be needed to increase the potency of the primary hit compounds.

Compound 7013338 activated human $GABA_A$Rs more than any other hit compound in the FLIPR assay (**Figure 2.2f**). However, its efficacy window was

relatively narrow (10–50 μM), raising questions about its structure activity relationship (SAR) (**Figure 2.6e**). To analyze its SAR, we generated 21 analogs with different substituents on the A-, B-, and C-rings (**Figure 2.2d, Supplemental Figure 2.18**), and tested these analogs for biological activity in vivo. The most active analog, JG-18, increased eASR magnitude and widened the efficacy window from 1 to 50 μM (**Figure 2.6e**). It had a chloro substituent on C2' of the B-ring, an ethyl substituent on C2 of the C-ring, and C-6 propyl and C7 hydroxyl substituents on the A-ring (**Supplemental Figure 2.18**). In congruence with previous SAR analyses of isoflavones[34], JG-18 and other analogs with more lipophilic substituents on position C6 of the A-ring and position C2 of C-ring exhibited increased biological activity (**Figure 2.6e**). By contrast, analogs with more dramatic enhancements in steric bulk and lipophilicity at these positions (i.e., phenethyl and propyl, respectively) exhibited reduced biological activity. Likewise, it was notable that capping the polar C7-hydroxy group of JG-18 with alkyl and acyl groups tended to lessen biological activity. Importantly, we found that the B-ring C2' chloro substituent was absolutely critical for biological activity, since analogs without it did not cause eASRs. Previously, it was reported that analogs with alkoxy or trifluoromethoxy substituents at multiple positions but especially at C3' on the B-ring were high affinity $GABA_AR$ binders in vitro[43]. Surprisingly, compound JG-17 (with a trifluoromethoxy substituent on C3' of the B-ring, an ethyl substituent on C2 of C-ring, and C6 propyl and C7 hydroxy substituents on the A-ring) had no biological activity in vivo (**Figure 2.6e**). It is not clear why these ligands were not active in zebrafish. Perhaps, the anomaly could be ascribed to low penetrance in vivo, receptor subtype selectivity, and/or structural differences between the human and zebrafish $GABA_ARs$. Together, these data suggest

that additional SAR analyses may yield analogs with greater potency and broader efficacy windows in vivo.

2.5 Discussion

These studies show that anesthetics and other $GABA_AR$ PAMs cause sedation and paradoxical excitation in zebrafish, and that this behavioral model has high predictive and construct validity for identifying modulators of human $GABA_ARs$. Indeed, these studies may have underestimated the number of hit compounds that targeted $GABA_ARs$ for several reasons. One reason is that the in vitro $GABA_AR$ FLIPR assay only tested a very small number of receptor subtypes and subunit isoforms ($\alpha_1\beta_2$ and $\alpha_1\beta_2\gamma_2$). As a result, these assays would have missed compounds that acted on other $GABA_AR$ subtypes. A second reason is that some of the hit compounds may act on zebrafish-specific $GABA_ARs$. Finally, some hit compounds that caused eASRs in zebrafish may need to be bioactivated in vivo, and would therefore not be be active in vitro. Therefore, even more of the hit compounds may have targeted $GABA_ARs$.

These studies also suggest that non-$GABA_AR$ mechanisms may also affect paradoxical excitation, including HTR6 antagonism. For example, we found that HTR6 antagonists produced sedation and paradoxical excitation in zebrafish (**Figure 2.4**). These HTR6 antagonists likely reduce neuronal excitation via different mechanisms than $GABA_AR$ PAMs. $GABA_ARs$ are widely distributed in the CNS, suggesting that GABA ligands likely inhibit most neurons directly. By contrast, HTR6s are restricted to discrete neuronal populations[44], suggesting that their effects are likely propagated through indirect signaling networks. HTR6 antagonists can reduce 5-HT neuronal

firing[45], presumably by blocking positive feedback[46] control of raphe neurons that broadly project throughout the brain and spinal cord[21]. Researchers have made remarkable progress applying the principles of systems pharmacology to structure-based target predictions[47], computer assisted design of multi-target ligands[48-50], and the large-scale prediction of beneficial drug combinations[10,51]. Although we focused on predicting targets of compounds one at a time, in future studies it may be possible to calculate multi-target enrichment factors among the hit compounds from large-scale phenocopy screens and identify multi-target mechanisms.

The HTR6 antagonists identified in this study add to a growing body of evidence implicating various serotonin ligands and receptors in phenotypes related to neuronal inhibition and excitation. Our finding that HTR6 antagonists activate a region in the zebrafish NST (**Figure 2.5h, i**), are consistent with previous work showing that HTR6 antagonists activate neurons in the mammalian NST[46]. In rodents, HTR6 antagonists promote sleep[47], reduce anxiety[48], and show anticonvulsant properties[49]. However, it is not clear if HTR6 causes these effects via specific neuronal circuits, or more generally by coordinating nervous system tone and arousal. Furthermore, there are substantial differences in the central nervous system distribution and pharmacology of the mouse, rat, and human HTR6 receptors[50]. So, although HTR6 antagonists phenocopied etomidate in zebrafish, these effects may not translate to anesthetic activity in humans. Despite promising effects in rodents, several HTR6 antagonists failed in clinical trials as cognitive enhancers for the treatment of Alzheimer's disease[51], underscoring the caveats of generalizing between humans and model organisms.

These data suggest at least two possible models by which $GABA_AR$ PAMs could cause paradoxical excitation of the acoustic startle response. One possibility is that the ligands disinhibit the acoustic startle neurons. Alternatively, the ligands may excite specific neurons directly, due to conditions that reverse the chloride equilibrium potential, such as the tonic activation of $GABA_ARs$[52]. Our observation that caudal hindbrain neurons were activated by acoustic stimuli in etomidate-treated zebrafish is not the first to link GABA signaling to auditory excitation. For example, in rodents, gaboxadol activates extrasynaptic $GABA_ARs$, hyperpolarizes resting membrane potential, and converts neurons in the auditory thalamus to burst mode[53]. In addition, etomidate causes purposeless muscle excitement that is exacerbated by acoustic stimuli in dogs[54]. In zebrafish, researchers have found that the offset of optogenetic-induced inhibition of caudal hindbrain neurons triggers swim responses[55]. In addition, zebrafish caudal hindbrain neurons have been shown to be activated during hunting behaviors, a behavior that requires strong inhibitory control[56]. However, exactly how these neurons impact motor activity, and why startle neurons remain active despite elevated inhibitory tone, remains unclear.

Although these studies show that $GABA_AR$ PAMs cause paradoxical excitation, pharmacological experiments to determine which $GABA_AR$ subtypes caused eASRs were ultimately inconclusive. While the majority of $GABA_ARs$ in the CNS are benzodiazepine-sensitive γ-containing subtypes, and multiple benzodiazepines did not cause strong eASRs (**Figure 2.1g**), γ-containing subtypes may still be very important for eASRs. One reason is that the benzodiazepines tested in this study only represent a very small subset of benzodiazepine analogs. Another reason is that diazepam

produced intermediate eASR phenotypes (**Figure 2.1g**, **Supplemental Figure 2.2**), suggesting that other benzodiazepines may cause even stronger eASR phenotypes. Although etomidate, propofol, neurosteroids, and other anesthetics are PAMs at δ-subunit containing $GABA_AR$ subtypes, these ligands also modulate γ-containing subtypes. Furthermore, although THIP and DS2 are reported to have preferential activity at δ-containing $GABA_ARs$, these compounds also modulate γ-containing receptors[57], and they did not cause eASRs. One alternative explanation is that β-isoforms[58,59] could drive the presence or absence of eASRs. Another possible explanation is that whereas PAMs may produce immobilizing effects effects via some receptor subtypes, they may produce eASRs via other subtypes. In summary, although a subset of $GABA_AR$ PAMs caused eASRs, these compounds may do so via a variety of receptor subtypes. In future studies, it would be interesting to test additional benzodiazepines for such effects including midazolam, which causes paradoxical excitation in humans[60]. The specificity of currently available pharmacological tools may be insufficient to determine which $GABA_AR$ subtypes produce eASRs. Therefore, future studies may require targeted knockouts and other genetic tools to help identify the key receptor subtypes.

While these studies focused on behavioral profiling, other types of phenotypic profiling data may further improve the accuracy of neuroactive compound classification, including whole-brain imaging. Whole-brain imaging allows researchers to record real-time firing patterns will likely add massive amounts data to the behavioral pharmacology field[61,62]. For example, recent advances in high-throughput brain activity mapping for systems neuropharmacology illustrate how whole-brain activity mapping can be used in

primary screening for compounds that activate specific circuits, or allow researchers to discriminate between compounds with similar behavioral phenotypes but that work on different neuronal populations[62]. These approaches enable primary screening for compounds that activate specific circuits and allow researchers to discriminate between compounds with similar behavioral phenotypes but that work on different neuronal populations.

In summary, we have shown that $GABA_AR$ PAMs cause sedation and paradoxical excitation in zebrafish. Whereas previous behavior-based chemical screens in zebrafish have identified neuroactive compounds related to behaviors including sleep[25], antipsychotics[23], learning[26], and appetite[63], we show here that behavioral profiling can also be used to rapidly identify compounds related to sedation and paradoxical excitation. Future studies will likely expand the utility of behavior-based chemical phenocopy screens to additional kinds of neuroactive ligands, targets, and pathways.

2.6 Acknowledgements

We thank members of our research groups for helpful advice and critical reading of the manuscript. Dr. Owen Randlett for his assistance with the pERK immunostaining and whole-brain imaging protocol. This work was supported by US National Institutes of Health (NIH) grants: R01AA022583 (D.K.), the Paul G. Allen Family Foundation (D.K. and M.K.), R01MH115705 (S.T.), and U01MH104984 (S.T.).

2.7 Figures

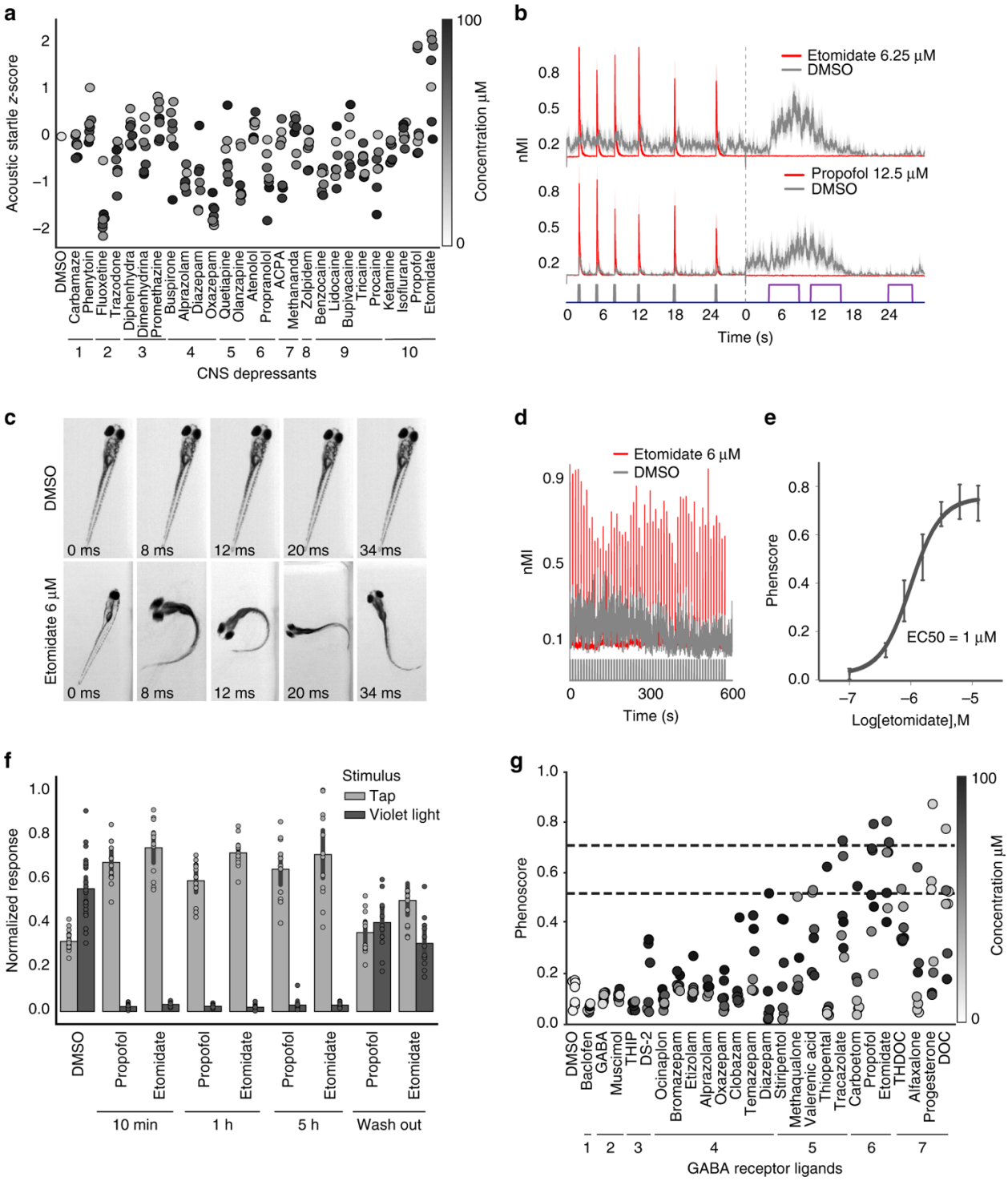
a
Acoustic startle z-score
Concentration µM
DMSO
Carbamaze
Phenytoin
Fluoxetine
Trazodone
Diphenhydra
Dimenhydrina
Promethazine
Buspirone
Alprazolam
Diazepam
Oxazepam
Quetiapine
Olanzapine
Atenolol
Propranolol
ACPA
Methananda
Zolpidem
Benzocaine
Lidocaine
Bupivacaine
Tricaine
Procaine
Ketamine
Isoflurane
Propofol
Etomidate
CNS depressants
b
Etomidate 6.25 µM
DMSO
Propofol 12.5 µM
DMSO
nMI
Time (s)
c
DMSO
Etomidate 6 µM
0 ms
8 ms
12 ms
20 ms
34 ms
d
Etomidate 6 µM
DMSO
nMI
Time (s)
e
Phenscore
EC50 = 1 µM
Log[etomidate],M
f
Stimulus
Tap
Violet light
Normalized response
DMSO
Propofol
Etomidate
10 min
1 h
5 h
Wash out
g
Phenoscore
Concentration µM
DMSO
Baclofen
GABA
Muscimol
THIP
DS-2
Ocinaplon
Bromazepam
Etizolam
Alprazolam
Oxazepam
Clobazam
Temazepam
Diazepam
Stiripentol
Methaqualone
Valerenic acid
Thiopental
Tracazolate
Carboetom
Propofol
Etomidate
THDOC
Alfaxalone
Progesterone
DOC
GABA receptor ligands

Figure 2.1. $GABA_AR$ PAMs enhance acoustic startle in zebrafish.
Zebrafish were treated with the indicated compounds and analyzed for changes in behavioral responses. **a** The scatter plot quantifies acoustic startle response as a z-score (*y*-axis) in zebrafish treated with the indicated CNS-depressants (*x*-axis) at the indicated concentrations (colorbar). Each point represents the average of $n = 12$ wells and 6 experimental replicates (also listed in **Supplemental Table 2.1**). **b** These plots show how the indicated compounds impact zebrafish motor activity (*y*-axis) over time (*x*-axis) ($n = 12$ wells, shaded boundary = 95% confidence interval; nMI, normalized motion index). Colored bars above the *x*-axis represent the timing and duration of low-volume acoustic stimuli (gray bars) and violet light stimuli (purple bars). The vertical dotted line indicates where the first assay ends and the second begins. **c** Representative images of animals treated with the indicated compounds. Time stamps indicate the time elapsed from the initial presentation of a low-volume acoustic stimulus. **d** These plots compare the motor activity (*y*-axis) over time (*x*-axis) of animals treated with DMSO (gray) or etomidate (red) ($n = 50$ larvae). Consecutive stimuli ($n = 60$) are indicated by vertical gray bars. **e** Dose-response curve showing phenoscores at the indicated concentrations (each point represents $n = 12$ wells/dose, error bars: ± SD). **f** Bar plot showing normalized response to the indicated stimulus (tap or violet light) of animals treated with DMSO, 6 μM propofol, or 6 μM etomidate ($n = 12$ wells, error bars: ± SD) for the indicated durations. **g** Average phenoscores (*y*-axis) of zebrafish treated with the indicated compounds. Dashed lines intersecting the *y*-axis at 0.51 and 0.71 correspond respectively to 1% and 5% significance cutoffs, as determined from statistical simulations. Compounds are grouped by ligand class: (1) $GABA_BR$ agonist, (2) $GABA_AR$ orthosteric agonist, (3) PAM of δ-subunit containing $GABA_ARs$, (4) $GABA_AR$ BZ-site PAM, (5) $GABA_AR$ non-BZ-site PAM, (6) $GABA_AR$ neurosteroid PAM, (7) $GABA_AR$ anesthetic PAM.

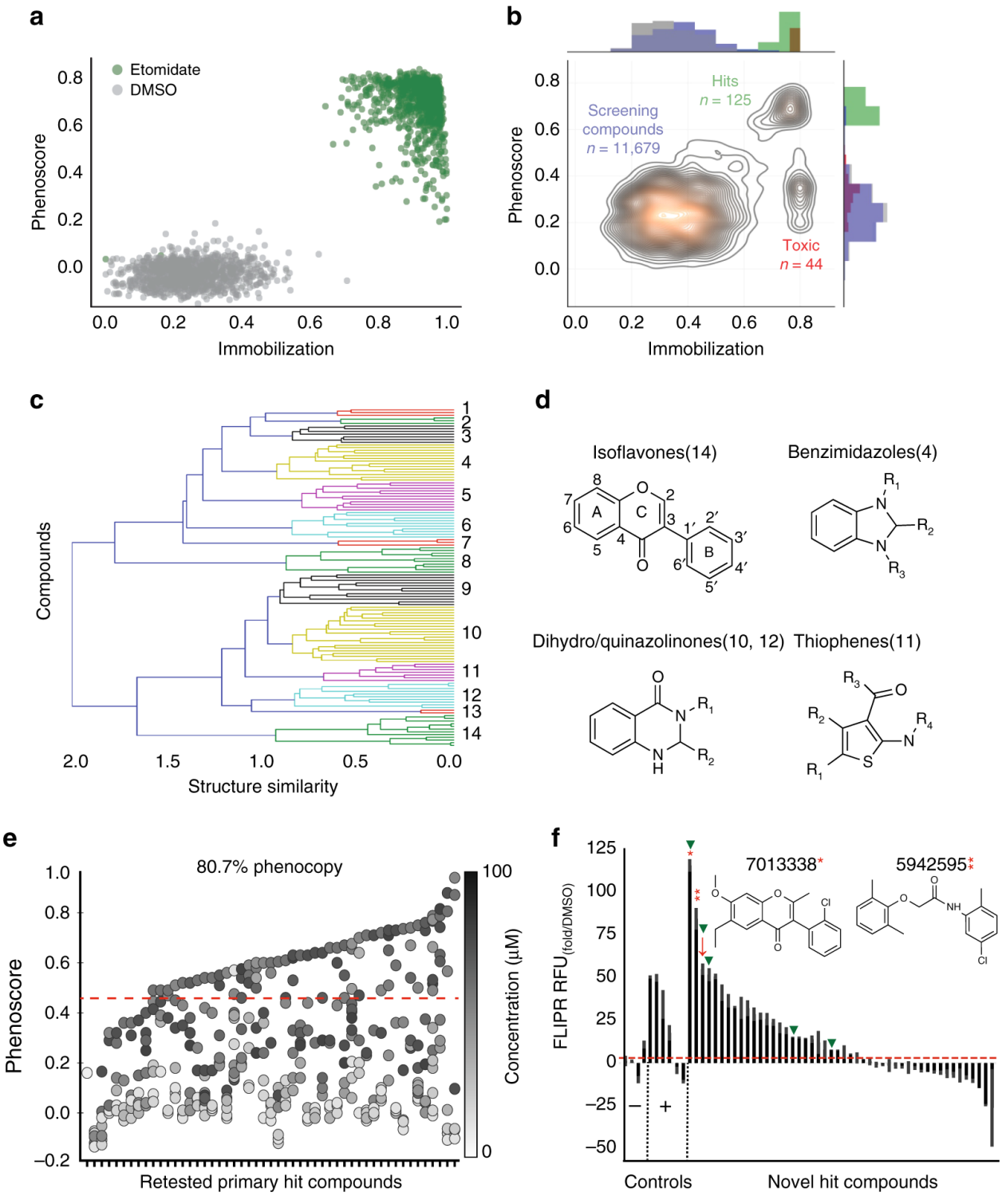
a
Etomidate
DMSO
Phenoscore
Immobilization
b
Hits
n = 125
Screening compounds
n = 11,679
Toxic
n = 44
Phenoscore
Immobilization
c
Compounds
Structure similarity
d
Isoflavones(14)
Benzimidazoles(4)
Dihydro/quinazolinones(10, 12)
Thiophenes(11)
e
80.7% phenocopy
Phenoscore
Concentration (µM)
Retested primary hit compounds
f
7013338*
5942595**
FLIPR RFU(fold/DMSO)
Controls
Novel hit compounds

Figure 2.2. A high-throughput behavioral screen identifies GABAergic compounds.
Zebrafish were treated with various compounds and analyzed for anesthetic-related behaviors. **a** This scatter plot compares phenoscores of individual wells treated with DMSO or etomidate (6.25 μM) (Z-factor = 0.7, $n = 944$ wells). **b** This contour plot scores each well from the large-scale behavior-based chemical screen (11,679 compounds, 2336 DMSO controls) by its phenoscore (*y*-axis) and immobilization index (*x*-axis). Labels indicate regions with 125 hit compounds (green), 44 toxic compounds (red), and the remaining screening compounds and DMSO controls (blue and gray, respectively). **c** Structural clustering of the top 125 hit compounds (*y*-axis) forms 14 clusters using a Tanimoto similarity metric (*x*-axis). **d** Example structures of selected compounds in the indicated clusters. **e** This scatter plot shows a 80.7% reproducibility rate for 57 primary hit compounds. Each point represents the average phenoscore of $n = 12$ wells at the indicated concentrations (colorbar). The first column represents DMSO controls. **f** Human $GABA_AR$ activation (*y*-axis) was measured by FLIPR analysis. Of 47 hit compounds, 23 potentiated $GABA_ARs$. Compounds 7013338 and 5942595 potentiated $GABA_ARs$ significantly greater than positive controls (red asterisk = 7013338, two red asterisks = 5942595, $P < 0.0001$, two-tailed *t*-test, $n = 2–4$ replicates as indicated). The hit threshold was defined as 2× the average DMSO control group. Picrotoxin, BGC 20-761, progesterone, and DMSO were used as negative controls (*x*-axis) while etomidate, tracazolate, propofol, diazepam, and thiopental were used as positive controls. Arrows indicate compounds that were predicted by SEA to bind $GABA_ARs$ (red arrows) and compounds that bound to TSPO in vitro (green arrowheads).

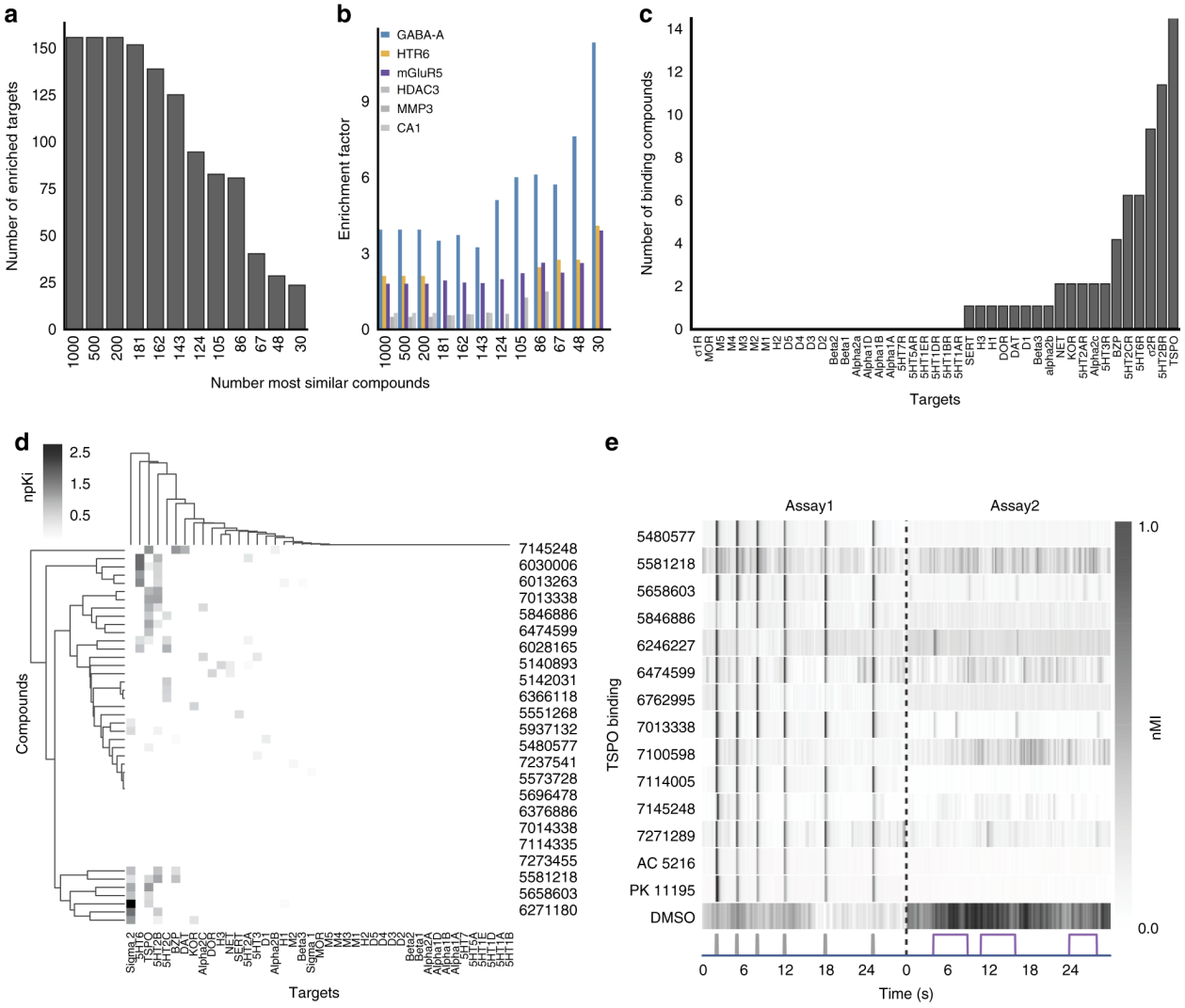

Figure 2.3. Potential targets include $GABA_AR$, mGluR, TSPO, and HTR6.
a SEA analysis was performed on decreasing numbers of hit compounds (1000-30). The bar plot shows the number of SEA enriched targets decreasing as the analysis focuses on the top 30 hit compounds. **b** The bar plot shows increasing enrichment of $GABA_AR$, HTR6, and mGluR5 as the top targets predicted for the top 30 hit compounds. **c** This bar plot shows the number of 46 primary hit compounds (*y*-axis) that bound to the indicated CNS receptors (*x*-axis). **d** The clustergram shows binding affinity profiles at the indicated CNS receptors. The colorbar indicates normalized Ki (npKI). **e** Heatmap of average motor activity profiles for TSPO binding compounds (*y*-axis) over time (*x*-axis) ($n = 12$ wells). Assay 1 is comprised of 6 low-amplitude acoustic stimuli (gray); Assay 2 is a series of 3 violet light pulses (violet). These two assays are separated by a dotted line. AC 5216 and PK 11195 are TSPO binding compounds. Abbreviations: nMI, normalized motion index; MMP3, matrix metallopeptidase 3; CA1, carbonic anhydrase 1; HDAC3, histone deacetylase 3.

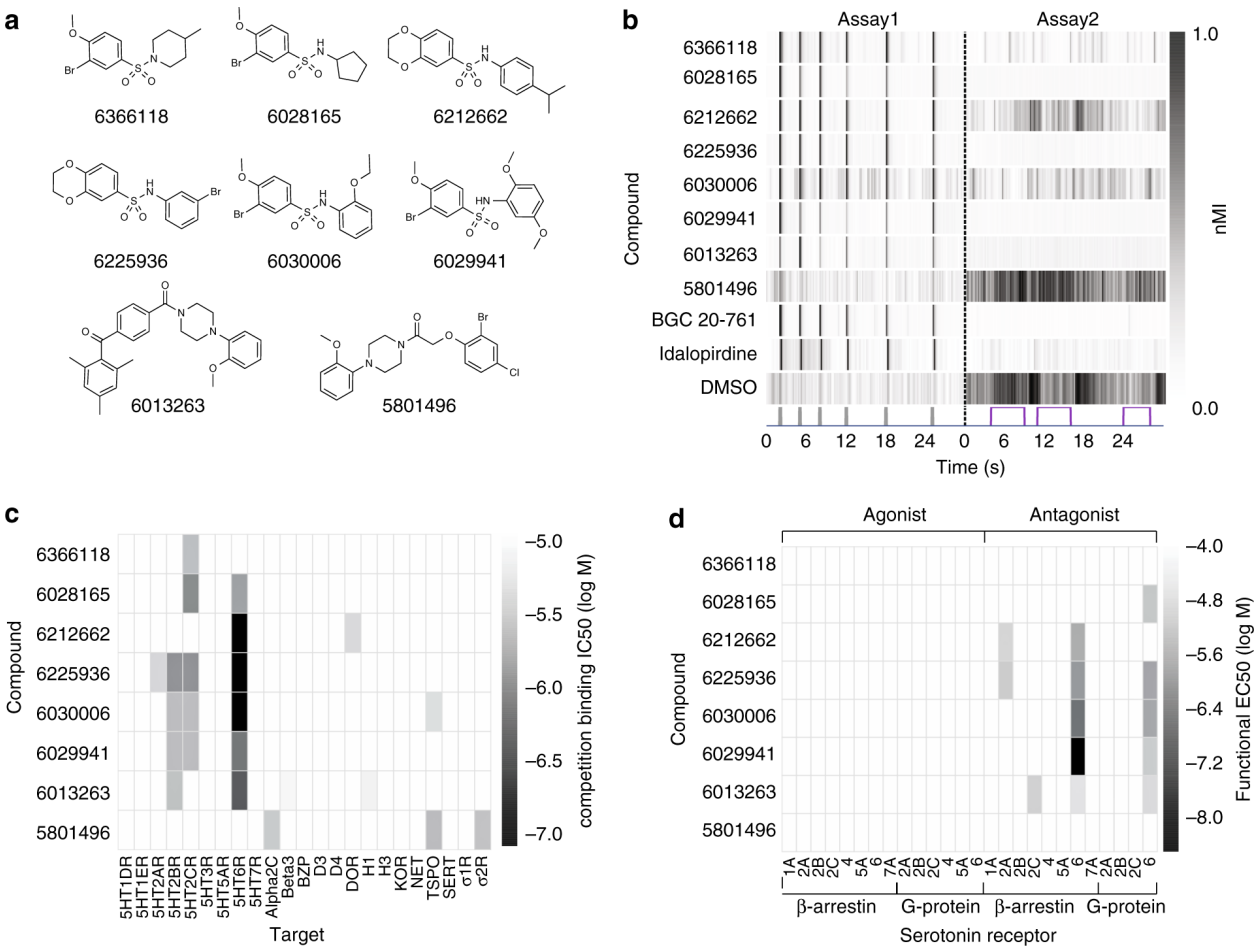

Figure 2.4. A subset of hit compounds are HTR6 antagonists.
a Structures of eight primary hit compounds predicted to bind HTR6. **b** Heatmap showing average ($n = 12$) motor activity profiles over time (x-axis) for compounds predicted to bind HTR6 (y-axis). Assay 1 is comprised of 6 low-amplitude acoustic stimuli; Assay 2 is a series of 3 violet light pulses (as indicated), these two assays are separated by a dotted line. BGC 20-761 and Idalopirdine are previously annotated HTR6 antagonists. **c** Heatmap showing binding affinities of primary hit compounds at 23 CNS receptors (x-axis). **d** Heatmap showing functional activity of primary hit compounds at the indicated GPCRs. (nMI, normalized motion index).

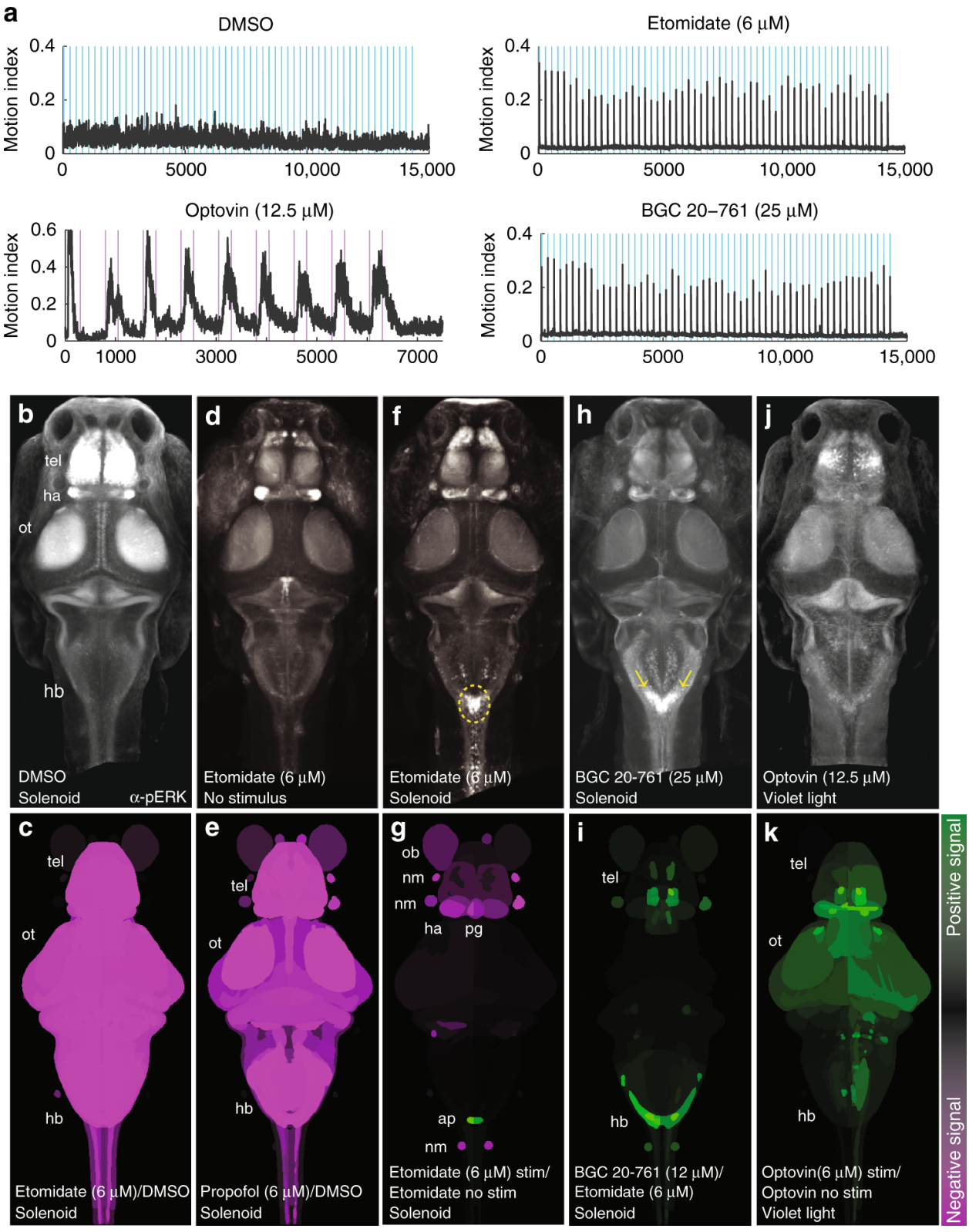
a
DMSO
Etomidate (6 μM)
Optovin (12.5 μM)
BGC 20–761 (25 μM)
Motion index
b
tel
ha
ot
hb
DMSO
Solenoid
α-pERK
d
Etomidate (6 μM)
No stimulus
f
Etomidate (6 μM)
Solenoid
h
BGC 20-761 (25 μM)
Solenoid
j
Optovin (12.5 μM)
Violet light
c
Etomidate (6 μM)/DMSO
Solenoid
e
Propofol (6 μM)/DMSO
Solenoid
g
ob
nm
ha
pg
ap
Etomidate (6 μM) stim/
Etomidate no stim
Solenoid
i
BGC 20-761 (12 μM)/
Etomidate (6 μM)
Solenoid
k
Optovin(6 μM) stim/
Optovin no stim
Violet light
Positive signal
Negative signal

Figure 2.5. Hit compounds activate hindbrain neurons.
Animals were exposed to the indicated drugs and stimuli and analyzed for pERK levels as a readout of neuronal activity. **a** Plots showing motor activity (*y*-axis) over time (*x*-axis) for animals treated with the indicated compounds ($n = 25–50$ larvae) in response to the indicated acoustic (blue) or violet light (purple) stimuli. **b**, **d**, **f**, **h**, **j** Confocal projections showing the average fluorescent intensity of image registered larval brains stained with α-pERK ($n = 10$ larvae/condition). Larvae were treated with the indicated compounds and exposed to the low-amplitude acoustic stimulus once every 10 s for 10 min, except for (**b**, no stimulus) and (**f**, violet light exposure). **c**, **e**, **g**, **i**, **k** Brain activity maps showing significant ΔpERK signals using the Z-brain online reference tool ($n = 5–10$ animals/condition). The heatmap indicates positive (green), negative (purple), and nonsignificant (black) changes in pERK labeling *(*$P < 0.0005$, Mann–Whitney *U* test). All activity maps are comparisons between the indicated treatment conditions. Abbreviations: tel, telencephalon; ot, optic tectum; hb, hindbrain; ob, olfactory bulb; nm, neuromast; ap, area postrema; pg, pineal gland.

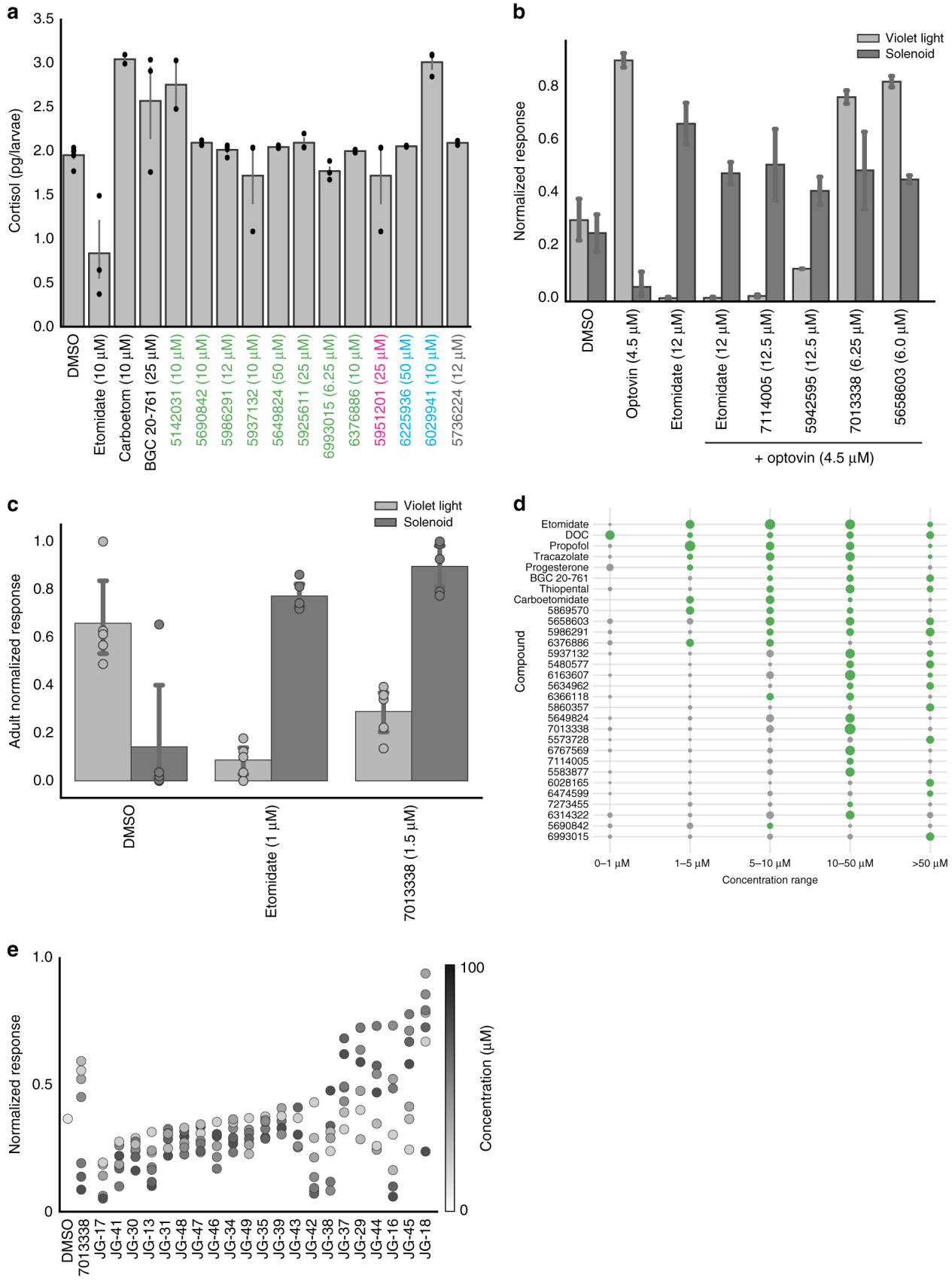
a
Cortisol (pg/larvae)
3.5
3.0
2.5
2.0
1.5
1.0
0.5
0.0
DMSO
Etomidate (10 µM)
Carboetom (10 µM)
BGC 20-761 (25 µM)
5142031 (10 µM)
5690842 (10 µM)
5986291 (12 µM)
5937132 (10 µM)
5649824 (50 µM)
5925611 (25 µM)
6993015 (6.25 µM)
6376886 (10 µM)
5951201 (25 µM)
6225936 (50 µM)
6029941 (10 µM)
5736224 (12 µM)
b
Violet light
Solenoid
Normalized response
0.8
0.6
0.4
0.2
0.0
DMSO
Optovin (4.5 µM)
Etomidate (12 µM)
Etomidate (12 µM)
7114005 (12.5 µM)
5942595 (12.5 µM)
7013338 (6.25 µM)
5658603 (6.0 µM)
+ optovin (4.5 µM)
c
Violet light
Solenoid
Adult normalized response
1.0
0.8
0.6
0.4
0.2
0.0
DMSO
Etomidate (1 µM)
7013338 (1.5 µM)
d
Compound
Etomidate
DOC
Propofol
Tracazolate
Progesterone
BGC 20-761
Thiopental
Carboetomidate
5869570
5658603
5986291
6376886
5937132
5480577
6163607
5634962
6366118
5860357
5649824
7013338
5573728
6767569
7114005
5583877
6028165
6474599
7273455
6314322
5690842
6993015
0–1 µM
1–5 µM
5–10 µM
10–50 µM
>50 µM
Concentration range
e
Normalized response
1.0
0.5
0
100
0
Concentration (µM)
DMSO
7013338
JG-17
JG-41
JG-30
JG-13
JG-31
JG-48
JG-47
JG-46
JG-34
JG-49
JG-35
JG-39
JG-43
JG-42
JG-38
JG-37
JG-29
JG-44
JG-16
JG-45
JG-18

Figure 2.6. Hit compounds show diverse efficacy windows and side effect profiles.
a This bar plot shows cortisol levels (*y*-axis) in animals treated with the indicated compounds (*x*-axis) including FLIPR-positive GABAergics (green), SEA predicted GABAergics (magenta), serotonergics (blue), and a compound with undetermined targets (gray) ($n = 2–5$ experiments, 15 animals/experiment, error bars: ± SEM). **b** This bar plot shows the normalized responses (*y*-axis) of animals treated with the indicated compounds (*x*-axis) in the pain-related optovin-response suppression assay. **c** This bar plot shows the magnitude of behavioral responses of adult zebrafish (y-axis) treated with with the indicated compounds (*x*-axis). **d** Dot plot showing efficacy windows for the indicated compounds with strong (green) or weak (gray) phenocopy scores. Marker size represents the magnitude of the eASR response ($n = 12$ wells/condition). Compounds with broad efficacy windows have large green dots at multiple concentrations (*x*-axis). **e** This strip plot shows the normalized acoustic startle response (*y*-axis) of larvae treated with increasing concentrations (colorbar) of multiple analogs of the screening hit 7013338 (*x*-axis) ($n = 4–6$ wells/condition, 8 fish/well).

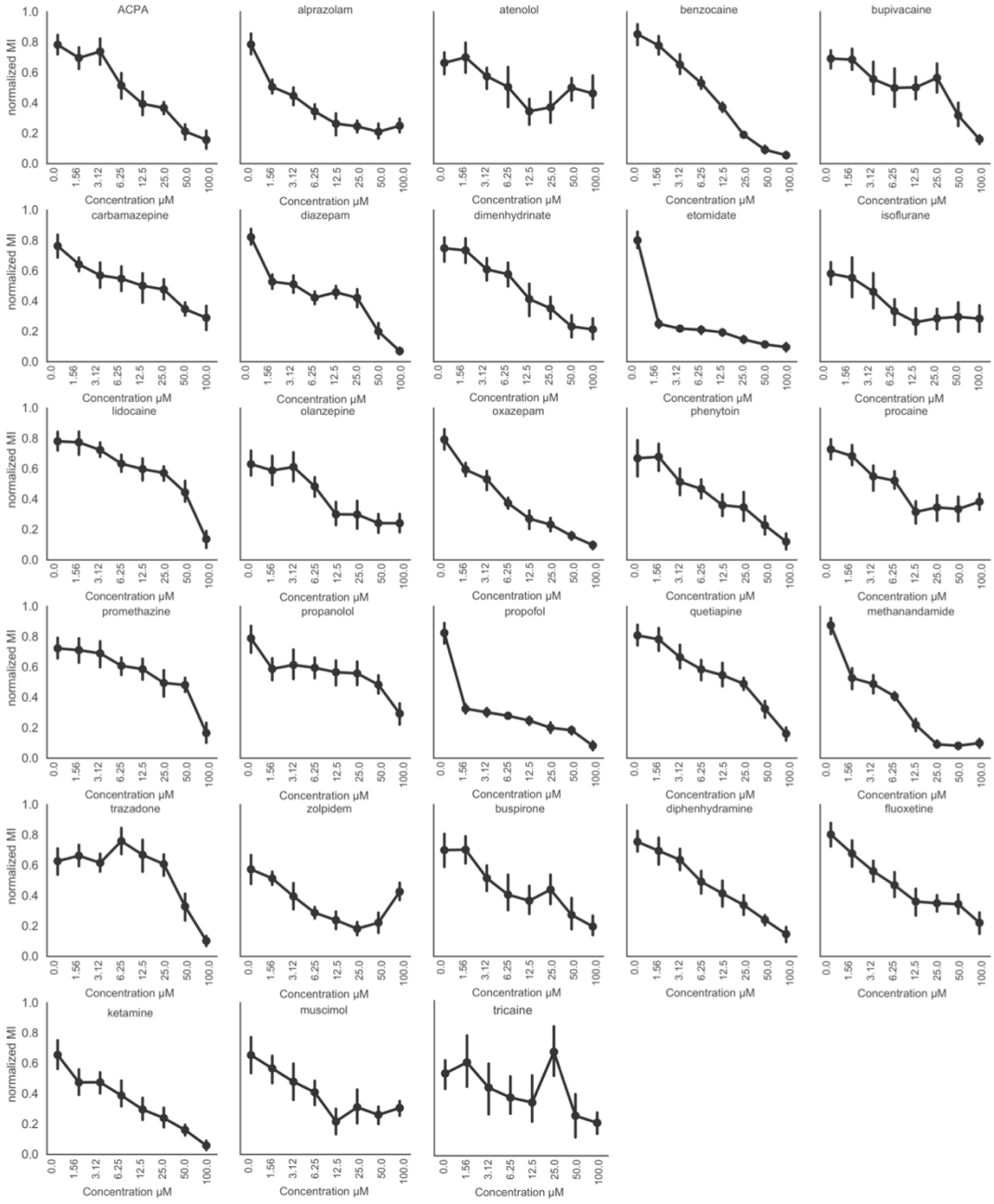

Figure 2.S1. Sedatives cause a dose dependent reduction in zebrafish motion. A panel of 30 known sedatives administered to 7dpf zebrafish larvae (n = 12 replicates; 96 fish/ condition) at a 2 fold dilution series. The y-axis represents motion index (MI) and the x-axis represents dose.

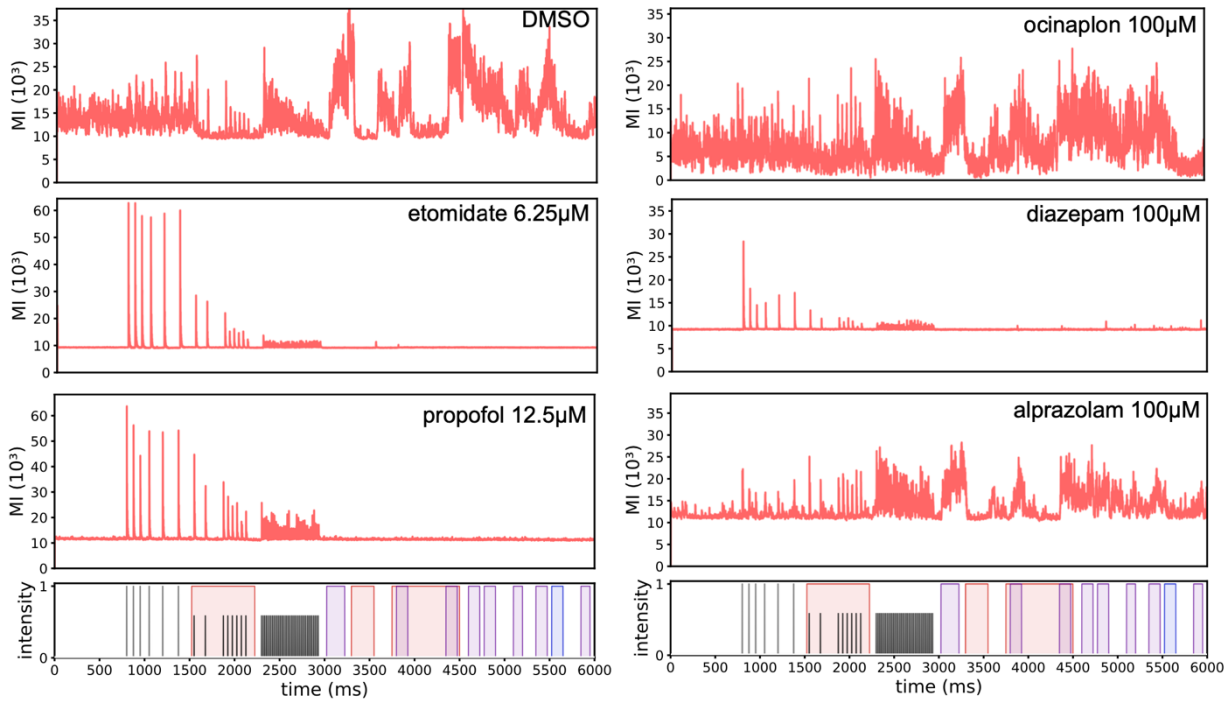

Figure 2.S2. Propofol and etomidate block light-induced behaviors but enhance the acoustic startle response.
The plots show motor activity (*y*-axis) of zebrafish treated with the indicated compounds (n = 12 wells). Colored bars above the *x*-axis represent the timing and duration of indicated stimuli.

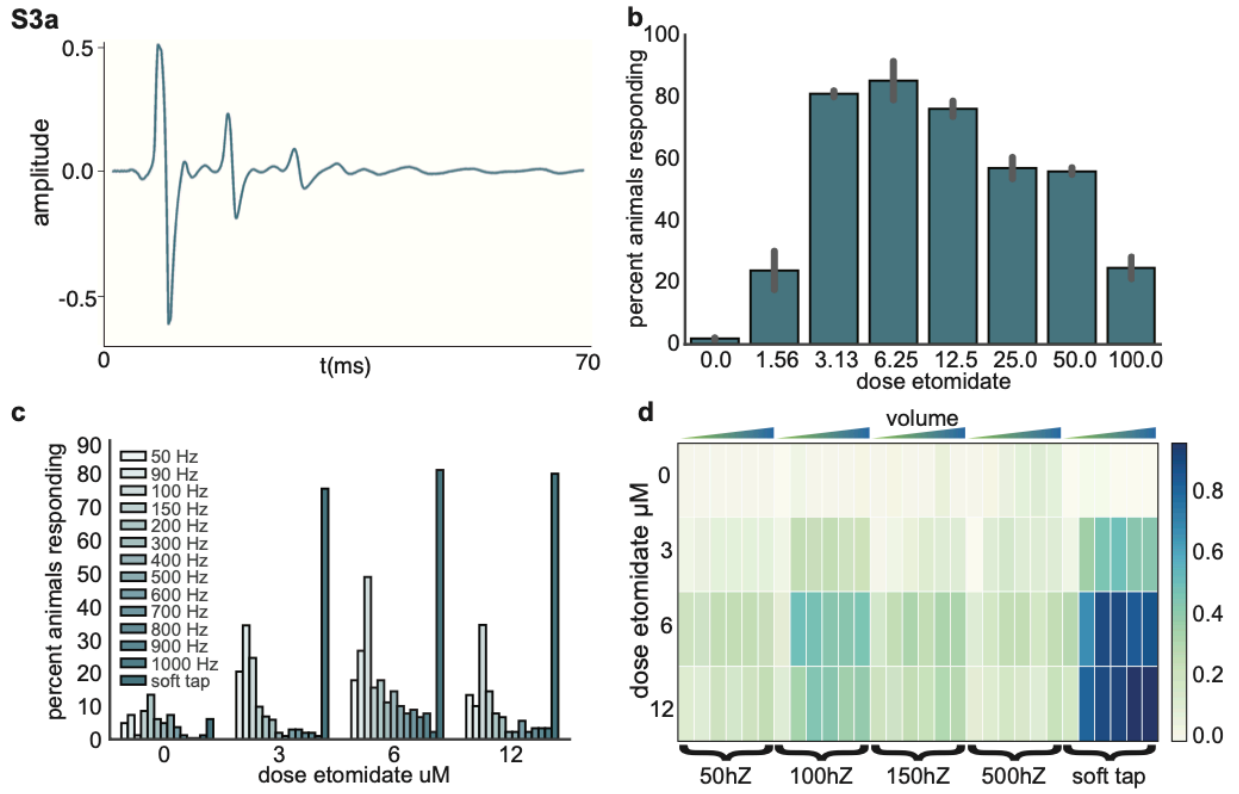

Figure 2.S3. eASR stimulus characterization.
We explored a range of digital, acoustic stimuli to understand which parameters were important for triggering eASRs. **(a)** Recorded waveform of the dampened solenoid. The original stimulus, generated by a dampened solenoid, approximated a 100 Hz inverse fading sine wave, with a 70 dB maximum volume and 70 ms duration. **(b)** Bar graph depicting startle frequency (y-axis) of 100 animals to the dampened solenoid stimulus at increasing concentrations of etomidate (x-axis), it elicited responses in 85% of etomidate-treated animals (6.25 µM) and in 2% of controls. **(c)** Startle frequency (y-axis) of 100 animals treated with indicated concentrations of etomidate (x-axis) in response to different frequencies of synthesized and dampened solenoid acoustic stimulus (colored bars). In frequency scans from 50-1000 Hz, the highest magnitude eASRs were elicited by 100 Hz stimuli. Interestingly, the most effective synthesized stimulus (a 100 Hz inverse fading sine wave; 70ms) was only 50% as effective as the original solenoid, suggesting that some unknown feature of the original solenoid-based stimulus was not captured by the synthesized waveform and/or the surface transducers. **(d)** Heat map of the startle frequency of 100 animals (color bar) in response to increasing volume (top y-axis) of different frequency synthesized acoustic stimulus and the solenoid stimulus (x-axis). Animals were treated with increasing concentrations of etomidate (y-axis). At 100Hz, all stimuli greater than 60 dB were effective, whereas those less than 55 dB were not.

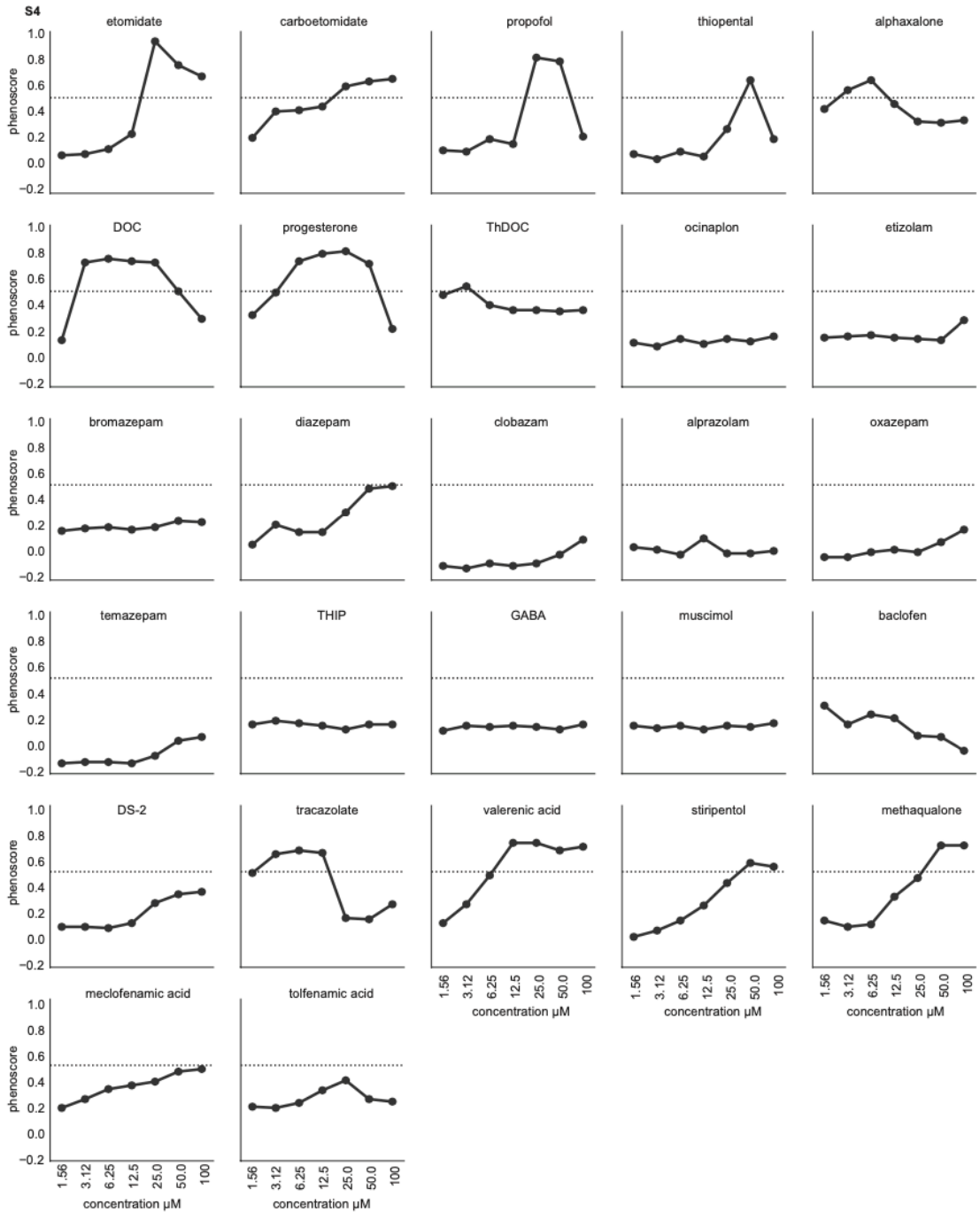

Figure 2.S4. Dose response analysis of GABA reference compounds.
Average phenoscores (*y*-axis) of zebrafish treated with the indicated compounds (n = 12 wells) at increasing concentrations (x-axis).

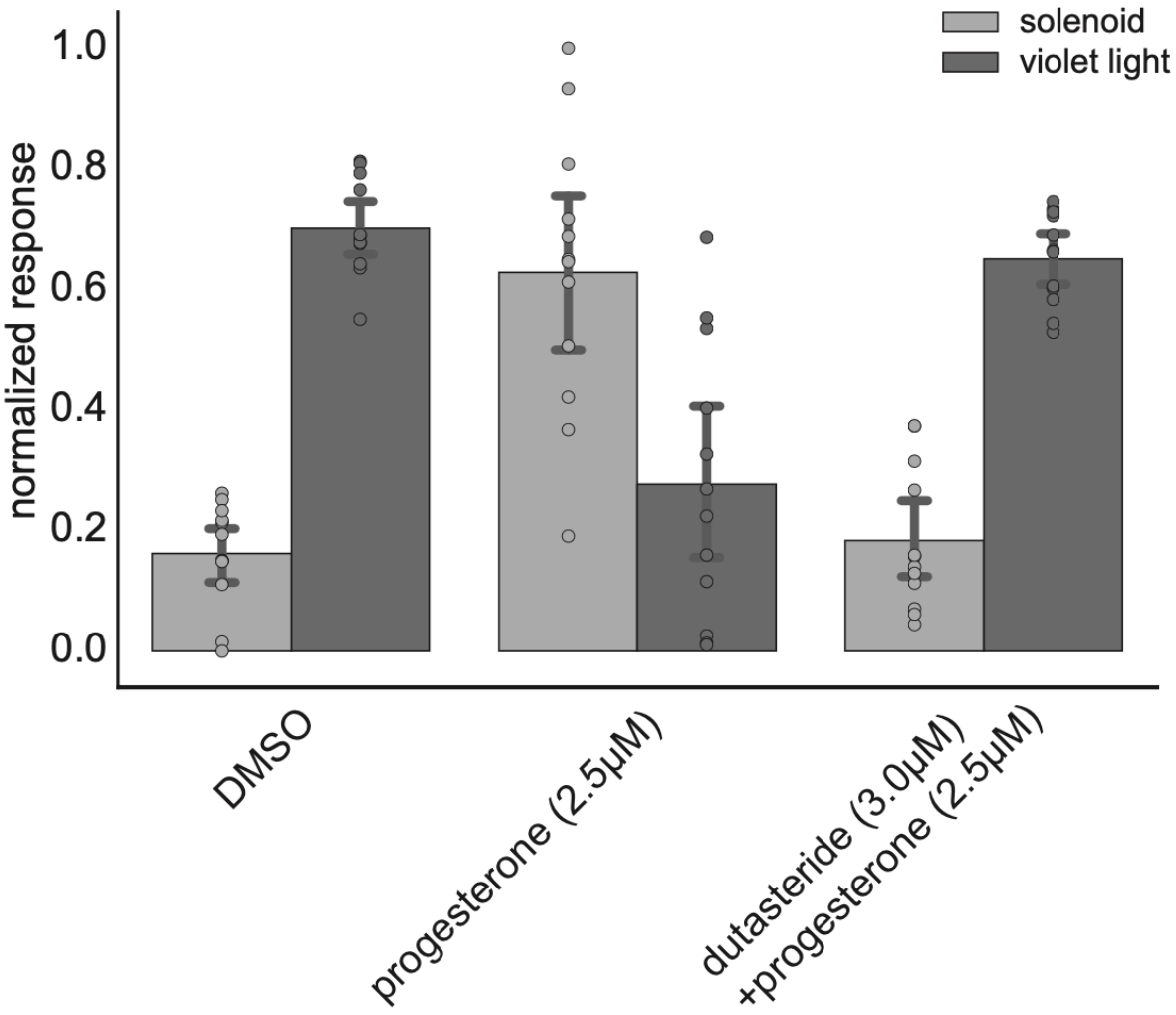

Figure 2.S5. Dutasteride inhibits progesterone-induced eASRs.
The plots show the normalized behavioral responses (y-axis), to acoustic (grey) or light (black) stimuli, in animals treated with the indicated compounds (x-axis).

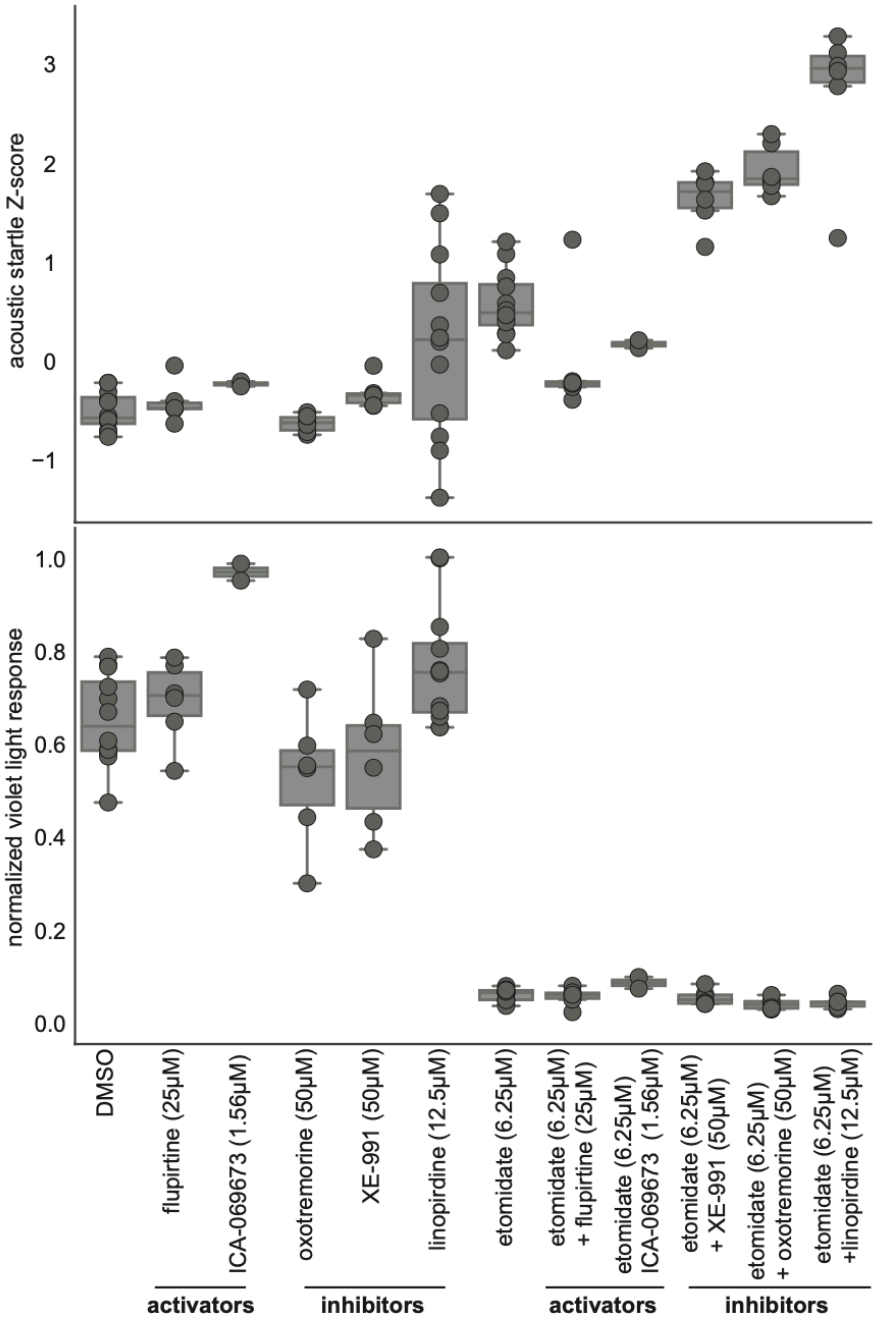

Figure 2.S6. M-current ligands modify eASRs.
Boxplots depicting the motor activity (y-axis) of animals treated with the indicated compounds (x-axis) in response response to acoustic (top) or violet light stimuli (bottom). M-current activators and inhibitors were analyzed alone or combined with etomidate, at the indicated concentrations.

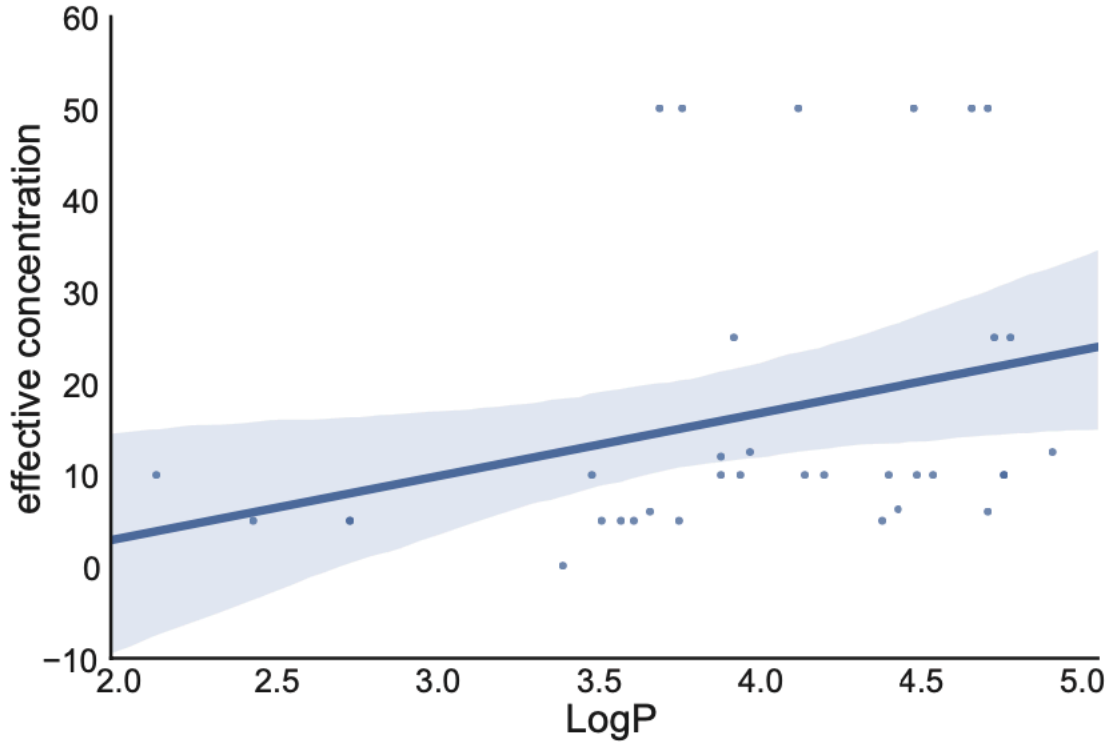

Figure 2.S7. Hit compound efficacy does not correlate with hydrophobicity. Animals were treated with hit compounds. For each compound, the cLogP (calculated partition coefficient) (x-axis) and minimum concentration required to cause the eASR phenotype, were plotted (y-axis). Unlike historical Myer-Overton analyses, the minimum effective concentration does not decrease with hydrophobicity. The best-fit line and shading represent the resulting regression line and a 95% confidence interval for that regression.

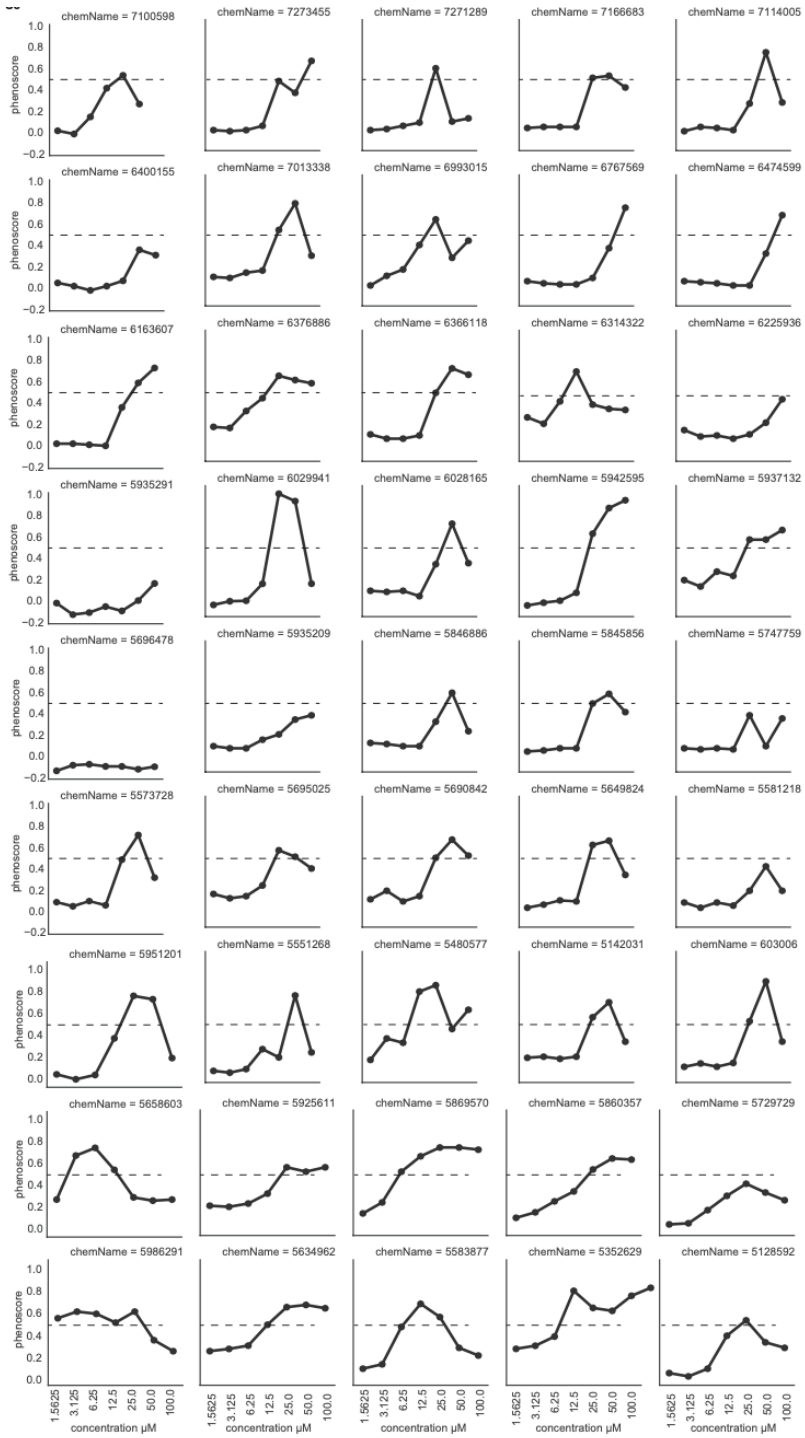

Figure 2.S8. Dose response retest of primary hit compounds.
Average phenoscores (*y*-axis) of zebrafish treated with the indicated compounds (n = 12 wells) at the indicated concentrations (x-axis).

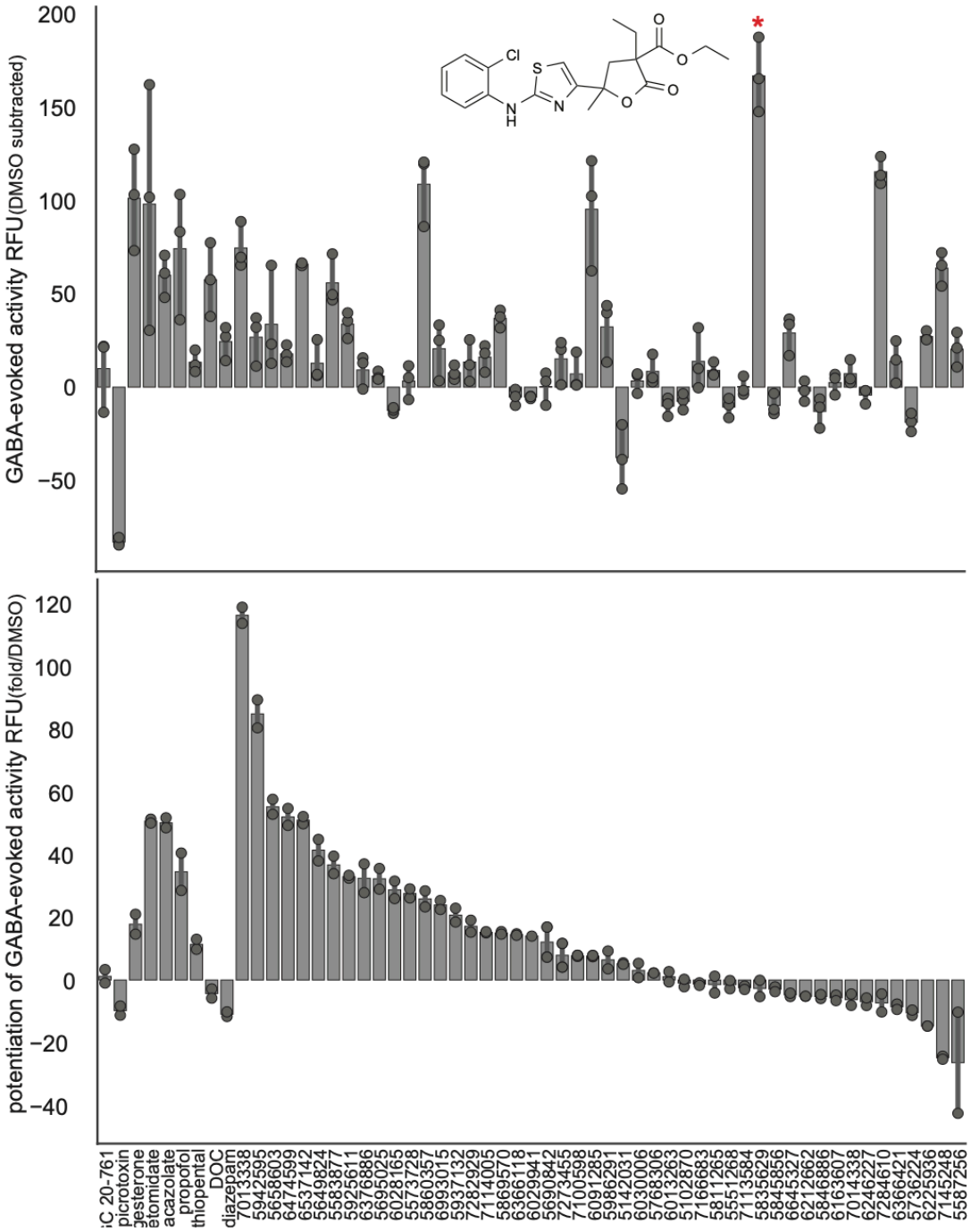

Figure 2.S9. Hit compounds cause direct and indirect activation of GABAARs. Human GABAAR activation (*y*-axis) was measured by FLIPR analysis in random fluorescent units (RFUs). Direct **(a)** and indirect **(b)** activation was analyzed for the indicated hit compounds (x-axis, n = 2-4).

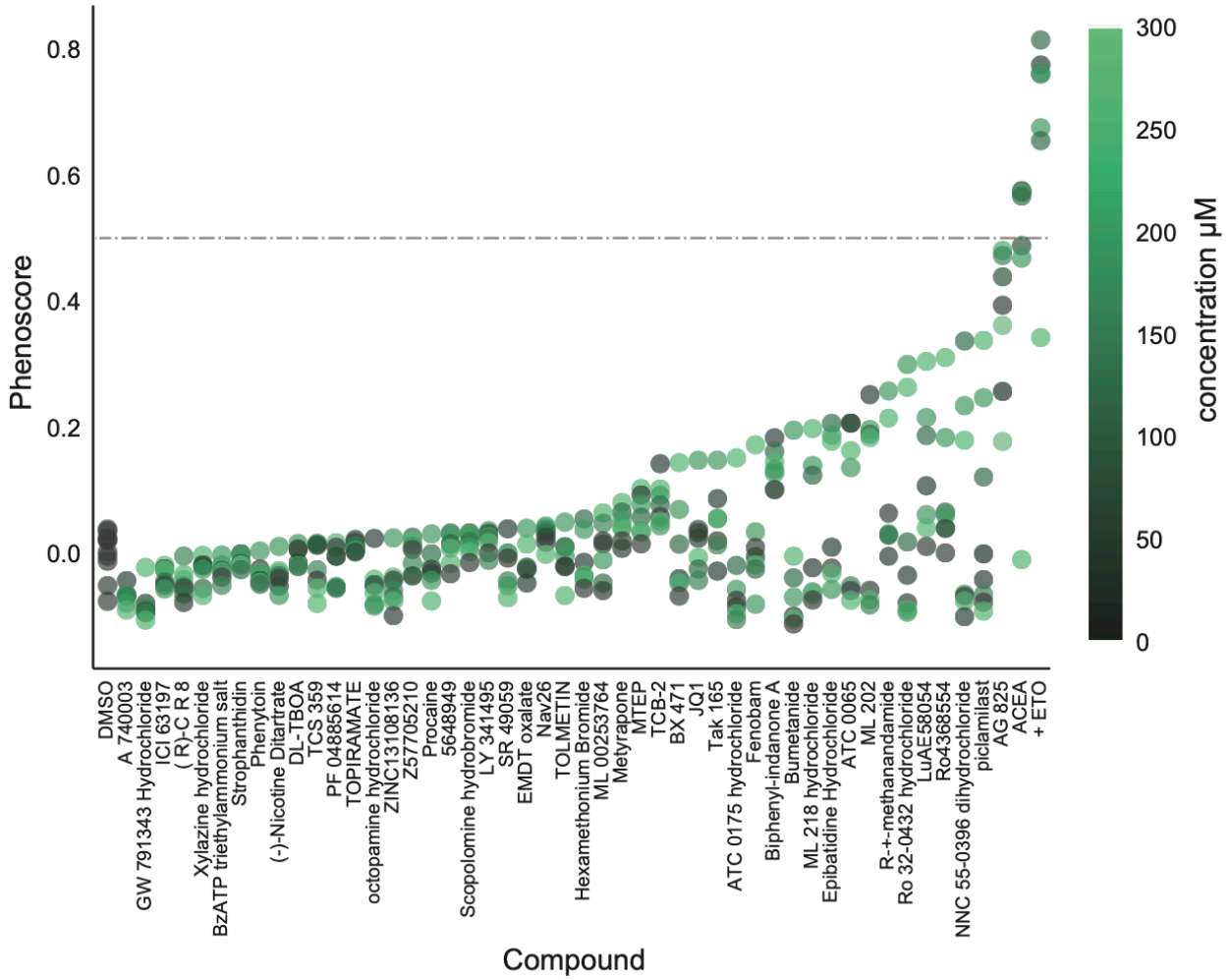

Figure 2.S10. Phenoscores of ligands at targets with low value EFs.
Ligands for targets with low (left of dotted line) and high (right of dotted line) EF scores. The plot shows the phenoscore (y-axis) of the indicated compounds (x-axis). Color bar represents concentration in µM.

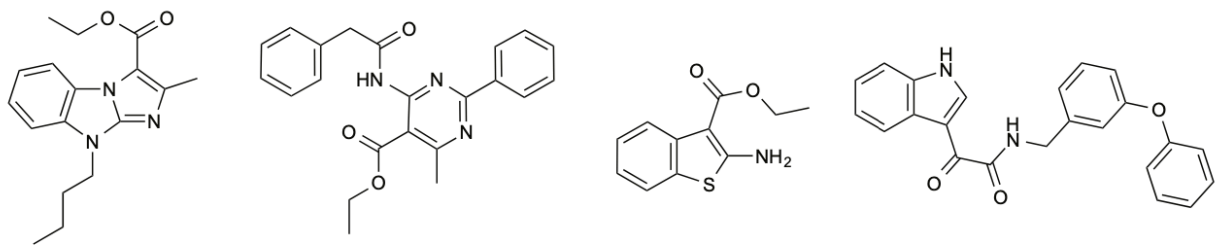

Figure 2.S11. Chemical structures of hit compounds predicted to target GABAARs by SEA.

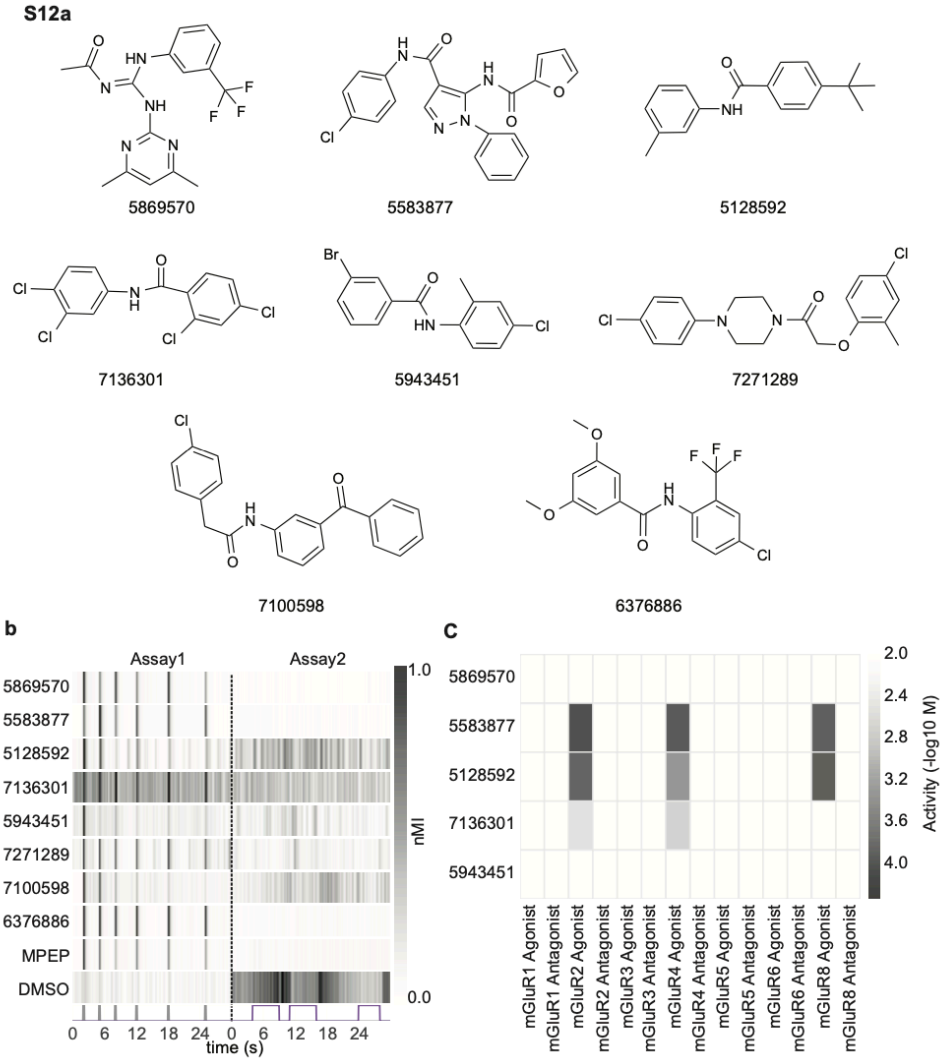

Figure 2.S12. Characterization of hit compounds predicted to target mGluR by SEA.

(a) Chemical structures of 8 hit compounds predicted to target mGluR. **(b)** The heatmap represents the normalized motion index (nMI) of larvae treated with the indicated compounds. Assay 1 is composed of 6 low amplitude acoustic stimuli; Assay 2 is a series of 3 violet light pulses as indicated on the *x*-axis. MPEP is a known mGluR4/5 ligand. Compounds were tested for agonist and antagonist activity in Gq functional assays in-vitro. **(c)** The heat map represents the activity of 5 novel mGluR predicted compounds (y-axis) at the indicated receptor (x-axis). Low-level activation of mGlur2/4 was detected for compounds 5583877, 5128592, and 7136301 (46.13 μM to 2871 μM).

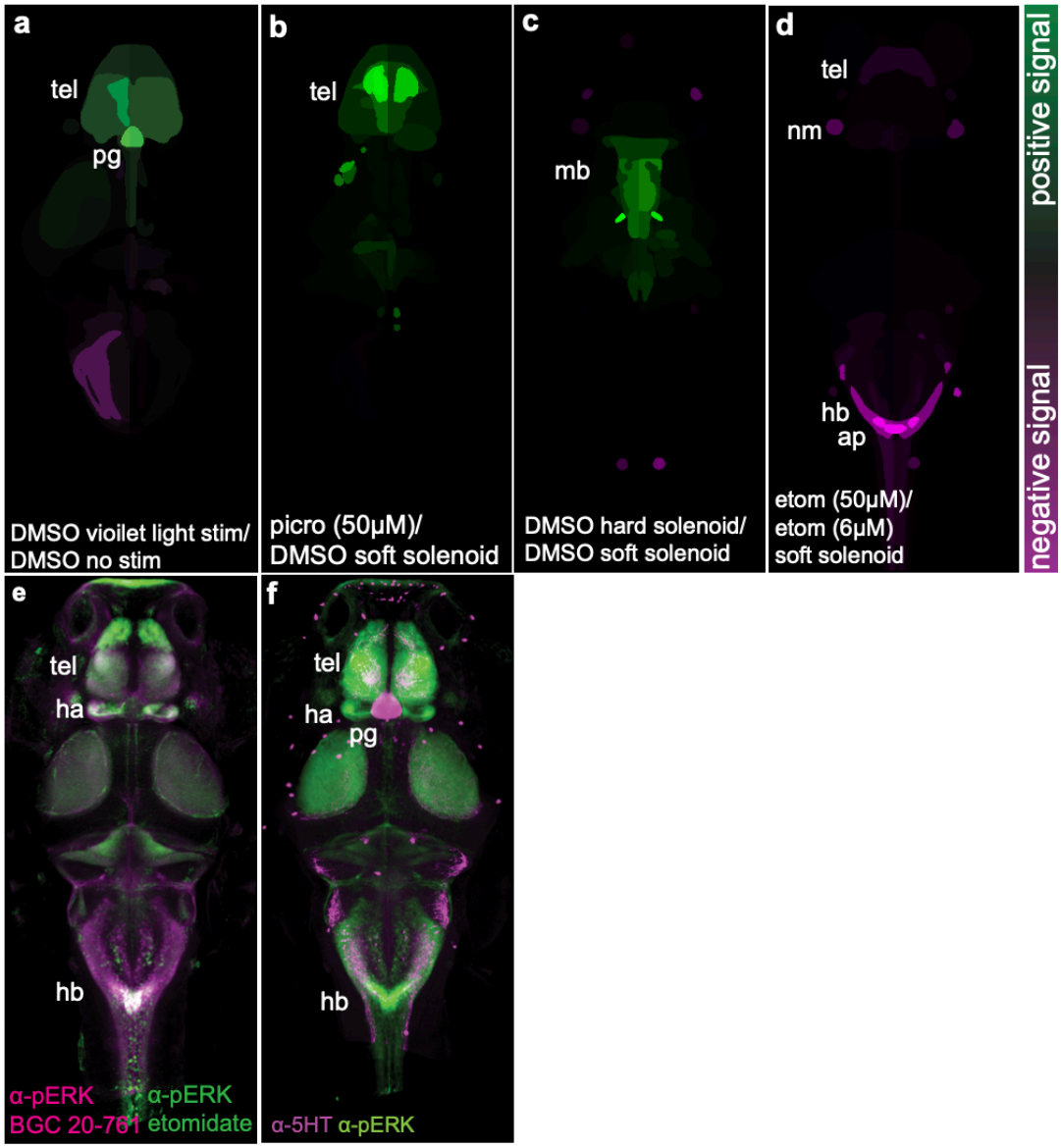

Figure 2.S13. pERK whole brain neural activity maps in control assays and 5-HT immunohistochemistry.
(a-d) Brain activity maps showing significant ΔpERK signals using the Z-brain online reference tool (n = 5-10 animals/condition). Heatmaps indicate positive (green), negative (purple), and nonsignificant (black) changes in pERK labeling ($p < 0.0005$, Mann-Whitney U test). All activity maps are comparisons between the indicated treatment conditions. (**e**) Overlay of average α-pERK signal for BGC 20-761(magenta), and etomidate treated animals (green). (**f**) Overlay of α-5HT staining (magenta) and the average α-pERK staining (green) for BGC 20-761 treatment. Abbreviations: tel, telencephalon; mb, midbrain; ot, optic tectum; hb, hindbrain; ha, habenula; ob, olfactory bulb; nm, neuromast; ap, area postrema; pg, pineal gland.

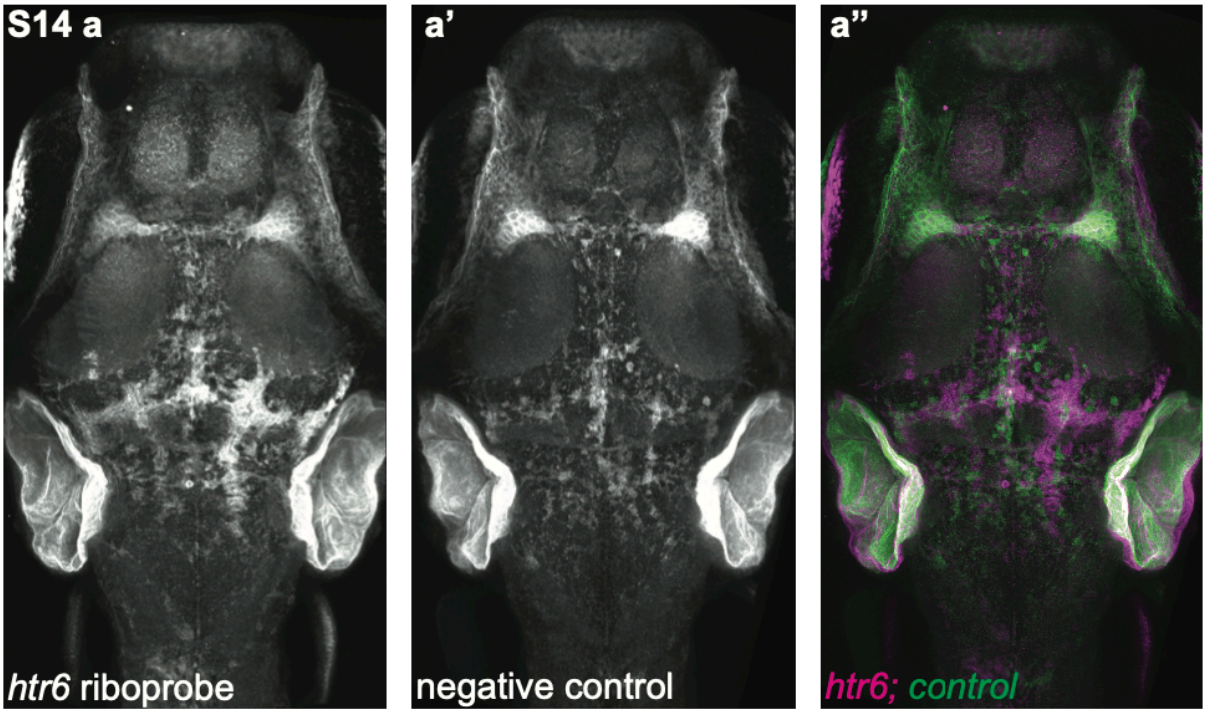

Figure 2.S14. Fluorescent in situ hybridization of the zebrafish *htr6* transcript shows low expression in the telencephalon.
Confocal projections from image registered animals showing transcripts for *htr6* (a) and non-specific negative control antisense probe (a'), overlay in (a'').

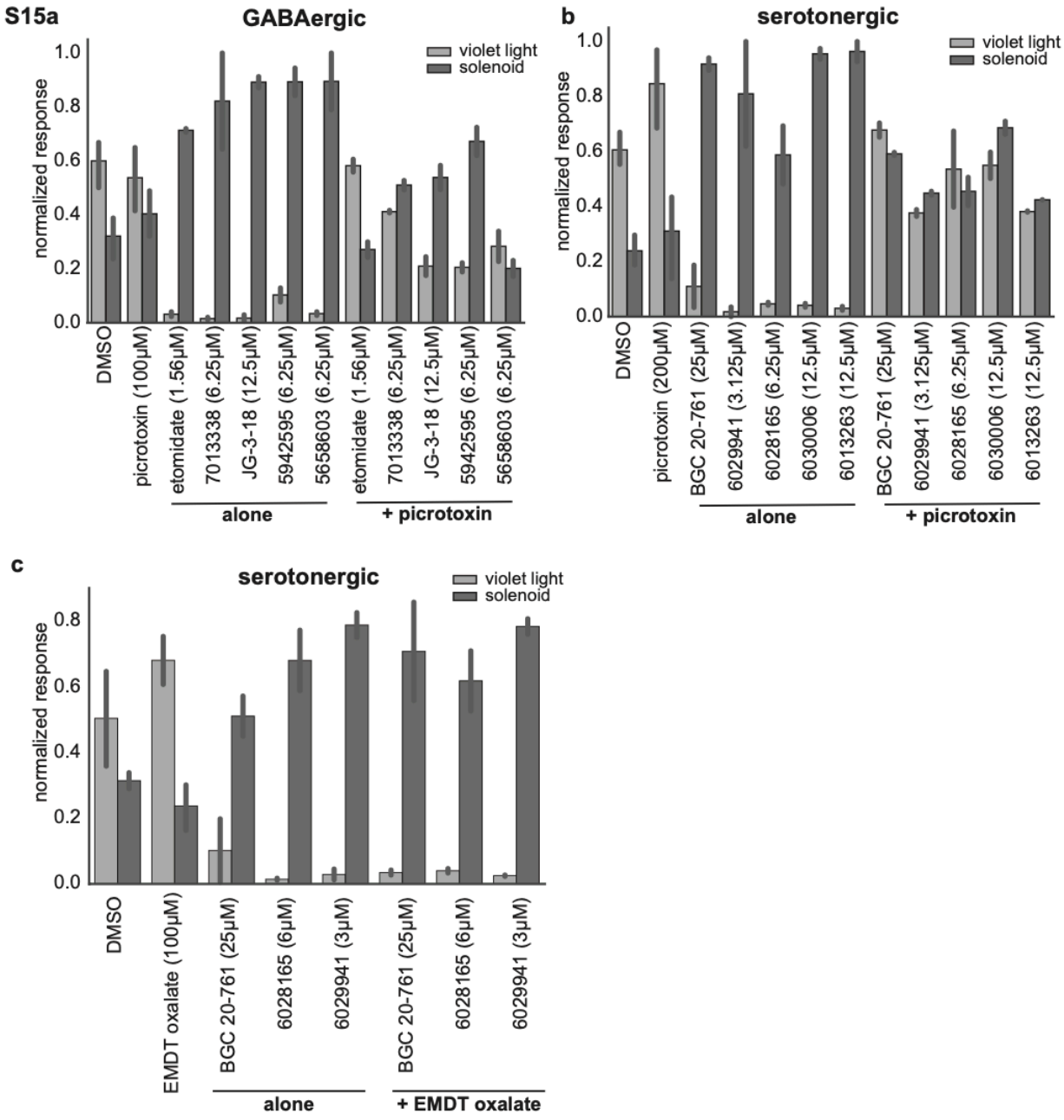

Figure 2.S15. The GABAergic antagonist picrotoxin reverses the eASRs-induced by some ligands, but the serotonergic agonist EMDT does not.
Normalized behavioral responses (y-axis) of animals treated with the indicated compounds (x-axis).

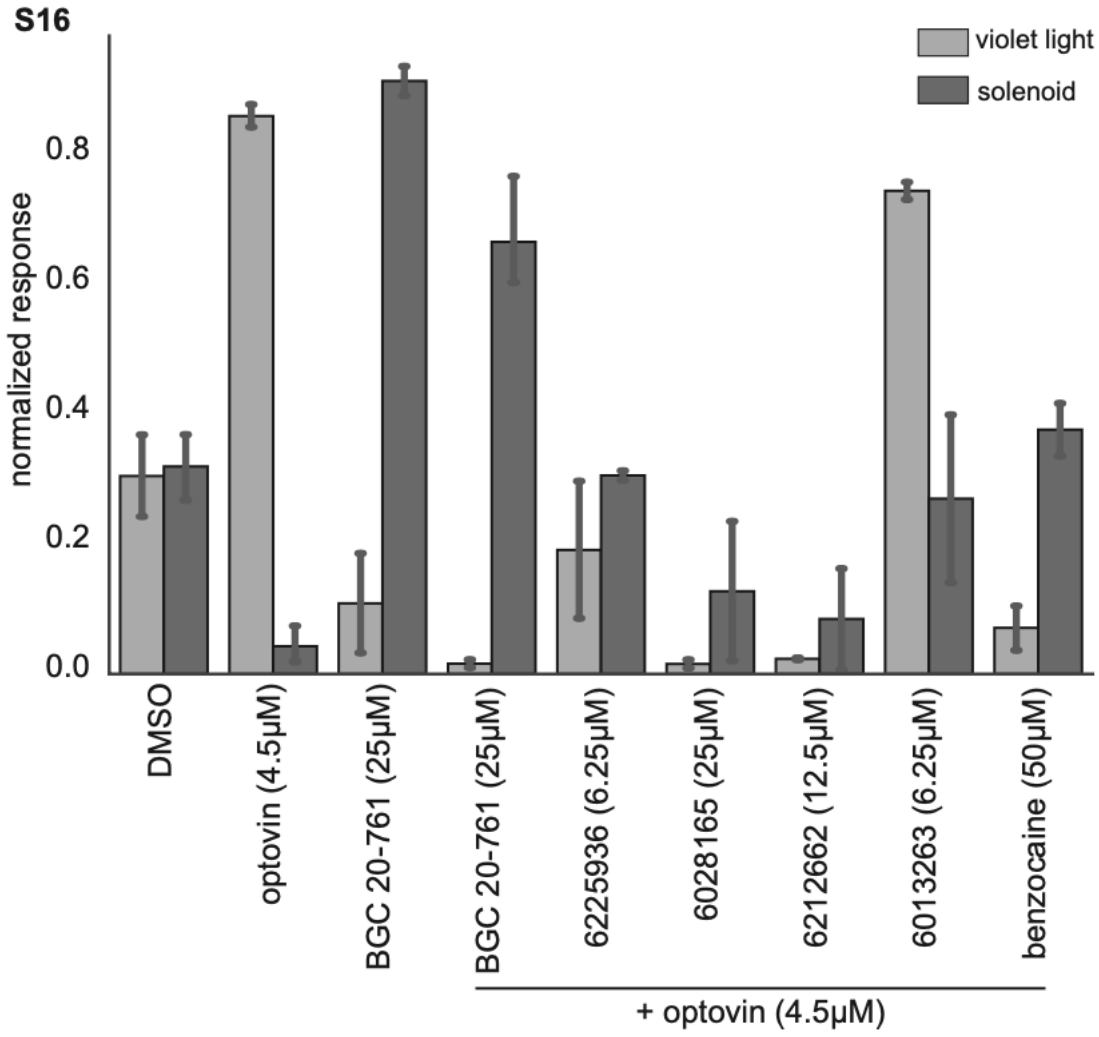

Figure 2.S16. Serotonergic hit compounds inhibit optovin response.
Normalized behavioral response (y-axis) of animals treated with the indicated compounds (x-axis).

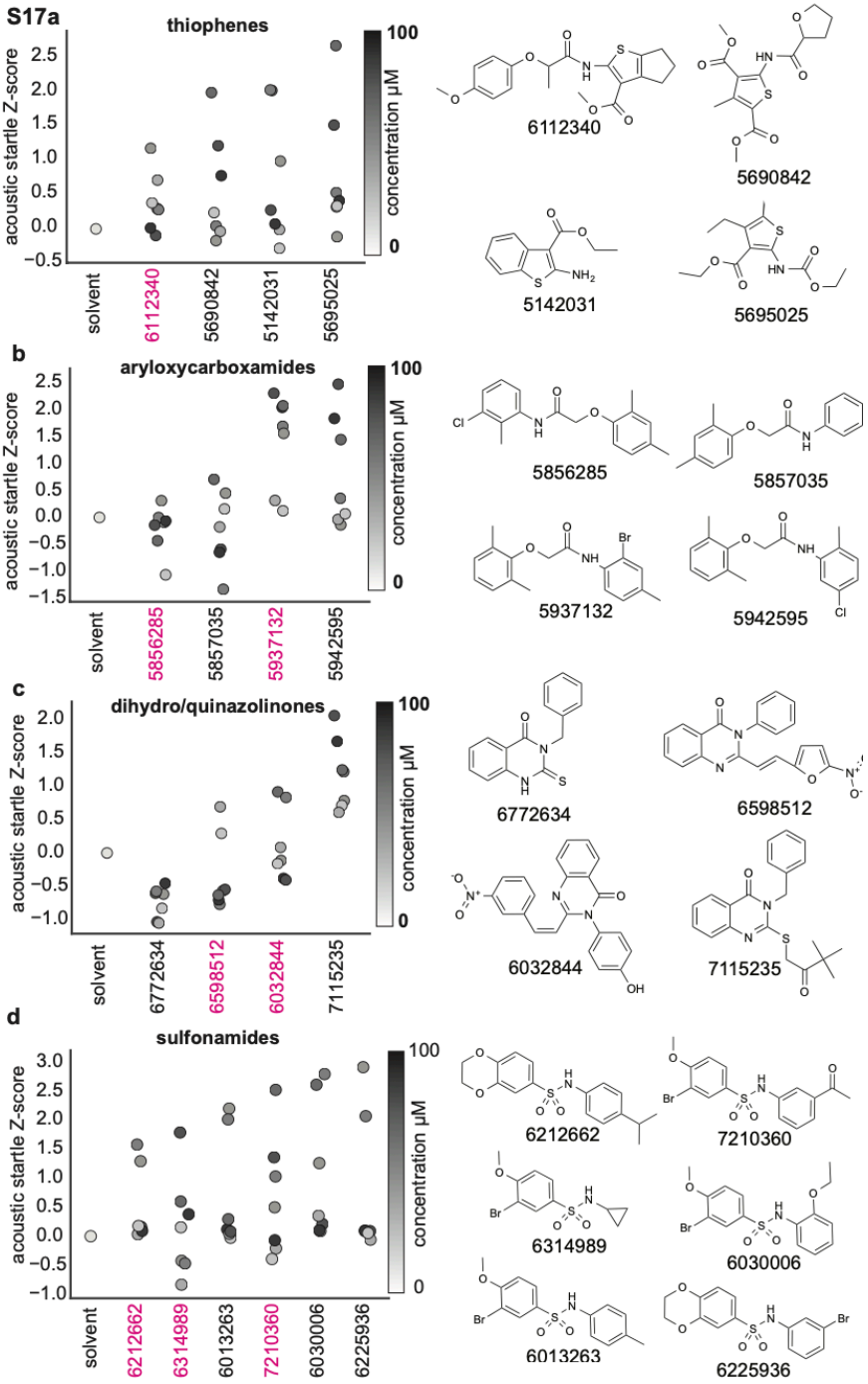

Figure 2.S17. Preliminary SAR of key compound classes.
(a-d) The plots show the Z-score of the acoustic startle response (y-axis) in animals treated with the indicated compounds (x- axis). The compound structures in each class are shown to the right of each plot including the original hit compounds (black) and their analogs (red). Many analogs did not cause the eASR behaviors.

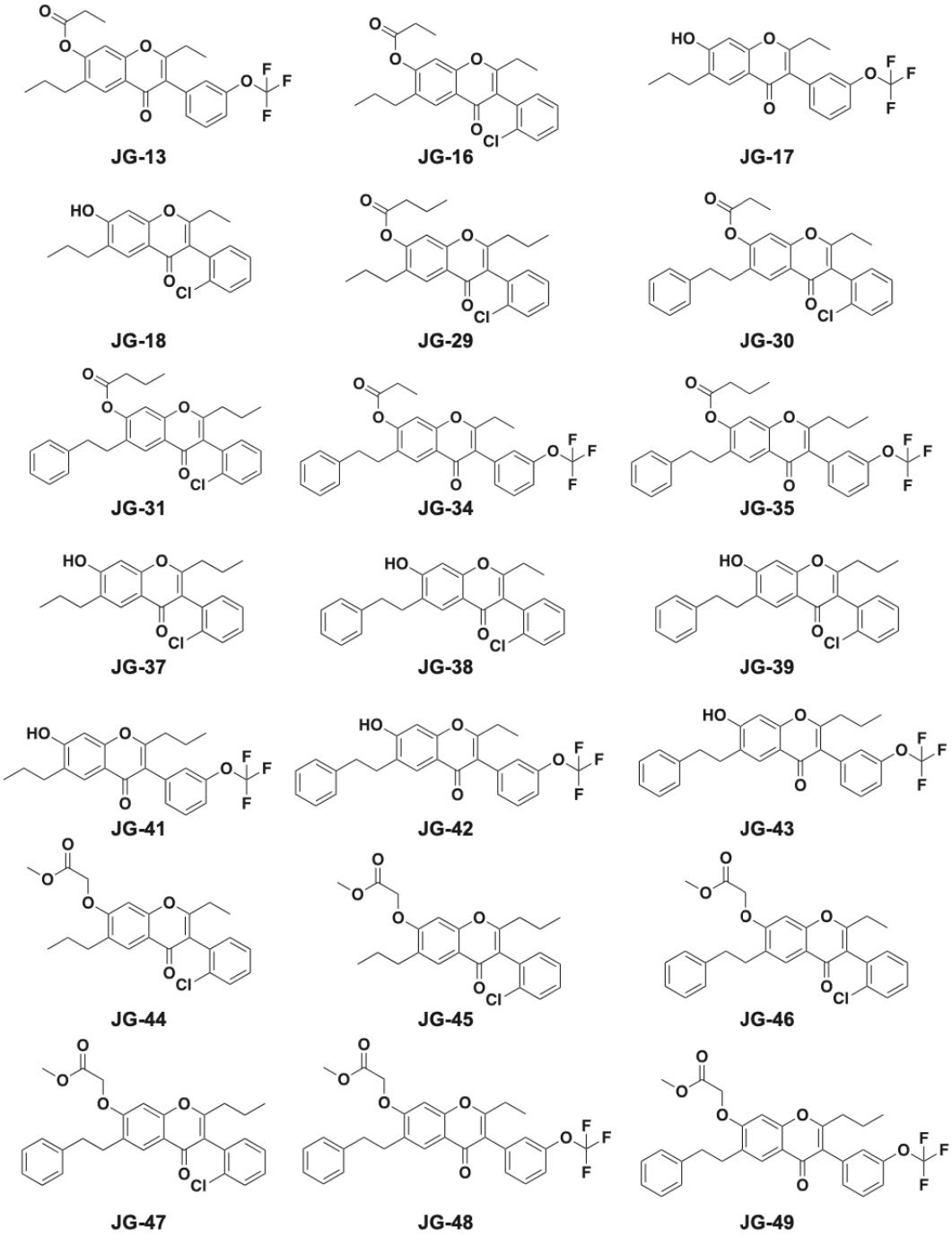

Figure 2.S18. Chemical structures of isoflavone analogs.

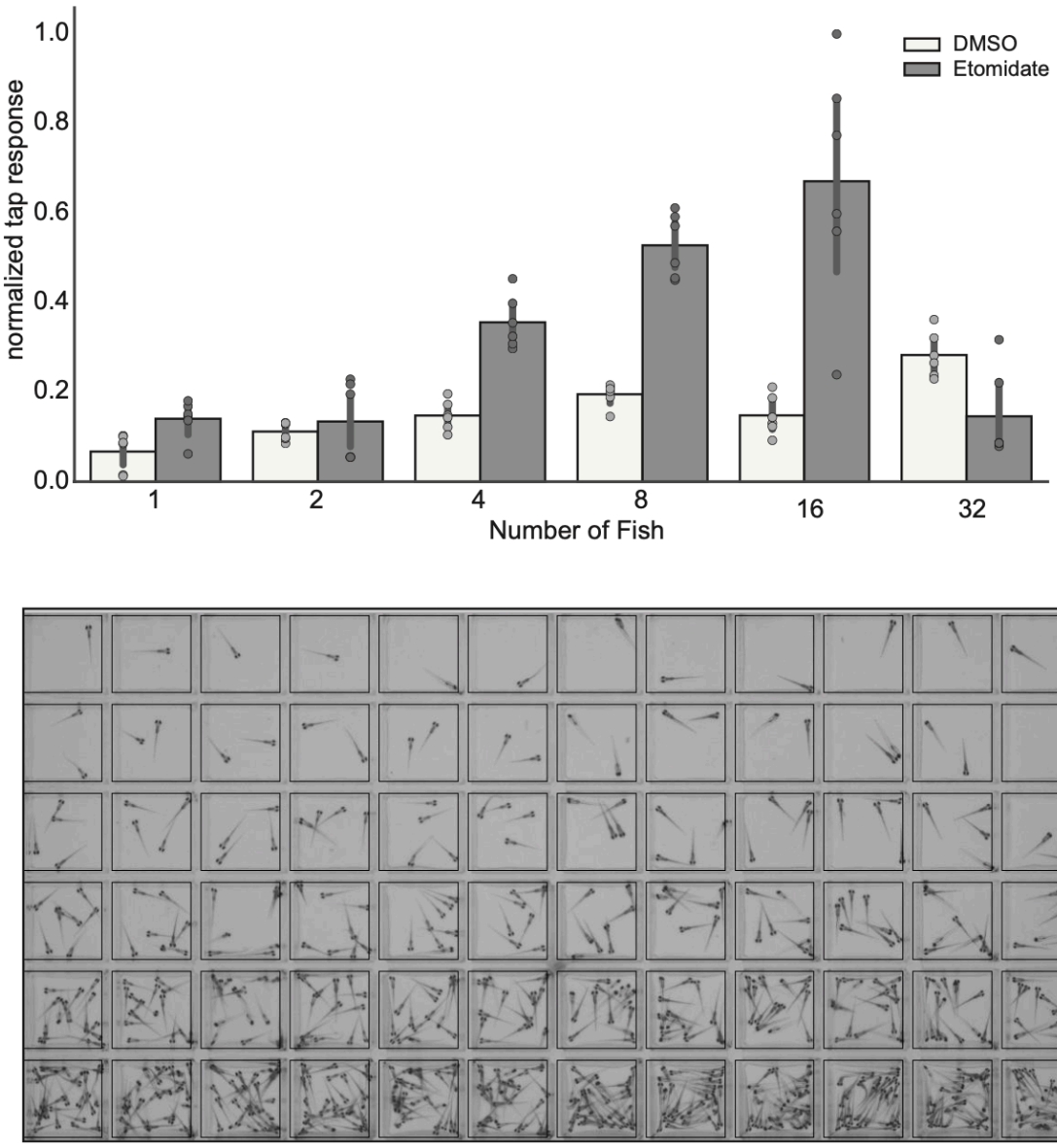

Figure 2.S19. Group size affects eASR quantification.
To determine the impact of group size on this assay, we analyzed eASR behaviors from animals in different group sizes (1, 2, 4, 8, 12, 16, 32 animals per well). Groups of 8 and 16 animals generated the most robust MI values. Here, we chose to use 8 animals per group because it balanced a small group size with high signal to noise using the MI metric. **(a)** Bar graph illustrating the average tap response (*y*-axis) per tap stimulus (each marker represents one of 6 total stimuli averaged over 6 replicate wells), for wells with the indicated number of fish larvae (*x*-axis) and treated with DMSO control or 6μM etomidate, as indicated. **(b)** Representative image of wells containing increasing numbers of animals.

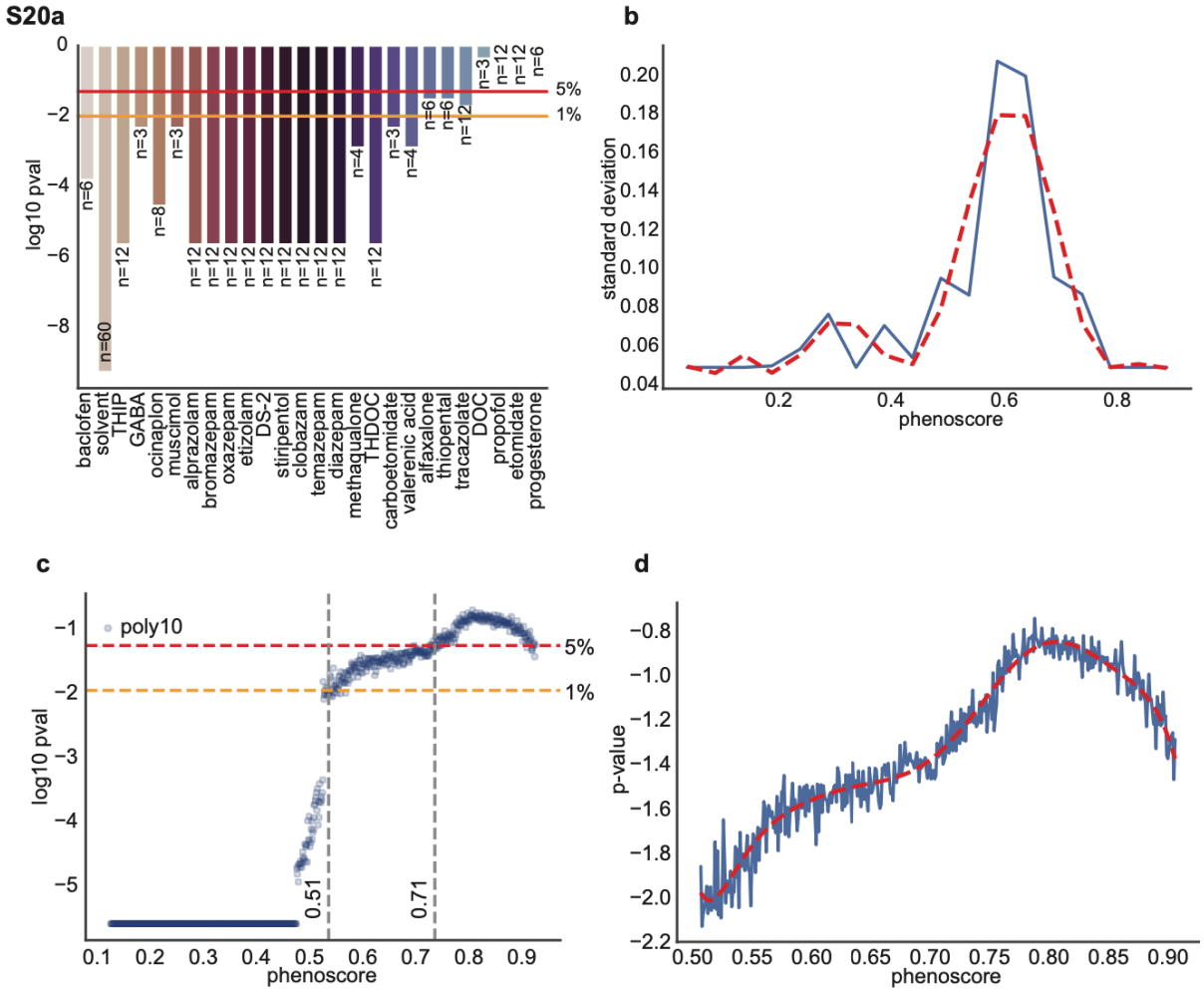

Figure 2.S20. Statistical analysis of phenotypic thresholds for GABA$_A$R ligands. **(a)** This plot shows the Kolmogorov-Smirnov (KS Test) statistic for the highest-scoring profiles produced by the indicated treatments *(y*-axis). On the x-axis, the ligands are sorted in order of ascending average phenoscore (left to right) from lowest to highest. Horizontal lines on the *y*-axis indicate the 1% (yellow) and 5% (red) *P* value significance thresholds **(b)** Plot showing the standard deviations for GABAAR ligands as a function of phenoscore with a 10th order polynomial. **(c)** Plot showing simulated *P* values as a function of phenoscore. Horizontal dashed lines indicate 1% and 5% P value thresholds, and vertical lines indicate the phenoscores at which these thresholds are met (0.51 and 0.71, respectively). **(d)** Plot showing a 10th order polynomial fit for the smooth region of the simulation where phenoscore > 0.5 in panel (c).

2.8 Tables

Supplemental Table 2.1. CNS depressants characterized on zebrafish larval behavior.

class ID	chemical name	class	citation
1	carbamazepine	anticonvulsant	19
1	phenytoin	anticonvulsant	20
2	fluoxetine	antidepressant	21
2	trazodone	antidepressant	22
3	diphenhydramine	antihistamine	23
3	dimenhydrinate	antihistamine	23
3	promethazine	antihistamine	23
4	buspirone	anxiolytic	24
4	alprazolam	anxiolytic	25
4	diazepam	anxiolytic	26
4	oxazepam	anxiolytic	27
5	quetiapine	atypical antipsychotic	28
5	olanzapine	atypical antipsychotic	29
6	atenolol	beta blocker	30
6	propranolol	beta blocker	31
7	ACPA	cannabinoid	32
7	methanandamide	cannabinoid	33
8	zolpidem	hypnotic	34
9	benzocaine	local anesthetic	35
9	lidocaine	local anesthetic	39
9	bupivacaine	local anesthetic	40
9	tricaine	local anesthetic	41
9	procaine	local anesthetic	42
10	ketamine	intravenous anesthetic	38
10	isoflurane	inhalational anesthetic	35
10	propofol	intravenous anesthetic	36
10	etomidate	intravenous anesthetic	37

Supplemental Table 2.2. Viability of anesthetic treated animals

treatment	concentration	alive/total 10 min	alive/total 1 hour	alive/total 5 hours
DMSO	0 μM	100/100	100/100	100/100
etomidate	3 μM	100/100	100/100	100/100
etomidate	6 μM	100/100	100/100	100/100
etomidate	12 μM	100/100	100/100	98/100
propofol	3 μM	100/100	100/100	100/100
propofol	6 μM	100/100	100/100	100/100
propofol	12 μM	100/100	100/100	99/100

Supplemental Table 2.3. GABAAR ligand reference set

Chemical Name	Class	Reference
dmso	vehicle control	NA
baclofen	$GABA_B$ agonist	4
GABA	orthosteric $GABA_AR$ agonist	5
muscimol	orthosteric $GABA_AR$ agonist	6
gaboxadol (THIP)	$GABA_AR$ delta subtype preferring PAM	7
DS-2	$GABA_AR$ delta subtype preferring PAM	7
ocinaplon	$GABA_AR$ BZ-site PAM	11
bromazepam	$GABA_AR$ BZ-site PAM	8
etizolam	$GABA_AR$ BZ-site PAM	12
alprazolam	$GABA_AR$ BZ-site PAM	5
oxazepam	$GABA_AR$ BZ-site PAM	8
clobazam	$GABA_AR$ BZ-site PAM	9
temazepam	$GABA_AR$ BZ-site PAM	10
diazepam	$GABA_AR$ BZ-site PAM	5
stripentol	$GABA_AR$ non BZ-site PAM	14
methaqualone	$GABA_AR$ non BZ-site PAM	15
valerinic acid	$GABA_AR$ non BZ-site PAM	16
thiopental	$GABA_AR$ non BZ-site PAM	18
tracazolate	$GABA_AR$ non BZ-site PAM	13
carboetomidate	$GABA_AR$ anesthetic PAM	18
propofol	$GABA_AR$ anesthetic PAM	18
etomidate	$GABA_AR$ anesthetic PAM	18
tetrahydrodeoxycorticosterone (THDOC)	$GABA_AR$ neurosteroid PAM	17
alphaxalone	$GABA_AR$ neurosteroid PAM	17
progesterone	$GABA_AR$ neurosteroid PAM	17
deoxycorticosterone (DOC)	$GABA_AR$ neurosteroid PAM	17

2.9 References

1. Jeong S, et al. Increase of paradoxical excitement response during propofol-induced sedation in hazardous and harmful alcohol drinkers. *Br. J. Anaesth.* 2011;107:930–933. doi: 10.1093/bja/aer275.
2. McCarthy MM, Brown EN, Kopell N. Potential network mechanisms mediating electroencephalographic beta rhythm changes during propofol-induced paradoxical excitation. *J. Neurosci.* 2008;28:13488–13504. doi: 10.1523/JNEUROSCI.3536-08.2008.
3. Sneyd JR. Excitatory events associated with propofol anaesthesia: a review. *J. R. Soc. Med.* 1992;85:288–291.
4. Fulton SA, Mullen KD. Completion of upper endoscopic procedures despite paradoxical reaction to midazolam: a role for flumazenil? *Am. J. Gastroenterol.* 2000;95:809–811. doi: 10.1111/j.1572-0241.2000.01866.x.
5. Zuleta-Alarcon A, et al. Anesthesia-related perioperative seizures: pathophysiology, predisposing factors and practical recommendations. *Austin J. Anesth. Analg.* 2014;2:1026.
6. Mancuso CE, Tanzi MG, Gabay M. Paradoxical reactions to benzodiazepines: literature review and treatment options. *Pharmacotherapy.* 2004;24:1177–1185. doi: 10.1592/phco.24.13.1177.38089.
7. Massanari M, Novitsky J, Reinstein LJ. Paradoxical reactions in children associated with midazolam use during endoscopy. *Clin. Pediatr.* 1997;36:681–684. doi: 10.1177/000992289703601202.

8. Orser BA, Canning KJ, Macdonald JF. Mechanisms of general anesthesia. *Curr. Opin. Anaesthesiol.* 2002;15:427–433. doi: 10.1097/00001503-200208000-00004.
9. Sachs BD, et al. The effects of brain serotonin deficiency on behavioural disinhibition and anxiety-like behaviour following mild early life stress. *Int. J. Neuropsychopharmacol.* 2013;16:2081–2094. doi: 10.1017/S1461145713000321.
10. Pothakos K, et al. Decreased serotonin levels associated with behavioral disinhibition in tissue plasminogen activator deficient (tPA-/-) mice. *Brain Res.* 2010;1326:135–142. doi: 10.1016/j.brainres.2009.12.095.
11. Fickbohm DJ, Katz PS. Paradoxical actions of the serotonin precursor 5-hydroxytryptophan on the activity of identified serotonergic neurons in a simple motor circuit. *J. Neurosci.* 2000;20:1622–1634. doi: 10.1523/JNEUROSCI.20-04-01622.2000.
12. Yun H-M, Rhim H. The serotonin-6 receptor as a novel therapeutic target. *Exp. Neurobiol.* 2011;20:159–168. doi: 10.5607/en.2011.20.4.159.
13. Griffin A, et al. Clemizole and modulators of serotonin signalling suppress seizures in Dravet syndrome. *Brain.* 2017;140:669–683.
14. Dinday, M. T. & Baraban, S. C. Large-scale phenotype-based antiepileptic drug screening in a zebrafish model of dravet syndrome. *eNeuro***2**, pii: ENEURO.0068-15 (2015).
15. Monti JM. Serotonin 5-HT(2A) receptor antagonists in the treatment of insomnia: present status and future prospects. *Drugs Today.* 2010;46:183–193. doi: 10.1358/dot.2010.46.3.1437247.

16. Matsunaga F, et al. Molecular interactions between general anesthetics and the 5HT2B receptor. *J. Biomol. Struct. Dyn.* 2015;33:211–218. doi: 10.1080/07391102.2013.869483.
17. James R, Glen JB. Synthesis, biological evaluation, and preliminary structure-activity considerations of a series of alkylphenols as intravenous anesthetic agents. *J. Med. Chem.* 1980;23:1350–1357. doi: 10.1021/jm00186a013.
18. Mathur P, Guo S. Use of zebrafish as a model to understand mechanisms of addiction and complex neurobehavioral phenotypes. *Neurobiol. Dis.* 2010;40:66–72. doi: 10.1016/j.nbd.2010.05.016.
19. Cocco A, et al. Characterization of the γ-aminobutyric acid signaling system in the zebrafish (Danio rerio Hamilton) central nervous system by reverse transcription-quantitative polymerase chain reaction. *Neuroscience.* 2017;343:300–321. doi: 10.1016/j.neuroscience.2016.07.018.
20. Monesson-Olson B, et al. Expression of the eight GABAA receptor α subunits in the developing zebrafish central nervous system. *PLoS One.* 2018;13:e0196083. doi: 10.1371/journal.pone.0196083.
21. Panula P, et al. The comparative neuroanatomy and neurochemistry of zebrafish CNS systems of relevance to human neuropsychiatric diseases. *Neurobiol. Dis.* 2010;40:46–57. doi: 10.1016/j.nbd.2010.05.010.
22. Norton WHJ, Folchert A, Bally-Cuif L. Comparative analysis of serotonin receptor (HTR1A/HTR1B families) and transporter (slc6a4a/b) gene expression in the zebrafish brain. *J. Comp. Neurol.* 2008;511:521–542. doi: 10.1002/cne.21831.

23. Bruni G, et al. Zebrafish behavioral profiling identifies multitarget antipsychotic-like compounds. *Nat. Chem. Biol.* 2016;12:559–566. doi: 10.1038/nchembio.2097.
24. Kokel D, et al. Photochemical activation of TRPA1 channels in neurons and animals. *Nat. Chem. Biol.* 2013;9:257–263. doi: 10.1038/nchembio.1183.
25. Rihel J, et al. Zebrafish behavioral profiling links drugs to biological targets and rest/wake regulation. *Science.* 2010;327:348–351. doi: 10.1126/science.1183090.
26. Wolman MA, Jain RA, Liss L, Granato M. Chemical modulation of memory formation in larval zebrafish. *Proc. Natl Acad. Sci. USA.* 2011;108:15468–15473. doi: 10.1073/pnas.1107156108.
27. Hill-Venning C, Belelli D, Peters JA, Lambert JJ. Subunit-dependent interaction of the general anaesthetic etomidate with the gamma-aminobutyric acid type A receptor. *Br. J. Pharm.* 1997;120:749–756. doi: 10.1038/sj.bjp.0700927.
28. McCarthy MM, Brown EN, Kopell N. Potential network mechanisms mediating electroencephalographic beta rhythm changes during propofol-induced paradoxical excitation. *J. Neurosci.* 2008;28:13488–13504. doi: 10.1523/JNEUROSCI.3536-08.2008.
29. Kornhuber J, et al. [Neuronal potassium channel opening with flupirtine] *Fortschr. Neurol. Psychiatr.* 1999;67:466–475. doi: 10.1055/s-2007-994997.
30. Popovici F, Dorostkar M, Boehm S. The non-opioid analgesic flupirtine is a modulator of GABAA receptors involved in pain sensation. *BMC Pharmacol.* 2008;8:A14. doi: 10.1186/1471-2210-8-S1-A14.
31. Devulder J. Flupirtine in pain management: pharmacological properties and clinical use. *CNS Drugs.* 2010;24:867–881. doi: 10.2165/11536230-000000000-00000.

32. Amato G, et al. N-Pyridyl and pyrimidine benzamides as KCNQ2/Q3 potassium channel openers for the treatment of epilepsy. *ACS Med. Chem. Lett.* 2011;2:481–484. doi: 10.1021/ml200053x.
33. Pérez C, Limón A, Vega R, Soto E. The muscarinic inhibition of the potassium M-current modulates the action-potential discharge in the vestibular primary-afferent neurons of the rat. *Neuroscience.* 2009;158:1662–1674. doi: 10.1016/j.neuroscience.2008.11.023.
34. Luk KC, Stern L, Weigele M, O'Brien RA, Spirt N. Isolation and identification of 'diazepam-like' compounds from bovine urine. *J. Nat. Prod.* 1983;46:852–861. doi: 10.1021/np50030a005.
35. Lounkine E, et al. Large-scale prediction and testing of drug activity on side-effect targets. *Nature.* 2012;486:361–367. doi: 10.1038/nature11159.
36. Papadopoulos V, Lecanu L, Brown RC, Han Z, Yao Z-X. Peripheral-type benzodiazepine receptor in neurosteroid biosynthesis, neuropathology and neurological disorders. *Neuroscience.* 2006;138:749–756. doi: 10.1016/j.neuroscience.2005.05.063.
37. Papadopoulos V, Mukhin AG, Costa E, Krueger KE. The peripheral-type benzodiazepine receptor is functionally linked to Leydig cell steroidogenesis. *J. Biol. Chem.* 1990;265:3772–3779.
38. Randlett O, et al. Whole-brain activity mapping onto a zebrafish brain atlas. *Nat. Methods.* 2015;12:1039–1046. doi: 10.1038/nmeth.3581.

39. Biacabe B, Chevallier JM, Avan P, Bonfils P. Functional anatomy of auditory brainstem nuclei: application to the anatomical basis of brainstem auditory evoked potentials. *Auris Nasus Larynx.* 2001;28:85–94.
40. Longatti P, et al. The human area postrema: clear-cut silhouette and variations shown in vivo. *J. Neurosurg.* 2015;122:989–995. doi: 10.3171/2014.11.JNS14482.
41. Kremeyer B, et al. A gain-of-function mutation in TRPA1 causes familial episodic pain syndrome. *Neuron.* 2010;66:671–680. doi: 10.1016/j.neuron.2010.04.030.
42. Kissin I, McGee T, Smith LR. The indices of potency for intravenous anaesthetics. *Can. Anaesth. Soc. J.* 1981;28:585–590. doi: 10.1007/BF03007157.
43. Gavande N, Karim N, Johnston GAR, Hanrahan JR, Chebib M. tors. *ChemMedChem.* 2011;6:1340–1346. doi: 10.1002/cmdc.201100120.
44. Ward RP, et al. Localization of serotonin subtype 6 receptor messenger RNA in the rat brain by in situ hybridization histochemistry. *Neuroscience.* 1995;64:1105–1111. doi: 10.1016/0306-4522(94)00439-C.
45. Brouard JT, et al. Pharmacological evidence for 5-HT6 receptor modulation of 5-HT neuron firing in vivo. *ACS Chem. Neurosci.* 2015;6:1241–1247. doi: 10.1021/acschemneuro.5b00061.
46. Garfield AS, Burke LK, Shaw J, Evans ML, Heisler LK. Distribution of cells responsive to 5-HT6 receptor antagonist-induced hypophagia. *Behav. Brain Res.* 2014;266:201–206. doi: 10.1016/j.bbr.2014.02.018.
47. Morairty SR, Hedley L, Flores J, Martin R, Kilduff TS. Selective 5HT2A and 5HT6 receptor antagonists promote sleep in rats. *Sleep.* 2008;31:34–44. doi: 10.1093/sleep/31.1.34.

48. Wesołowska A, Nikiforuk A. Effects of the brain-penetrant and selective 5-HT6 receptor antagonist SB-399885 in animal models of anxiety and depression. *Neuropharmacology.* 2007;52:1274–1283. doi: 10.1016/j.neuropharm.2007.01.007.
49. Routledge C, et al. Characterization of SB-271046: a potent, selective and orally active 5-HT6 receptor antagonist. *Br. J. Pharm.* 2000;130:1606–1612. doi: 10.1038/sj.bjp.0703457.
50. Setola V, Roth BL. Why mice are neither miniature humans nor small rats: a cautionary tale involving 5-hydroxytryptamine-6 serotonin receptor species variants. *Mol. Pharmacol.* 2003;64:1277–1278. doi: 10.1124/mol.64.6.1277.
51. Atri A, et al. Effect of idalopirdine as adjunct to cholinesterase inhibitors on change in cognition in patients with Alzheimer disease: three randomized clinical trials. *JAMA.* 2018;319:130–142. doi: 10.1001/jama.2017.20373.
52. Gulledge AT, Stuart GJ. Excitatory actions of GABA in the cortex. *Neuron.* 2003;37:299–309. doi: 10.1016/S0896-6273(02)01146-7.
53. Richardson BD, Ling LL, Uteshev VV, Caspary DM. Reduced GABA(A) receptor-mediated tonic inhibition in aged rat auditory thalamus. *J. Neurosci.* 2013;33:1218–27a. doi: 10.1523/JNEUROSCI.3277-12.2013.
54. Muir WW, 3rd, Mason DE. Side effects of etomidate in dogs. *J. Am. Vet. Med. Assoc.* 1989;194:1430–1434.
55. Arrenberg AB, Del Bene F, Baier H. Optical control of zebrafish behavior with halorhodopsin. *Proc. Natl. Acad. Sci. U. S. A.* 2009;106:17968–17973. doi: 10.1073/pnas.0906252106.

56. Del Bene F, et al. Filtering of visual information in the tectum by an identified neural circuit. *Science.* 2010;330:669–673. doi: 10.1126/science.1192949.

57. Ahring PK, et al. A pharmacological assessment of agonists and modulators at α4β2γ2 and α4β2δ GABAA receptors: The challenge in comparing apples with oranges. *Pharmacol. Res.* 2016;111:563–576. doi: 10.1016/j.phrs.2016.05.014.

58. Zeller A, Arras M, Jurd R, Rudolph U. Mapping the contribution of beta3-containing GABAA receptors to volatile and intravenous general anesthetic actions. *BMC Pharmacol.* 2007;7:2. doi: 10.1186/1471-2210-7-2.

59. Gee KW, et al. Limiting activity at beta1-subunit-containing GABAA receptor subtypes reduces ataxia. *J. Pharmacol. Exp. Ther.* 2010;332:1040–1053. doi: 10.1124/jpet.109.161885.

60. Golparvar M, Saghaei M, Sajedi P, Razavi SS. Paradoxical reaction following intravenous midazolam premedication in pediatric patients–a randomized placebo controlled trial of ketamine for rapid tranquilization. *Pediatr. Anesth.* 2004;14:924–930. doi: 10.1111/j.1460-9592.2004.01349.x.

61. Ahrens MB, et al. Brain-wide neuronal dynamics during motor adaptation in zebrafish. *Nature.* 2012;485:471–477. doi: 10.1038/nature11057.

62. Lin X, et al. High-throughput brain activity mapping and machine learning as a foundation for systems neuropharmacology. *Nat. Commun.* 2018;9:5142. doi: 10.1038/s41467-018-07289-5.

63. Jordi J, et al. High-throughput screening for selective appetite modulators: a multibehavioral and translational drug discovery strategy. *Sci. Adv.* 2018;4:eaav1966. doi: 10.1126/sciadv.aav1966.

64. Besnard J, et al. Automated design of ligands to polypharmacological profiles. *Nature.* 2012;492:215–220. doi: 10.1038/nature11691.

65. Yeh C-M, Glöck M, Ryu S. An optimized whole-body cortisol quantification method for assessing stress levels in larval zebrafish. *PLoS One.* 2013;8:e79406. doi: 10.1371/journal.pone.0079406.

Publishing Agreement

It is the policy of the University to encourage open access and broad distribution of all theses, dissertations, and manuscripts. The Graduate Division will facilitate the distribution of UCSF theses, dissertations, and manuscripts to the UCSF Library for open access and distribution. UCSF will make such theses, dissertations, and manuscripts accessible to the public and will take reasonable steps to preserve these works in perpetuity.

I hereby grant the non-exclusive, perpetual right to The Regents of the University of California to reproduce, publicly display, distribute, preserve, and publish copies of my thesis, dissertation, or manuscript in any form or media, now existing or later derived, including access online for teaching, research, and public service purposes.

DocuSigned by:
Reid Kinser
A58A6E32B4B6451...
Author Signature

3/15/2022
Date